remote sensing

MDPI

Review

A Meta-Analysis of Remote Sensing Technologies and Methodologies for Crop Characterization

Hazhir Bahrami [1], Heather McNairn [2], Masoud Mahdianpari [3,4] and Saeid Homayouni [1,*]

[1] Centre Eau Terre Environnement, Institut National de la Recherche Scientifique, Québec, QC G1K 9A9, Canada
[2] Ottawa Research and Development Centre, Agriculture and Agri-Food Canada, Ottawa, ON K1A 0C6, Canada
[3] C-CORE, St. John's, NL A1B 3X5, Canada
[4] Department of Electrical and Computer Engineering, Memorial University of Newfoundland, St. John's, NL A1B 3X5, Canada
* Correspondence: saeid.homayouni@ete.inrs.ca

Abstract: Climate change and population growth risk the world's food supply. Annual crop yield production is one of the most crucial components of the global food supply. Moreover, the COVID-19 pandemic has stressed global food security, production, and supply chains. Using biomass estimation as a reliable yield indicator, space-based monitoring of crops can assist in mitigating these stresses by providing reliable product information. Research has been conducted to estimate crop biophysical parameters by destructive and non-destructive approaches. In particular, researchers have investigated the potential of various analytical methods to determine a range of crop parameters using remote sensing data and methods. To this end, they have investigated diverse sources of Earth observations, including radar and optical images with various spatial, spectral, and temporal resolutions. This paper reviews and analyzes publications from the past 30 years to identify trends in crop monitoring research using remote sensing data and tools. This analysis is accomplished through a systematic review of 277 papers and documents the methods, challenges, and opportunities frequently cited in the scientific literature. The results revealed that research in this field had increased dramatically over this study period. In addition, the analyses confirmed that the normalized difference vegetation index (NDVI) had been the most studied vegetation index to estimate crop parameters. Moreover, this analysis showed that wheat and corn were the most studied crops, globally.

Keywords: crop characterization; biomass; leaf area index; yield; agriculture; remote sensing; Earth observation data; meta-analysis; systematic review

Citation: Bahrami, H.; McNairn, H.; Mahdianpari, M.; Homayouni, S. A Meta-Analysis of Remote Sensing Technologies and Methodologies for Crop Characterization. *Remote Sens.* **2022**, *14*, 5633. https://doi.org/10.3390/rs14225633

Academic Editors: Jiali Shang, Miao Zhang, Xiaodong Huang, Chunhua Liao and Taifeng Dong

Received: 29 August 2022
Accepted: 30 October 2022
Published: 8 November 2022

1. Introduction

Providing adequate agricultural production is critical to a nation's economic development and social stability [1,2]. This sector continues to be challenged by climate change, increasingly unpredictable weather patterns, and global population growth [3]. As such, ongoing monitoring of crop conditions and production estimates can assist in building short-term and long-term resilience for national and international food security and trade and market management [4–9]. Moreover, the COVID-19 pandemic has stressed global food security, production, and supply chain systems [10]. Accurate in-season monitoring of crop conditions and yield estimation can positively impact economic development, national food security, and risk assessment of agricultural production [11,12]. To achieve accurate and precise crop production forecasts, various input data, including incoming solar radiation, temperature, precipitation, soil moisture, and crop phenology, are needed [7,13,14]. The performance of crop models depends on the quality of these input data. Traditionally, crop yield forecasts have been made using in situ and field measurements in which a small part or whole plant is cut as ground samples. However, this approach is destructive,

time-consuming, and expensive [15–19]. Furthermore, the information provided by in situ measurements is restricted to small geographies and may be limited in applicability to the entire growing season. Estimating crop production over large areas is vital for assessing national and regional food security.

Remote sensing can provide data to assist with monitoring and mapping crops at spatial and temporal scales that are difficult to achieve with in situ approaches [2,20–25]. Various sensor technologies and observing platforms have been developed to acquire these data. Sensors mounted on space-based orbiting platforms collect frequent images of the Earth, often with large swath coverage and over regions where on-the-ground access is challenging [26–30]. Typically, airborne sensors provide better spatial resolutions at the expense of temporal revisit and spatial coverage. Airborne systems are more flexible than satellite ones, with deployment dictated primarily by the operator and local weather conditions. These systems also offer choices for acquisition configurations such as incident angles, flight paths, and flying heights [31–33]. Various sensors can be mounted on aircraft, helicopters, unmanned aerial vehicles (UAVs), or drones [34]. In particular, UAV or drone platforms can collect very high-resolution data and are cost efficient relative to satellite remote sensing platforms if the required spatial coverage is small [2,35–37].

Various remote sensing technologies can measure and estimate crop biophysical parameters. These technologies include passive optical, multi- or hyper-spectral, active microwave or synthetic aperture radar (SAR), and optical light detection and ranging (LiDAR) sensors. Multispectral optical sensors have extensively been used for in-season crop mapping and monitoring [38,39]. In particular, vegetation indices (VIs) computed from multispectral data have been widely studied for agriculture applications, while far less research has examined the use of SAR to monitor crops [40]. The results of several studies showed that optical data, particularly VIs, outperform the use of SAR data alone in crop parameter estimation and crop mapping [41–45]. Reflectance and absorption of visible and infrared wavelengths are linked with plant pigmentation and internal leaf structure. Thus, optical VIs respond well to crop condition dynamics and have been used to estimate crop biophysical parameters and yield [46–50]. VIs are typically expressed as normalized ratios. This normalization decreases the impacts of atmospheric effects and bi-directional reflectance and mitigates the effect of soil background reflectance [51,52]. For instance, the normalized difference vegetation index (NDVI) is used to estimate crop biomass and leaf area index (LAI) [53–55]. Despite the sensitivity of optical wavelengths to crop biophysical and biochemical conditions, optical remote sensing is limited in the presence of clouds, cloud shadows, and other atmospheric conditions [56,57]. This limitation complicates the use of optical sensors for operational monitoring, considering that clouds cover two-thirds of the Earth for at least part of the growing season [58]. Optical reflectance saturates when significant biomass accumulates, and the crop canopy is dense, impacting the sensitivity of these VIs during periods of peak growth [59–61].

Synthetic aperture radars are active microwave sensors that generate their energy source and can thus operate independent of solar illumination [20,62]. SARs transmit microwave signals that are significantly longer than wavelengths in the optical and infrared regions of the electromagnetic spectrum. Given these characteristics, SARs are essential for imaging regions of the Earth that experience prolonged periods of cloud cover and in high latitude regions during periods of the year with low solar illumination [62,63]. SARs can collect images of agricultural landscapes regardless of the presence of clouds, and as such, this technology is an attractive option when operational monitoring is essential [20,64]. SARs measure the intensity and phase of target scattered signals [13]. The intensity and phase of microwave scattering depend on system configurations (incident angle, frequency, and polarization), as well as on the characteristics of the agricultural target (dielectric properties, soil surface roughness, and canopy structure) [4,56,65–68]. SARs can provide important information about crop development throughout the growing season because the scattering, intensity, and phase are impacted by canopy structure and water content [69]. When longer wavelengths are used, the sensitivity of SARs to crop characteristics can

extend to larger biomass canopies and periods in the growing season when optical signals saturate [70]. However, regardless of whether optical or SAR is used, methods to retrieve biophysical parameters (e.g., biomass, LAI) developed for one site and one season may not be easily transferable over space or time [71].

LiDAR systems can accurately generate and measure the profile of the terrain and vegetation height [72,73]. The primary measurement acquired by LiDAR systems is the distance between the sensor and target, determined by calculating the elapsed time between the emission of a laser pulse and the arrival of the backscattered pulse to the sensor. Time to and from the target, and the speed of light, determine the distance [74]. LiDAR systems usually utilize near-infrared pulses for topography profile retrieval. The data acquired by the LiDAR system typically have a high resolution because the instrument is mounted on UAVs or aircraft, which can fly at low altitudes [75]. Terrestrial laser scanning (TLS) systems collect data at a higher spatial resolution than airborne or spaceborne platforms [76]. TLS provides a dense 3D point cloud of the target [77,78] and is used extensively in close-range remote sensing.

There are fundamental differences between optical, SAR, and LiDAR and their technical functionalities. Agrawal and Khairnar [75] conducted comprehensive research and demonstrated the primary differences between optical, SAR, and LiDAR systems. The electromagnetic range for SAR systems is from approximately 1 mm to 1 m; however, this range is from 0.4 µm to 1 mm for optical sensors and 250 nm to 10 µm for LiDARs. For optical and SAR systems, information about reflection or scattering is stored in pixels. In contrast, data gathered by LiDARs form 3D point clouds that contain information about the point's coordinates, altitudes, and intensity. Because LiDAR systems are usually mounted on UAVs, aircraft, and ground platforms, the coverage area is relatively small compared to optical and SAR systems. Moreover, the cost of gathering LiDAR data is typically high.

Various review studies, summarized in Table 1, have documented the potential of remote sensing to retrieve crop biophysical parameters. Despite the diversity of this research, no paper comprehensively reviews optical and SAR sensors across platforms (spaceborne, airborne, and ground-based). Furthermore, most review papers on crop parameter estimation did not address the application of machine learning methods.

Table 1. Review studies on crop parameter estimation and remote sensing methods.

No.	Title	Ref.	Journal	Year	Citation
1	Systematic mapping study on remote sensing in agriculture	[79]	Applied Sciences	2020	3
2	Review of machine learning approaches for biomass and soil moisture retrievals from remote sensing data	[80]	Remote Sensing	2015	148
3	Estimation methods developing with remote sensing information for energy crop biomass: A comparative review	[81]	Biomass and Bioenergy	2018	10
4	Applications of vegetative indices from remote sensing to agriculture: past and future	[82]	Inventions	2019	6
5	Estimating the crop leaf area index using hyperspectral remote sensing	[83]	Journal of Integrative Agriculture	2016	44
6	Research advances of SAR remote sensing for agriculture applications: A review	[1]	Journal of Integrative Agriculture	2019	22
7	A review of multitemporal synthetic aperture radar (SAR) for crop monitoring	[39]	Multitemporal Remote Sensing	2016	43
8	A review on drone-based data solutions for cereal crops	[10]	Drones	2020	0
9	Radar remote sensing of agricultural canopies: A review	[84]	IEEE JSTARS	2017	104
10	Optical remote sensing and the retrieval of terrestrial vegetation bio-geophysical properties—A review	[85]	ISPRS J. of Photogrammetry and Remote Sensing	2015	297
11	Remote sensing for agricultural applications: A meta-review	[86]	Remote Sensing of Environment	2020	228

García-Berná et al. [79] defined eight mapping questions and analyzed the various platforms, methodologies, and spectral information used in published studies to estimate vegetation parameters, growth vigor, and water usage. Their results showed that most experiments applied multi- and hyperspectral data classification techniques. Ali et al. [80] reviewed machine learning algorithms to retrieve crop biomass and soil moisture, but these authors did not cover a range of sensors or platforms. Chao et al. [81] analyzed five approaches to estimate vegetation biomass, including the use of VIs, SAR backscatter, net primary productivity (NPP), crop height, and assimilation of state variables from remote sensing into crop growth models (CGMs). This article did not describe the details of the crops and machine learning algorithms investigated, nor did it provide a detailed review of sensors and platforms.

Hatfield et al. [82] evaluated the potential of various VIs to estimate several crop characteristics, including leaf chlorophyll, plant biomass, leaf area, phenological development, plant type, photosynthetic activity, and ground cover. The focus of this study was to investigate the applicability of VIs extracted from optical remote sensing data for crop biophysical parameter retrieval. In another review study by Ke et al. [83], research into the estimation of crop LAI using hyperspectral remote sensing data was described. Three papers by Liu et al. [1], McNairn and Shang [39], and Steele-Dunne et al. [84] reviewed the application of SAR systems in agriculture, including crop mapping, monitoring, and biophysical parameter estimation. None of these three studies included a review of the application of optical data.

Verrelst et al. [85] comprehensively described retrieval methods using optical data to estimate crop biophysical parameters. Panday et al. (2000a) reviewed airborne remote sensing using various methods for local-scale crop monitoring and yield estimation. Weiss et al. [86] published a meta-analysis that presented an overview of different remote sensing techniques to retrieve crop parameters but did not provide details of the platforms and sensors used.

Our research is the first comprehensive meta-analysis, and we pay particular attention to addressing the gaps and limitations of the existing review publications, as described above. This paper provides a robust analysis of the current status and general trends in crop biophysical estimation studies from remotely sensed observations. An extensive literature review is invaluable in pulling together disparate research findings to deliver a clearer understanding of where we stand on the science and better inform new research to overcome challenges and address gaps. The complete database was created based on critical information needed by researchers, including platforms, sensors, methodologies, and geographic location. The database was analyzed to determine the following:

1. Research studies with the highest citation;
2. Platforms used;
3. Most frequently exploited sensors;
4. Most widely used SAR frequency and polarization;
5. Countries that lead in research;
6. Most commonly used VIs;
7. Crop parameters studied most; and
8. Most widely used algorithms.

Several parameters were extracted from the database, including authors with the highest publications in this field, temporal trends in the studies based on the article's published date, sensor spatial and temporal resolution, study area size, and the total number of sampling points in each study.

2. Methods

A set of comprehensive queries was selected to search in the Web of Science (WoS) and Scopus knowledge websites to find review articles, book chapters, and conference papers and establish a database for this review. The search queries were created based on five basic categories to encompass all the papers with a crop parameter estimation focus.

1. Finding relevant keywords to crops and agriculture in the title;
2. Finding relevant studies on the topic of remote sensing (i.e., title, abstract, and keywords);
3. Finding relevant methods in crop parameter estimation on the topic;
4. Finding several relevant terms to crops on the topic;
5. Choosing several terms to exclude irrelevant studies on crops and agriculture.

"Or" is set between the keywords, and "and" is set between the categories (Figure 1). We tried to include only relevant articles in the search queries. According to Figure 1, the keyword in the 'title' column searches only among the title of articles. However, the "Topic" column searches keywords among title, abstract, and keywords of papers. The star sign (*) is to replace the character chain after the main word. For example, in the 'agricultur', both 'agriculture' and "agricultural' would be accepted for the title.

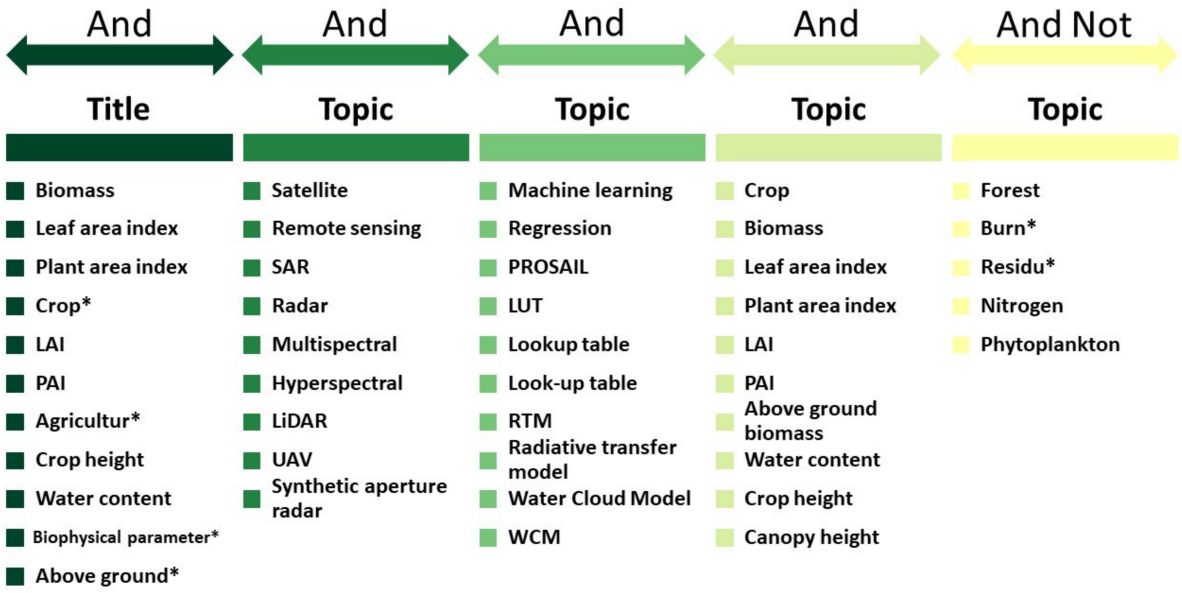

Figure 1. Designed search query and corresponding search phrases for crop parameter estimation review. Key terms in the first column were imported as input data in the topic, and the other columns were in the title. (Leaf area index (LAI), plant area index (PAI), look-up table (LUT), radiative transfer model (RTM), water cloud model (WCM)). The star marks mean that the system identified all suffixes, including the primary word.

In total, 1039 and 444 articles, including conference papers, reviews, and book chapters, were found in Scopus and WoS, respectively. In this study, only journal articles were included in the meta-analysis database. The selected studies were published from 1990 to 2020. After removing duplicate articles, 381 studies remained. Only related titles and abstracts for research on estimating crop parameters were selected from these studies. Finally, 277 published articles were included in the meta-analysis (Figure 2).

Figure 3 shows a cloud graphic of the most frequently utilized keywords in the final 277 papers. In this figure, the text size represents the number of keywords repeated in the research papers. These keywords are selected based on the occurrence of higher than 50. This image is captured by VOS viewer, free accessible software for constructing bibliometric networks.

The meta-analysis database was created using 21 attributes (Table 2). These attributes comprise broad terms that capture comprehensive information regarding the studies reviewed. This database contains general information about articles, including title, year, citation, publication, author(s), and affiliation. Furthermore, additional terms were created to extract specific information from each study, such as geographic location, crop type, platform, sensor, and methodology. The details of the attributes selected in this study are

shown in Table 2. These attributes were imported into an excel sheet, and each article's data was inserted.

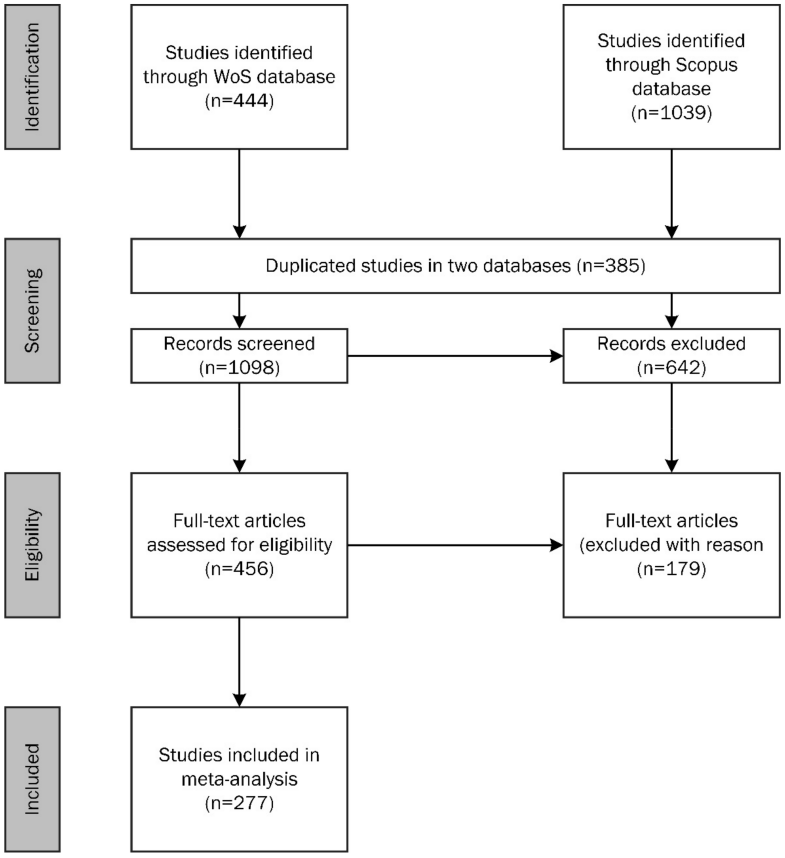

Figure 2. Preferred reporting items for systematic reviews and meta-analyses (PRISMA) flow diagram for selecting relevant manuscripts. PRISMA aims to help researchers improve the reporting of systematic and meta-analyses reviews.

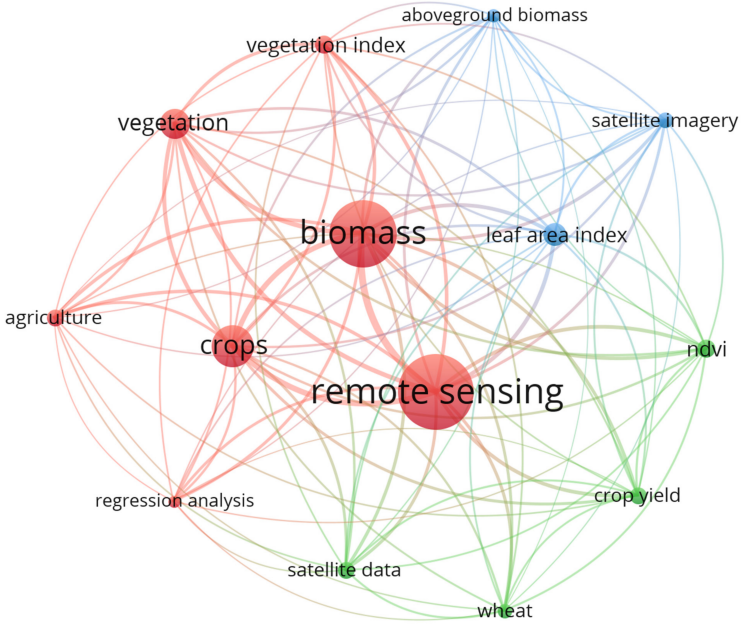

Figure 3. A cloud graphic of frequent terms in journal papers studying crop retrieval using remote sensing. The size of the text reflects the frequency of each specific term.

Table 2. Attributes extracted from screened articles in the database for comprehensive meta-analysis. These attributes were imported into an excel sheet for further analysis.

No.	Attribute	Description
1	Title	-
2	Year	-
3	Citation	-
4	Publication	Journal name
5	Author(s)	-
6	Affiliation	-
7	Geographic location	Country name
8	Study area size	km^2
9	Crop type	-
10	Platform	Spaceborne, airborne, or ground sensor
11	Sensor	Optical, synthetic aperture radar (SAR), point cloud, and integrating
12	SAR single or multifrequency	-
13	Used SAR frequency	X, C, P, L, Ku bands
14	Used VI(s)	Normalized difference vegetation index (NDVI), enhanced vegetation index (EVI), or ...
15	Polarization	Single, dual, or quad polarization
16	SAR Incident angle	Range of incidence angle
17	Spatial resolution	Meters
18	Methodology	Regression, etc.
19	Single or multi-date	-
20	Crop parameter estimation	Biomass, LAI, crop height, ...
21	Accuracy Assessment	The value of coefficient of determination (R^2), root mean square error (RMSE), mean absolute error (MAE), ...

Accuracy Assessment

In regression models, the most widely used evaluation criteria are coefficient of determination (R^2), root mean square error (RMSE), mean absolute error (MAE), normalized RMSE (nRMSE), and simple correlation coefficient (R). RMSE is a commonly used statistical measure that calculates the average differences between observed and estimated values as follows:

$$\mathrm{RMSE} = \sqrt{\frac{\sum_{i=1}^{N}(\hat{y}_i - y_i)^2}{N}}, \quad (1)$$

where $\hat{y}_i$ is the predicted value for ith sample, y_i is the observed value for the ith sample, and N is the number of observations. MAE is also a measure of errors between the predicted and observed data and is calculated as follows:

$$\mathrm{MAE} = \frac{\sum_{i=1}^{N}|\hat{y}_i - y_i|}{N}, \quad (2)$$

In addition, R^2 is calculated as follows:

$$R^2 = 1 - \frac{\sum_{i=1}^{N}(\hat{y}_i - y_i)^2}{\sum_{i=1}^{N}(\hat{y}_i - \overline{y})^2}, \quad (3)$$

where $\overline{y}$ is the average value of observations. R is used in statistics problems to measure the relationship between the estimated and observed samples and is calculated as follows:

$$R = \frac{\left(N\sum_{i=1}^{N}(\hat{y}_i y_i)\right) - \left(\sum_{i=1}^{N}\hat{y}_i\right)\left(\sum_{i=1}^{N}y_i\right)}{\sqrt{\left(N\sum_{i=1}^{N}\hat{y}_i{}^2 - \left(\sum_{i=1}^{N}\hat{y}\hat{i}\right)^2\right)\left(N\sum_{i=1}^{N}y_i{}^2 - \left(\sum_{i=1}^{N}y_i\right)^2\right)}}, \quad (4)$$

Finally, nRMSE is the RMSE normalized by the average value of the respective crop parameter.

3. Results of Bibliographic Analysis

3.1. General Characteristics

Figure 4a represents the number of published full-text articles per year. This figure shows that from 2008 up to now, the number of studies has steadily increased. Years without any published articles were excluded from this figure. Manuscripts that tackled the estimation of crop parameters received significant attention post-2011. This may be due to new technologies from satellite sensors and UAV and ground remote sensing sensors, which have become more accessible or have improved capability. An expansion in the availability of satellite remote sensing data, such as WorldView-1 and -2 (launched in 2007 and 2009, respectively), RapidEye (launched in 2008), RADARSAT-2 (launched in 2007), and other satellites/sensors launched just before this period (Landsat 5 and 7, MODIS) could explain the increase in research publications. Another driving factor is likely related to the rise in the development of computing power systems enabling the scalability of parametric and non-parametric regression methods. Recognition of the importance of large-scale agricultural monitoring using remote sensing technologies could further explain the increasing number of published papers.

The first paper on remotely sensed data for crop parameter estimation was published in 1990. There might be other papers published before 1990, but they did not satisfy our queries or were not in the Scopus or WoS database. Figure 4b documents the number of studies published in each journal. A significant number of studies were published in the Remote Sensing journal (44 articles), followed by Remote Sensing of Environment (RSE) with 29 articles, and the International Journal of Remote Sensing (IJRS) with 25. Journals with one or two published articles were removed. The "Other" bar plot (Figure 4b) included the Journal of Applied Remote Sensing (JARS) (6), Precision Agriculture (PA) (6), Journal of Photogrammetry, Remote Sensing and Geoinformation Science (JPHRSG) (3), and Photogrammetric Engineering and Remote Sensing (PEERS) (3). Cumulatively, 18 manuscripts were published in these journals.

Figure 5 maps the distribution of the sites of study for the research. The countries with more than 10 studies are China (75), Canada (37), the United States of America (USA) (34), Spain (17), Italy (16), France and Germany (15 each), India (13), and Brazil (10). In addition, the Netherlands (6), South Africa and Finland (5 each), Japan, Reunion Island, Iran, and Australia (4 each), and Senegal, Switzerland, Austria, and Greece (3) are also noteworthy. The impact of extensive experiments, for example, the Soil Moisture Active Passive Validation Experiment 2012 (SMAPVEX12) and 2016 (SMAPVEX16) over Canada, received significant attention given efforts to share these data broadly and considering the range of crops studied in these experiments [7,87–93].

Wheat is an important staple, and the significance of this crop is reflected in the attention paid to it in remote sensing research (Figure 6). Remote sensing to estimate wheat parameters was studied in 110 manuscripts. Other globally important crops followed, including corn (91 studies), soybean (32), rice (26), potato (24), barley (18), sunflower (18), canola (15), sugar beet (14), onion (12), and oats (10). Crops cited in less than 10 manuscripts are shown as others in the bar chart. Perennial crops and other agricultural land covers are essential in supporting livestock production. In the papers reviewed, remote sensing of grasslands was studied in 42 papers, while alfalfa was investigated in 22 and pasture lands in 12.

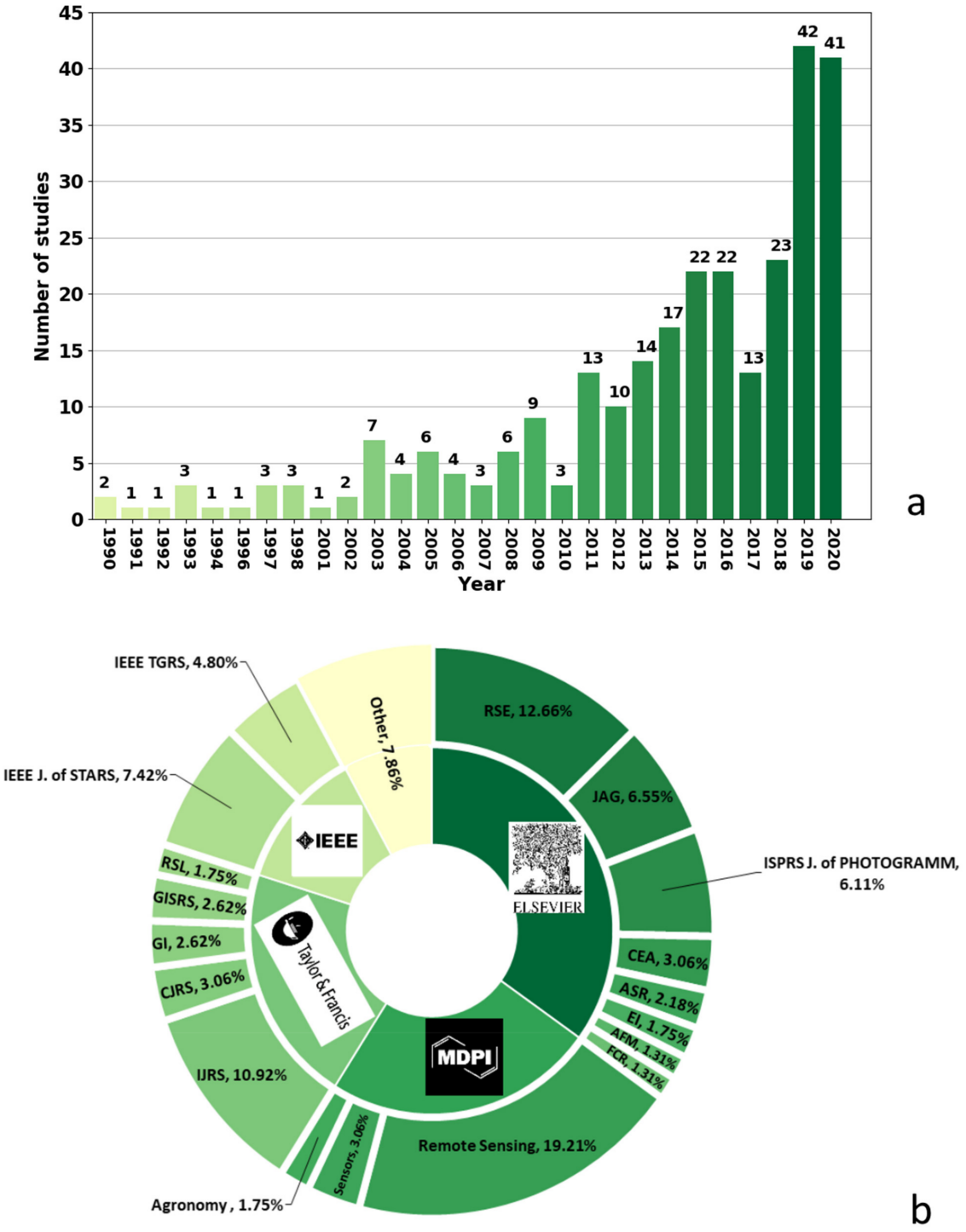

Figure 4. (**a**) The number of studies per year; (**b**) the number of papers published in each journal from 1990 to 2020. The journals with more than two articles were plotted here. In addition, the journals with fewer than five studies are included in the other plot. The journals include the International Journal of Applied Earth Observation and Geoinformation (JAG), ISPRS Journal of Photogrammetry and Remote Sensing (ISPRS J. of PHOTOGRAMM), Computers and Electronics in Agriculture (CEA), Advances in Space Research (ASR), Ecological Indicators (EI), Agricultural and Forest Meteorology (AFM), Field Crops Research (FCR), Canadian Journal of Remote Sensing (CJRS), Geocarto International (GI), GIScience and Remote Sensing (GISRS), Remote Sensing Letters (RSL), IEEE Journal of Selected Topics in Applied Earth Observations and Remote Sensing (IEEE J. of STARS), IEEE Transactions on Geoscience and Remote Sensing (IEEE TGRS).

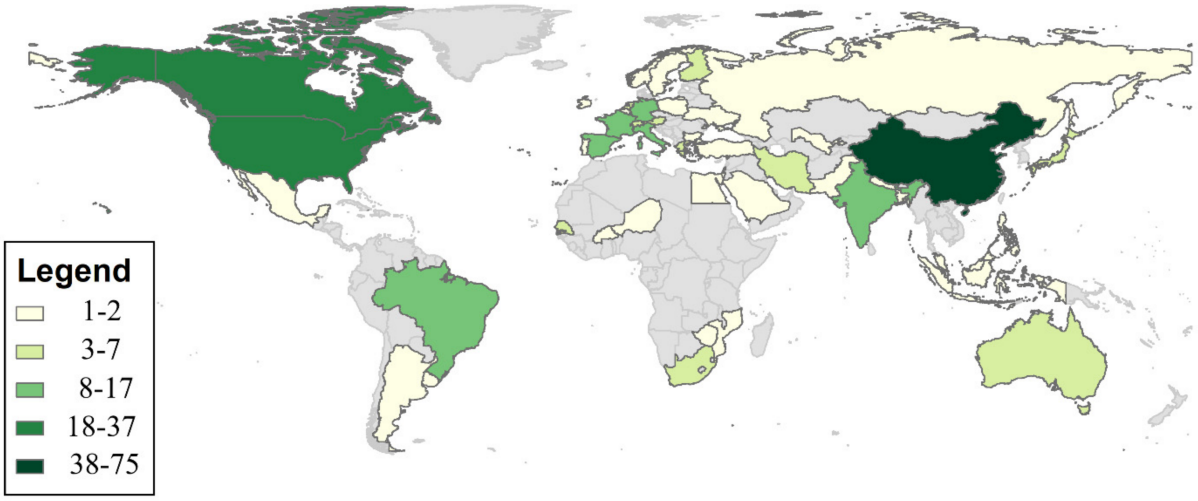

Figure 5. World map illustrating the number of published articles based on the location of the study site.

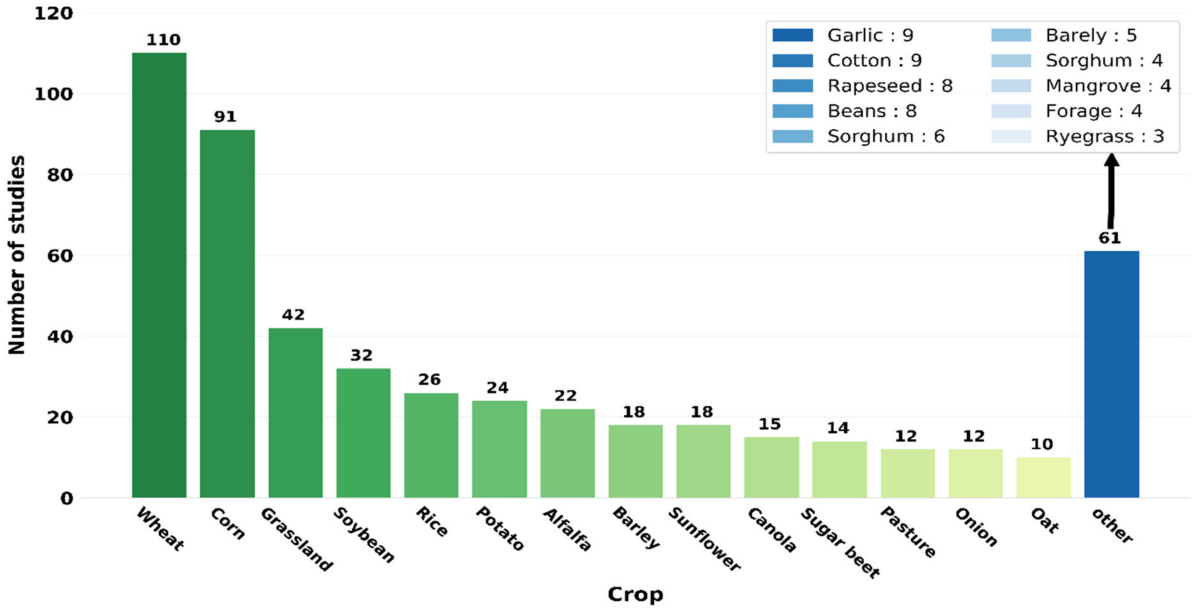

Figure 6. The number of manuscripts studying different crop types.

Figure 6 shows that wheat and corn received more attention than other crops. According to the Food and Agriculture Organization, wheat is cultivated more than any other commercial crop. It plays a significant role as the most critical food grain for humans (http://www.fao.org/3/y4011e/y4011e00.htm) (accessed on 31 October 2022). According to Shewry and Hey [94], wheat is an important staple crop in temperate and moderate zones. In addition, wheat produces essential by-products, such as proteins and vitamins, crucial for human health. Farmers are encouraged to increase wheat acreages, especially in Asia, because of this crop's potential high yield, affordability, and institutional support [95]. Corn, another globally important crop, can be grown under diverse agro-environmental conditions, including different climate zones and varying soils and landscapes [96]. Compared to other cereal crops, corn produces high yields. To this end, the cultivation of corn has become more attractive to farmers, particularly in areas with high population pressures [96]. The United States Department of Agriculture estimates that for China's marketing year (2021/2022), corn production is 273 million metric tons, a 5% increase from the previous year. According to the International Maize and Wheat

Improvement Center, wheat products are consumed by 2.5 billion people in 89 countries. Furthermore, wheat and corn acreages total 218 and 197 million hectares (https://www.cimmyt.org/news/ten-things-you-should-know-about-maize-and-wheat/) (accessed on 31 October 2022), respectively (https://www.cimmyt.org/) (accessed on 31 October 2022).

3.2. Data Processing

In general, papers that examined remote sensing to estimate crop biophysical parameters followed four primary steps (Figure 7). The remote sensing data collection included sensors mounted on spaceborne, airborne, and ground-based platforms. The sensor technology varied, but the most common experiments exploited SAR, optical, and laser-based sensors. The methodologies developed to estimate crop parameters and yield fell into one of four categories: parametric models, non-parametric models, physical-based models, and empirical models [85]. Researchers primarily studied the retrieval of LAI, biomass (wet and dry), and crop height using these varied methods and remote sensing technologies.

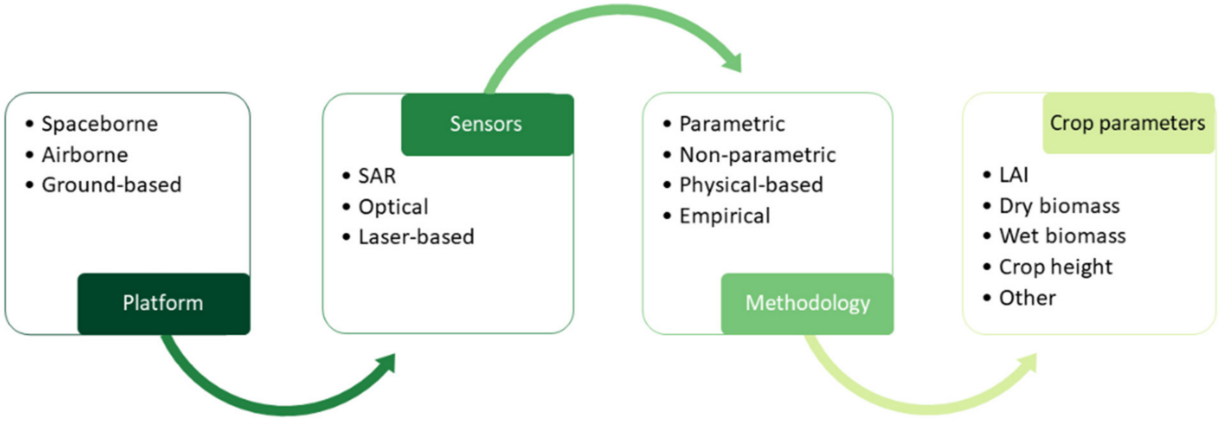

Figure 7. Essential parameters of meta-analysis articles assessed in this study.

3.2.1. Remote Sensing Platform

A further breakdown of the various platforms used in the manuscripts examined in our analysis is shown in Figure 8. Spaceborne platforms were most commonly used in these agriculture monitoring studies (169 articles), followed by airborne (45) and ground-based (35) platforms. All papers using ground SAR or optical sensors, including ground spectrometers and scatterometers, camera and imaging systems onboard ground platforms, such as a tripod or hand-held systems, are categorized into ground-based platforms. Many authors combined data from multiple platforms, such as spaceborne and airborne (15 studies), or spaceborne and ground-based (13 studies). Figure 8 presents the cumulative summation of platforms used in the studies examined in our meta-analysis, starting from 1990. Notably, spaceborne platforms for crop studies increased significantly in 2011. This uptake in research using space-based sensors may be partially due to the release of the Landsat data archive by the US Geology Survey on 9 January 2009 (https://www.usgs.gov/landsat-missions/january-9-2009-usgs-announcement-opening-landsat-archive) (accessed date on 31 October 2022). According to the USGS announcement, data from Landsat 1 to Landsat 7 could be downloaded for free, and users could begin accessing a collective archive of data dating back 35 years. In addition, this period witnessed an increase in the launch of new satellite SAR and optical systems. For example, TerraSAR-X and its companion TanDEM-X were launched in 2007 and 2010. Canada launched the C-band RADARSAT-2 satellite in 2007. In addition to satellite SAR data, the increase in available optical satellite data accelerated research to monitor croplands and assess crop parameters using these space-based technologies.

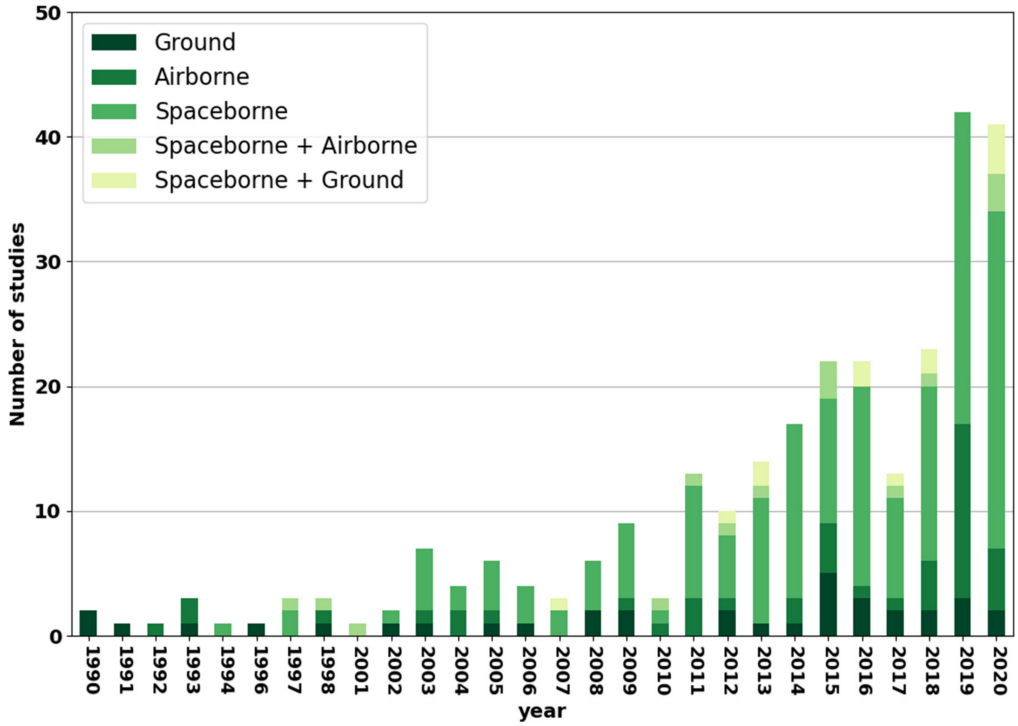

Figure 8. The variability of platforms used in screened articles, based on publication year.

3.2.2. Sensors

Using one spectral region is likely to yield acceptable results in the characterization of crop conditions, yet most researchers focus on combining two or more spectral regions (Figure 9). Examination of 182 articles (optical-based studies) and those which used a combination of optical with SAR and laser-based sensors showed that many studies used VIs extracted from optical sensors compared to exploiting spectral bands alone. Most studies examined visible and infrared sensors for biophysical retrieval (182 studies), which is expected given the long history of data available from optical sensors. The link between optical reflectance and crop metrics is physically meaningful and intuitive. Of the 53 studies that used SAR technologies, 32 examined the integration of SAR with optical data. A much smaller number of studies (10) used LiDAR data, with few combining LiDAR with optical data.

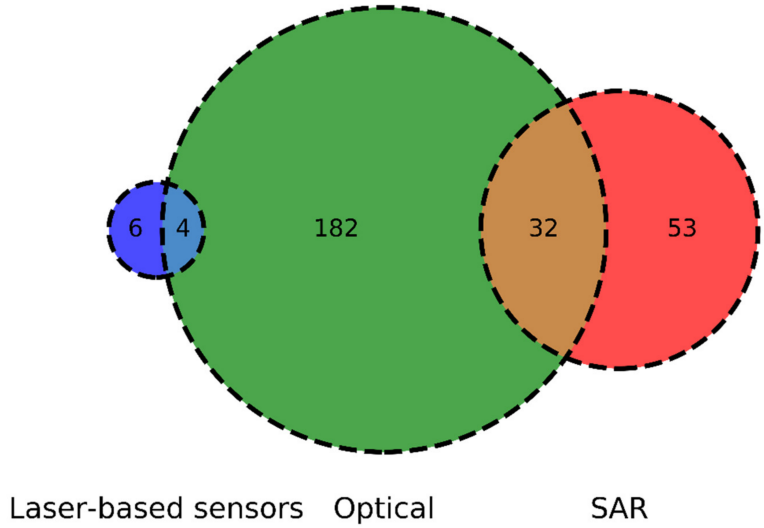

Figure 9. Sensors utilized in screened articles.

In those manuscripts that used optical multispectral data for crop biophysical retrievals, a wide range of VIs were evaluated (Figure 10). NDVI is the most studied VI, appearing in 161 papers. It should be noted, although NDVI is the most popular VI [97], it may not always be the best VI to use. The exploitation of NDVI for vegetation condition assessment dates back to the earliest optical remote sensing technologies, the NOAA series of satellites that carried the AVHRR sensor. Justice et al. [89] reported the first agricultural research using AVHRR images. Donald Deering and Robert Hass first introduced NDVI, with the assistance of mathematician John Schell, to normalize the effect of the solar zenith angle on vegetation reflectance [98]. The vast area coverage and consistency in data availability from NOAA's AVHRR sensors encouraged the uptake of NDVI as an essential remote sensing method for crop monitoring [99,100].

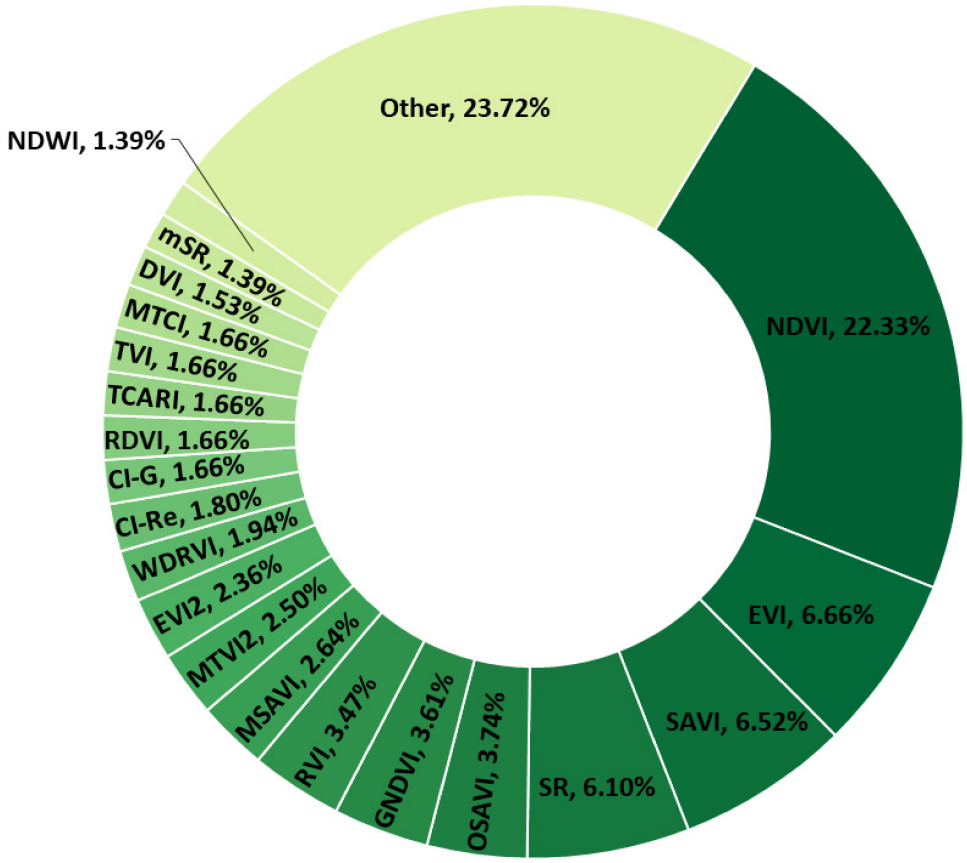

Figure 10. A representation of the most-utilized VIs.

NDVI is simple to calculate from optical sensors carrying one red and one NIR band, and its meaning is intuitive to vegetation conditions [97]. Chlorophyll, an indicator of vegetation health, strongly absorbs energy in the visible region of the electromagnetic region; however, the cellular part of leaves strongly reflects the infrared light. When the plant becomes sick or afflicted with disease, it absorbs near-infrared light instead of reflecting it. Therefore, NDVI provides important information on chlorophyll content and is strongly correlated with plant health. Multispectral sensors are typically less costly to design, manufacture, and deploy than SAR sensors. Thus, multispectral sensors are attractive as payloads for spaceborne, airborne, and ground platforms [97]. For this reason, NDVI has been widely adopted for field-scale national and global monitoring. Many other VIs were studied in three or more manuscripts. These included the enhanced vegetation index (EVI) (48 papers), soil-adjusted vegetation index (SAVI) (47), simple ratio (SR) (44), optimized soil-adjusted vegetation index (OSAVI) (27), green NDVI (GNDVI) (26), ratio vegetation index (RVI) (25), modified soil-adjusted vegetation index (MSAVI) (19), modified triangular vegetation index 2 (MTVI2) (18), EVI2 (17), wide dynamic range vegetation index

(WDRVI) (14), red-edge chlorophyll index (CI-Re) (13), green chlorophyll index (CI-G) (12), renormalized difference vegetation index (RDVI), transformed chlorophyll absorption ratio index (TCARI), transformed vegetation index (TVI), MERIS terrestrial chlorophyll index (MTCI) (12), difference vegetation index (DVI) (11), modified SR (mSR) and normalized difference water index (NDWI) (10). The list of the top 10 VIs with their formula is shown in Table 3.

Table 3. The formula of the top 10 VIs.

Index	Formula	Ref.
NDVI	$\frac{R_{NIR}-R_R}{R_{NIR}+R_R}$	[98]
EVI	$2.5\frac{R_{NIR}-R_R}{R_{NIR}+6R_R-7.5R_B+1}$	[101]
SAVI	$(1+L)\frac{R_{NIR}-R_R}{R_{NIR}+R_R+L}$	[102]
SR	$\frac{R_{NIR}}{R_R}$	[103]
OSAVI	$(1+0.16)\frac{R_{0.86}-R_{0.67}}{R_{0.86}+R_{0.67}+0.16}$	[104]
GNDVI	$\frac{R_{NIR}-R_G}{R_{NIR}+R_G}$	[105]
RVI	$\frac{R_R}{R_{NIR}}$	[106]
MSAVI	$\frac{2(R_{NIR}+1)-\left((2R_{NIR}+1)^2-8(R_{NIR}-R_R)^{0.5}\right)}{2}$	[107]
MTVI2	$\frac{1.5(1.2(R_{NIR}-R_G)-2.5(R_R-R_G))}{\sqrt{(2R_{NIR}+1)^2-\left(6R_{NIR}-5\sqrt{R_R}\right)-0.5}}$	[59]
EVI2	$2.5\frac{R_{NIR}-R_R}{R_{NIR}+2.4R_R+1}$	[108]

Concerning SAR research, Figure 11a illustrates the dominance of C-band SAR in crop biophysical retrieval studies. Routine collections of C-band SAR data from space first became readily available in 1991 with the launch of the ERS-1 satellite, followed by several other C-band missions (ERS-2, Envisat ASAR, RADARSAT-1, RADARSAT-2, Sentinel-1 A/B, RISAT, and the RADARSAT Constellation Mission). Although the C-band frequency was beneficial for ocean and ice monitoring, the availability of C-band data over land encouraged agricultural research (65 studies). Fewer studies reported the use of X-band (27 studies), L-band (19 studies), Ku-band (7 studies), P-band (2 studies), S-band (2 studies), and Ka-band (1). This is likely partially due to the limited data available at these frequencies. Of interest is the number of studies that examined only one frequency versus those researchers who could use SAR data collected at multiple frequencies (Figure 11b). Again, this would be related to the availability of satellite, airborne, or ground-based platforms that acquire data at more than one SAR frequency. The limited number of multi-frequency studies shows a significant gap in research, given the expected benefits of multi-frequency SAR for agricultural monitoring and mapping. For example, [109,110] showed the utility of multi-frequency data in crop monitoring and mapping. In addition, Mohan et al. [111] reported that multi-frequency data provided better accuracy in forest biomass estimation. Although many airborne platforms carry SAR sensors capable of acquiring data in more than one frequency, these data collections are more limited because of the cost of airborne campaigns. A movement toward free and open SAR satellite data has lagged behind initiatives such as the release of the Landsat archives. However, the Sentinel-1 constellation is an excellent example of the efforts of SAR data providers toward open and easy data access.

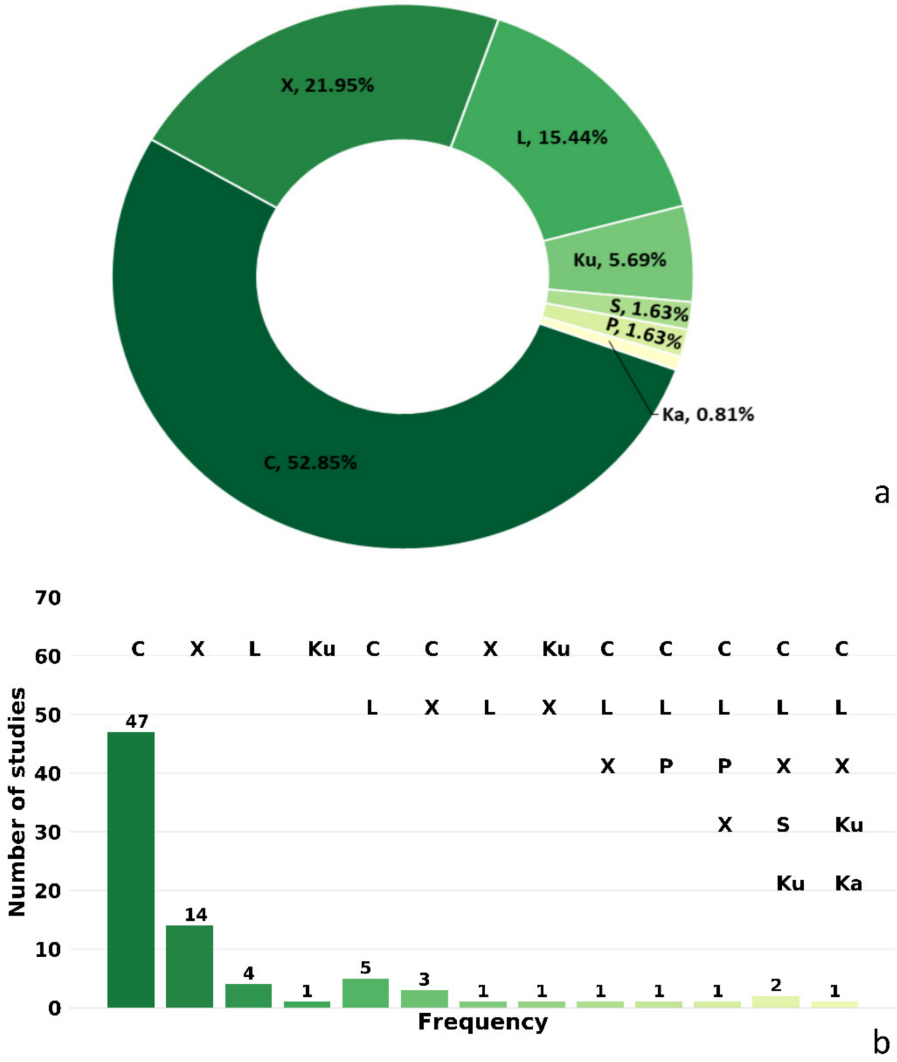

Figure 11. (**a**) SAR frequencies used, and (**b**) the combination of SAR frequencies studied in screened articles.

Our metadata analysis revealed that of the satellites used, the Landsat series of satellites (74 manuscripts in total), Sentinel-2 (51), and the moderate-resolution imaging spectroradiometer (MODIS) (39), which is a sensor on board the Aqua and Terra satellites, were exploited the most (Figure 12). The emphasis on these platforms is likely related to the accessibility of the data and a longer data record. UAV platforms are also used extensively (57), a function of the growth in technologies to fit these platforms, the reduced cost, and the spatial scale associated with these data acquisitions. Ground-based spectrometers and scatterometers (categorized here as ground-based optical-SAR; 45 studies) offer flexibility in deployment under controlled experimental settings and are often used to build and test models scaled to satellite platforms [112,113]. Sentinel-1, RADARSAT-2, and Envisat ASAR have been used in 19, 18, and 11 studies, respectively. A smaller number of studies have completed research using other optical satellites (HJ-1 (12), SPOT-4 (12), and RapidEye (11)).

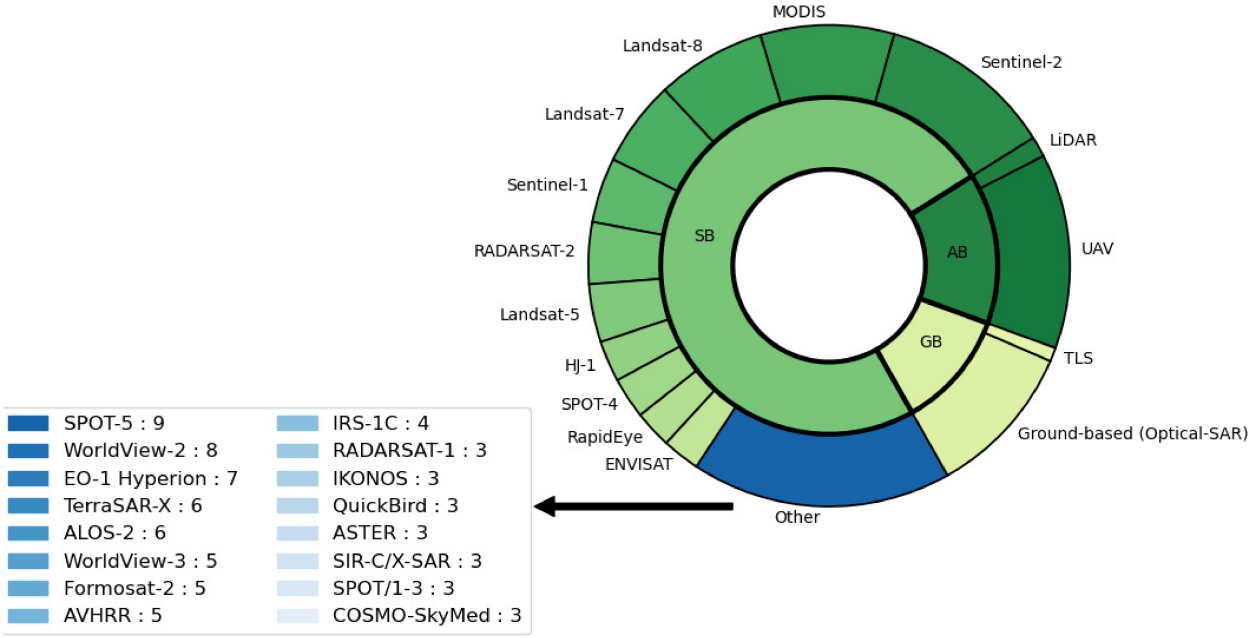

Figure 12. A detailed breakdown of remote sensing sensors used in screened articles.

3.2.3. Methodology

There are four main approaches for retrieving crop biophysical parameters, including parametric and non-parametric regression models, physically based models, and empirical models. In regression models, the number of parameters is a priori specified; accordingly, they can be categorized as parametric regression models. In parametric regression methods, two aspects are considered: (1) the type and the number of independent variables and (2) the mathematical model which defines the relationship between the dependent and independent variables. Unlike parametric regression methods, non-parametric regression methods build a non-explicit relationship, transformation, or fitting function on the independent variable(s). Generally, machine learning (ML) methods are considered non-parametric techniques in the literature. Non-parametric methods are divided into two common groups: (1) linear non-parametric methods (e.g., stepwise multiple linear regression (SMLR), principal components regression (PCR), partial least squares regression (PLSR)), and (2) nonlinear non-parametric methods (e.g., random forest (RF), support vector machine (SVM), and neural network (NN)). Non-parametric models, particularly machine learning regression-based algorithms, have outperformed parametric regression methods in crop parameter estimation [114]. These algorithms are widely applied to complex data; therefore, they can learn the nonlinear relationship between input variables and target parameters. RF is an ensemble learning model used in both regression and classification problems. RF is the first successful bagging model that combines all estimator predictions to produce an accurate model. Since the execution of RF is based on averaging all decision tree predictions, it significantly reduces the variance of the model. Among various machine learning algorithms for classification and regression problems, RF has been considered one of the more robust methods because of the nonlinear modeling relationships between features and target parameters [55]. RF models have several advantages as they can run efficiently on a large amount of data and use a relatively low number of hyper-parameters compared to other machine learning algorithms [55]. RFs are less sensitive to noise and overfitting [115].

NNs are popular machine learning algorithms inspired by the human brain. NN consists of interconnected neurons that learn by modifying their weights. NN models typically consist of one input layer, one hidden layer, and one output layer. In the NN model, the neurons of one layer can be connected to all previous and following layers' neurons but not to the same layer's neurons. NNs are an excellent alternative to classic

mathematical algorithms and are promising alternatives to these classic mathematic models [116]. Deep NNs are increasingly studied because of their performance and automatic feature extraction [117]. Numerous studies have discussed the advantage of using NNs in crop parameter estimation [7,41,116,118].

The SVM model is a robust kernel-based machine learning algorithm. SVM aims to identify a hyperplane that maximizes the margins between different classes of training samples. Using support vector regression (SVR), a flexible tube is formed comparably around the estimation function such that the absolute amount of error less than a specified threshold is ignored. In contrast to outside points, those inside points above or below the prediction function are not penalized. SVR has produced promising results in retrieving crop parameters. However, SVR is inappropriate when working with data that may have substantial errors and uncertainty, particularly in remote sensing data. This is because SVR exploits a fixed cost function, independent of its statistical nature, that assumes a specific density model [119].

Physical-based models are built upon physical laws, creating cause–effect relationships between a physical crop parameter and remote sensing observations [120]. Typically, physically based models derive variables using the radiative transfer model (RTM). Finally, empirical and semi-empirical methods build a simple statistical model between vegetation remote sensing observations, e.g., backscattering or reflectance, and crop parameter(s). Of the approaches taken to estimate crop biophysical parameters, linear regression (LR) parametric methods are the most common (136 studies) (Figure 13), likely because of the simplicity of applying these models. Other parametric methods include multiple linear regression (MLR) (43 studies), exponential regression (Exp-R) (28), logarithmic regression (Log-R) (20), polynomial regression (Poly-R) (16), and power regression (Pow-R) (11). There are also various non-parametric approaches, including neural network (NN) (32 studies), random forest (RF) (27), partial least square regression (PLSR) (24), support vector regression (SVM) (23), Gaussian process regression (GPR) (12), stepwise multiple linear regression (SMLR) (11), gradient boosting decision tree (GB) (4), and K-nearest neighbor (K-NN) (3)). Thirty-five manuscripts reported research using physical-based methods (i.e., RTM), and 20 used the semi-empirical water cloud model (WCM).

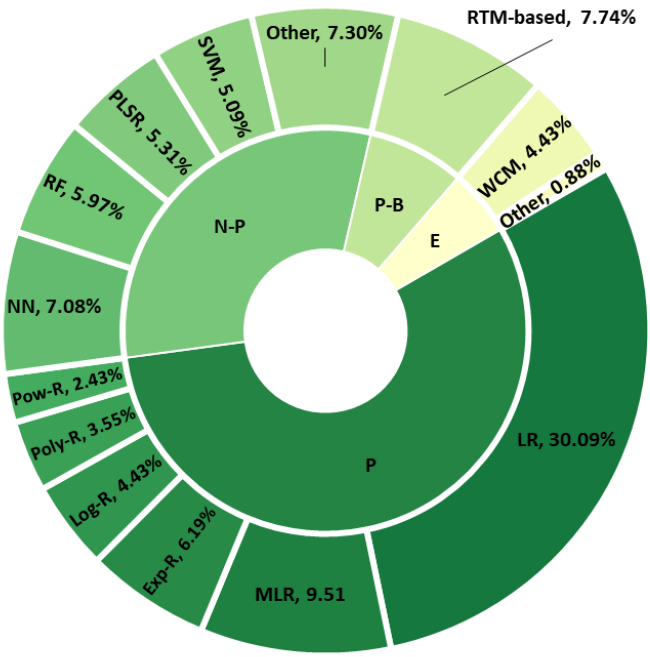

Figure 13. Methods used to estimate crop parameters from remote sensing data.

Figure 14 shows the results of various models based on the publication year. As seen in this figure, when considering parametric models, the number of publications has

been increasing rapidly since around 2010. The number of publications of non-parametric models from 2010 is also increasing.

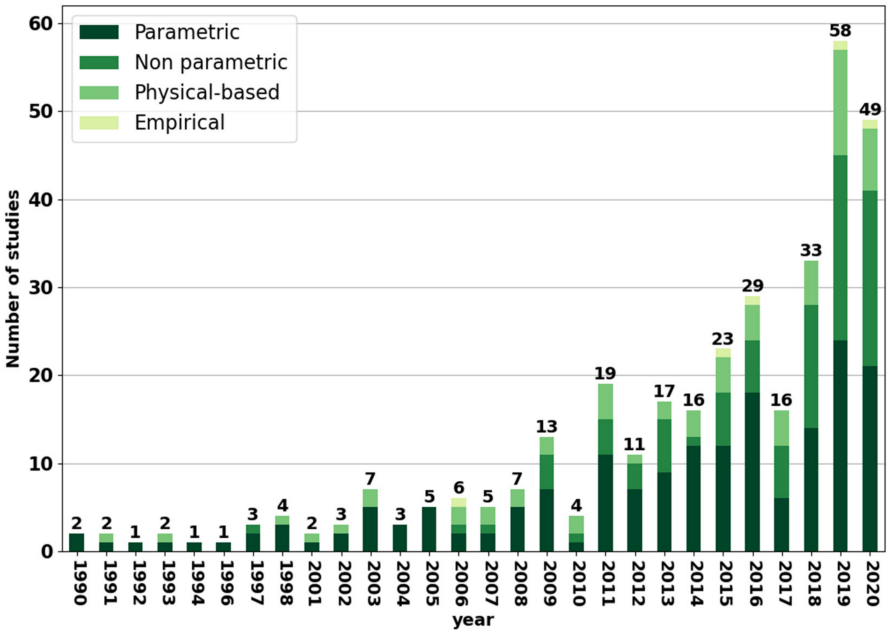

Figure 14. Methods used to estimate crop biophysical methods by year.

3.2.4. Crop Parameters

Crop parameters, such as biomass and LAI, correlate with essential crop productivity outcomes such as yield [70]. Most research has focused on wet and dry biomass, crop height, vegetation water content (VWC), and LAI retrievals (Figure 15). Crop height is more easily measured in the field as a quick metric of crop growing status. Although yield is the ultimate measure of agricultural productivity, collecting yield data at the field scale is tedious and expensive. Other parameters (i.e., biomass and LAI) are often used as surrogates for crop productivity [92]. VWC is typically a secondary measure derived from biomass drying and has received less attention in the literature.

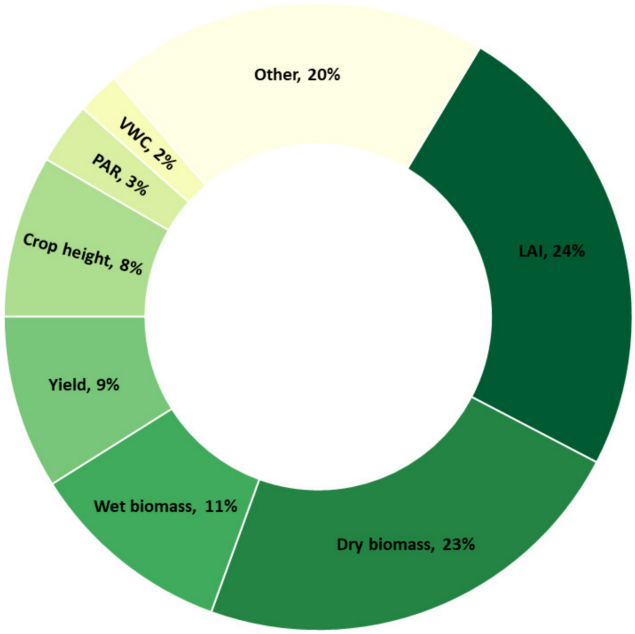

Figure 15. Most studied crop biophysical parameters.

3.2.5. Accuracy Assessment

We summarized the coefficient of determination (R^2) associated with retrieving crop physical parameters, as reported in each screened article. This meta-analysis provided insight into retrieval performance by crop type, biophysical parameter, sensor type and platform, and methodologies. The boxplots are used to visualize these results. Note that the coefficient of determination is not always the square of R. It would provide a sum square error greater than the sum squares total (computed from the flat reference line). It produces a ratio value above one and thus the negative R^2 value when subtracted from one (Equation (3)). Except for barley, the median R^2 was above 0.6 (Figure 16). Although accuracies could reach as high as 0.9, significant variance in results is revealed in these plots. This range in results could be associated with the variety of sensor technologies or methodologies exploited in the literature. Some crops have a lower standard deviation in the reported results (canola and sunflower) (Table 4). The significant variation in results from grasslands may be due to the varied nature of these land covers, even within a single experiment. Rice has the highest median and mean accuracies (i.e., R^2 = 0.79 and 0.74). The count row in the table is the amount of data in the analysis. Some papers utilized various vegetation indices for crop parameter estimation. To this end, they precisely calculated the value of R^2 for each index. Therefore, the amount of data in the analysis is greater than the number of papers screened in this research.

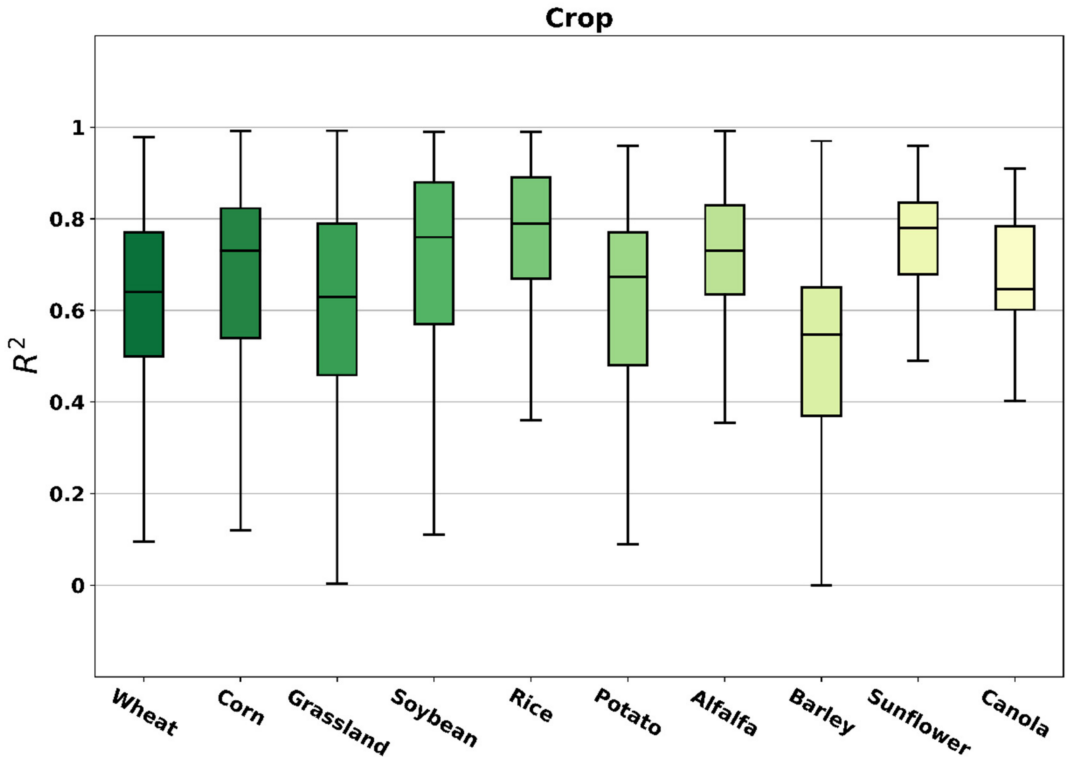

Figure 16. The coefficient of determination (R^2) of biophysical retrievals as a function of crop type.

The boxplots of the accuracies of various non-parametric and parametric regression methods are provided in Figure 17. The details of R^2 values for non-parametric and parametric regression methods are provided in Tables 5 and 6. However, the highest accuracy among all non-parametric methods was reported for the RF algorithm (i.e., R^2 of 0.998), and GPR achieved the highest median accuracy (i.e., R^2 of 0.88) (Table 5). GPR and RF have the highest mean of R^2 (0.8 and 0.76, respectively) (Table 5). The exponential regression model had the highest accuracy among parametric methods, while polynomial and exponential regression methods had the highest median (Table 6). In addition, polynomial regression has the highest average of R^2 (0.628) (Table 6). Compared to parametric methods

(Figure 17b), most non-parametric methods yielded lower accuracy variances as a collective of research results. A comparison between non-parametric and parametric models showed that the median of non-parametric algorithms is higher than parametric regression models.

Table 4. Statistical analysis of R^2 in various crops.

	Wheat	**Corn**	**Grassland**	**Soybean**	**Rice**
Mean	0.61	0.66	0.59	0.69	**0.74**
STD	0.22	0.23	0.24	0.24	0.20
Min	0.00	−0.07	0.00	−0.07	0.01
1st quartile	0.50	0.54	0.46	0.57	0.67
Median	0.64	0.73	0.63	0.76	**0.79**
3rd quartile	0.77	0.82	0.79	0.88	0.89
Max	0.979	0.992	**0.993**	0.990	0.990
Count	**789**	666	660	237	176
	Potato	**Alfalfa**	**Barley**	**Sunflower**	**Canola**
Mean	0.61	0.71	0.51	0.73	0.67
STD	0.22	0.18	0.24	0.17	**0.13**
Min	0.09	0.12	0.00	0.12	0.29
1st quartile	0.48	0.63	0.37	0.68	0.60
Median	0.67	0.73	0.55	0.78	0.65
3rd quartile	0.77	0.83	0.65	0.84	0.78
Max	0.959	0.992	0.970	0.959	0.910
Count	213	147	125	83	43

Table 5. Statistical analysis of R^2 in various non-parametric algorithms.

	ANN	**RF**	**SVR**	**GB**	**PLSR**	**K-NN**	**GPR**
Mean	0.65	0.76	0.71	0.57	0.75	0.74	**0.80**
STD	0.20	0.18	0.17	0.19	**0.15**	0.16	0.16
Min	0.01	0.31	0.10	0.36	0.14	0.40	0.29
1st quartile	0.51	0.67	0.62	0.42	0.67	0.68	0.71
Median	0.71	0.80	0.74	0.53	0.79	0.75	**0.88**
3rd quartile	0.81	0.92	0.85	0.69	0.85	0.77	0.93
Max	0.930	**0.998**	0.990	0.854	0.970	0.994	0.970
Count	88	111	105	9	**188**	19	42

Table 6. Statistical analysis of R^2 in various parametric algorithms.

	LR	**MLR**	**Power**	**Exponential**	**Logarithmic**	**Polynomial**
Mean	0.59	0.63	0.61	0.62	0.62	**0.63**
STD	0.25	0.20	**0.19**	0.20	0.23	0.25
Min	−0.07	0.02	0.01	0.00	0.03	0.00
1st quartile	0.43	0.51	0.52	0.57	0.44	0.52
Median	0.62	0.64	0.63	0.67	0.64	**0.69**
3rd quartile	0.79	0.79	0.76	0.76	0.81	0.80
Max	0.99	0.98	0.900	**0.99**	0.97	0.99
Count	**1363**	260	150	199	172	180

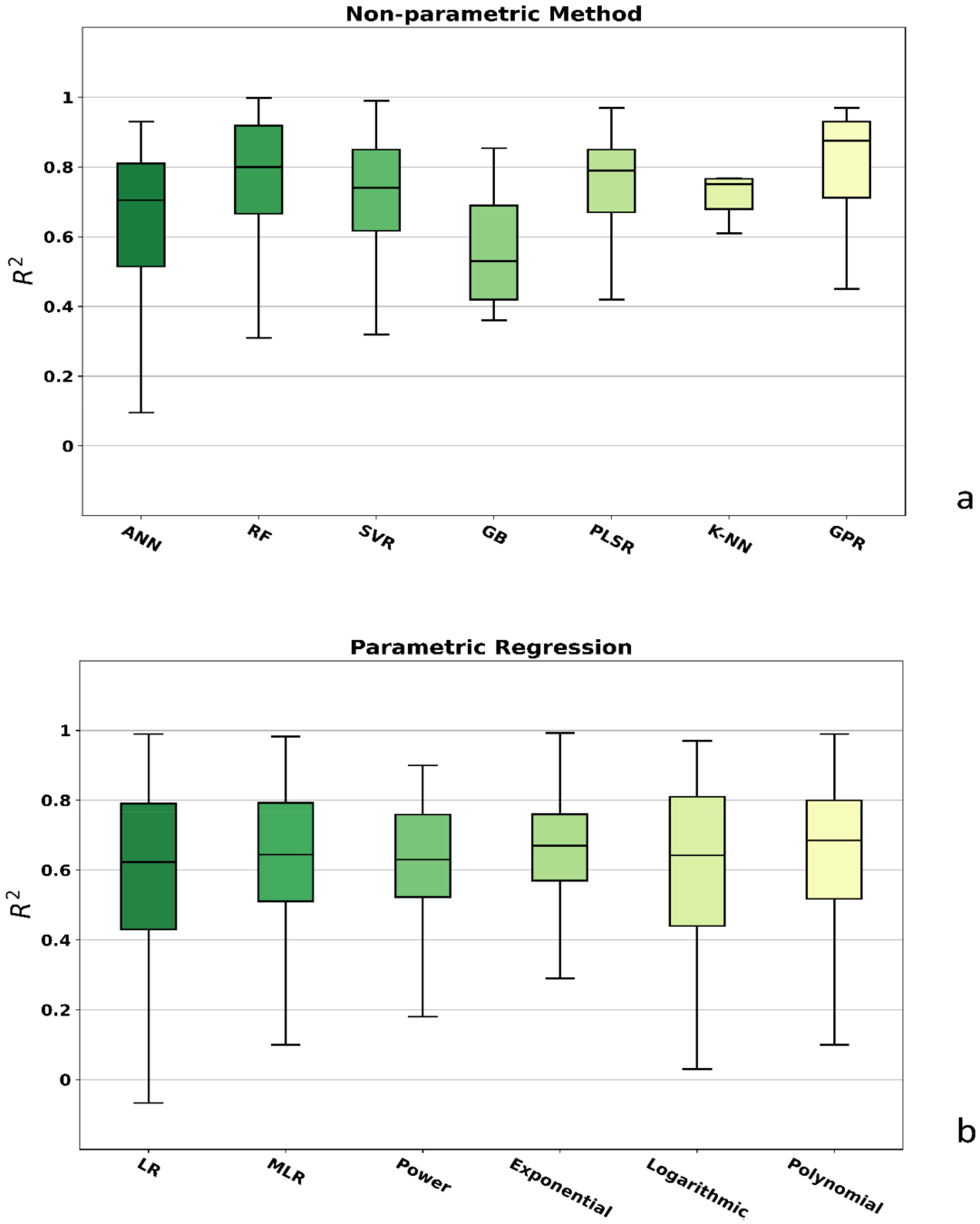

Figure 17. The coefficient of determination of (**a**) non-parametric algorithms and (**b**) parametric regression models. LR: Linear Regression; MLR: Multiple Linear Regression; GPR: Gaussian Process Regression.

As with the analysis of methods, the accuracy of retrievals for most biophysical models also had high variance; albeit, high median accuracies were reported when all studies were considered (Figure 18). LAI and fAPAR had high median correlations, and VWC and fAPAR had lower standard deviation among studies relative to other biophysical parameters; however, the amount of data in the analysis by the papers for fAPAR and VWC is significantly lower than the other crop parameters (Table 7). Among the three biophysical parameters that received the greatest attention (i.e., LAI, dry and wet biomass), LAI has the highest mean and median (0.67 and 0.7, respectively).

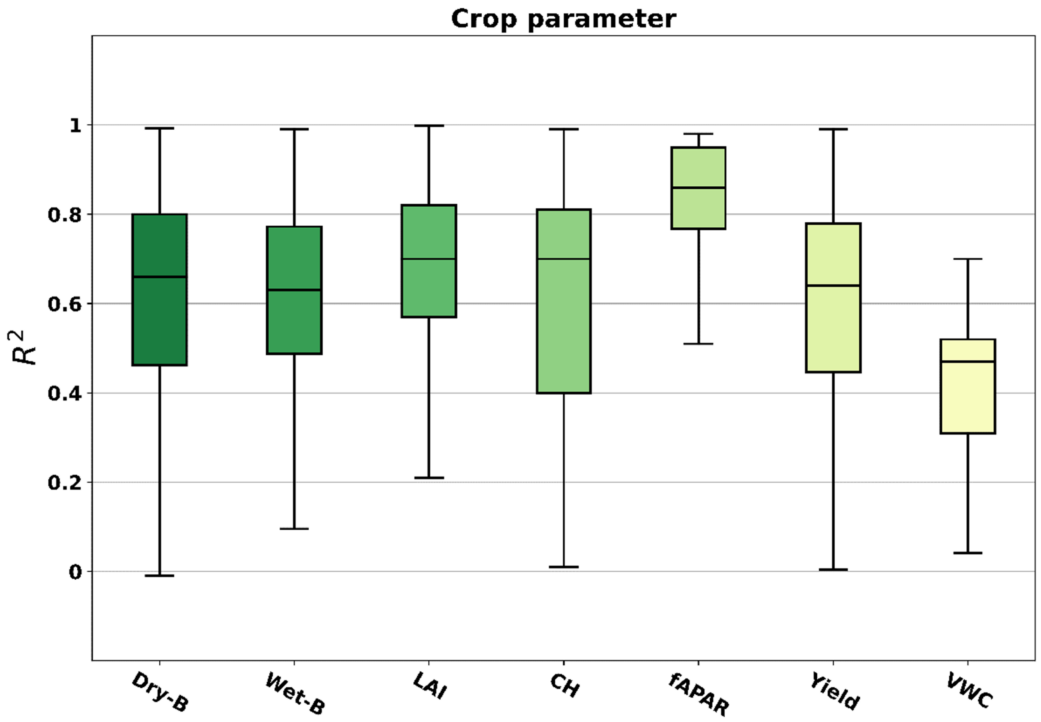

Figure 18. The coefficient of determination (R^2) of crop parameter estimation of screened studies (Dry-B: dry biomass; Wet-B: wet biomass; CH: crop height; VWC: vegetation water content).

Table 7. Statistical analysis of R^2 in various crop biophysical parameters.

	Dry-B	Wet-B	LAI	Height	fAPAR	Yield	VWC
Mean	0.62	0.62	0.67	0.61	**0.82**	0.59	0.42
STD	0.23	0.22	0.20	0.27	**0.18**	0.24	**0.18**
Min	−0.07	0.01	0.00	0.01	0.15	0.00	0.04
1st quartile	0.46	0.49	0.57	0.40	0.77	0.45	0.31
Median	0.66	0.63	0.70	0.70	**0.86**	0.64	0.47
3rd quartile	0.80	0.77	0.82	0.81	0.95	0.78	0.52
Max	0.993	0.990	**0.998**	0.990	0.980	0.990	0.837
Count	**1240**	288	1116	165	60	284	47

In Figure 19, accuracy results are broken down by platform and sensor. Among various platforms, spaceborne remote sensing data have higher accuracy (Figure 19). However, spaceborne data coupled with airborne have a higher mean and median, although this combination has a lower standard deviation in the reported coefficient of determination (Table 8).

Table 8. Statistical analysis of R^2 in various platforms.

	SB	AB	G-B	SB + AB	SB + G-B
Mean	0.64	0.63	0.61	**0.71**	0.65
STD	0.22	0.23	0.25	0.21	**0.16**
Min	−0.07	0.00	0.00	0.08	0.02
1st quartile	0.50	0.50	0.46	0.64	0.56
Median	0.67	0.68	0.67	**0.75**	0.63
3rd quartile	0.81	0.80	0.80	0.85	0.75
Max	**0.998**	0.990	0.990	0.960	0.990
Count	**1802**	633	562	104	95

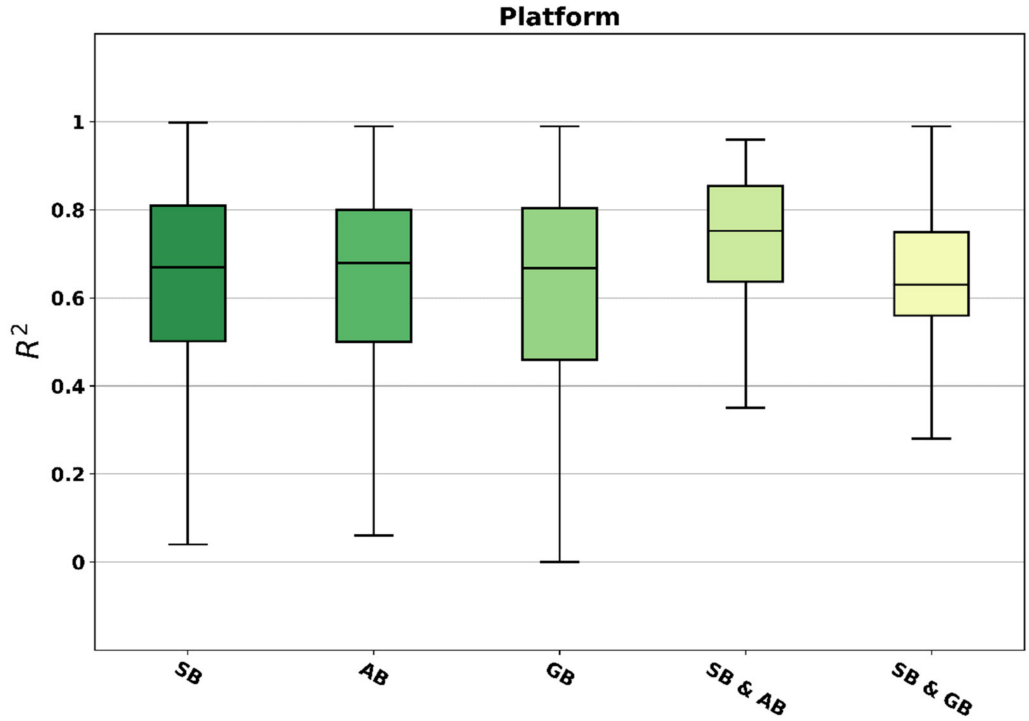

Figure 19. Various platforms' coefficient of determination (R^2) (SB: spaceborne; AB: airborne; GB: ground-based sensors).

Among various sensors, an examination of the mean results showed that the combination of multispectral and SAR data provided better accuracy for crop biophysical parameter estimation compared to the exclusive use of either optical or SAR data (Figure 20). However, the median of point-cloud data was higher than the other data types. Nevertheless, the amount of data in the analysis used by the papers for point-cloud sensors was less than the others. The publications that modeled biophysical parameters from SAR data reported slightly higher accuracies than those that used multispectral data (0.72 compared to 0.66) (Table 9). Nevertheless, several studies have shown that optical spectral bands or VIs obtained better accuracy than only using SAR backscatter and polarimetric features. Some papers examined a large number of VIs individually for estimation of plant parameters. However, some of VIs might produce poor results, impacting the overall mean and median results reported in our research. In addition, the combination of SAR and multispectral data can provide better accuracies than multispectral data alone. This is evident from the size of the boxes (i.e., values from first to third quartiles) in the boxplots for the combination of SAR and multispectral, compared to boxes of only SAR or only optical data.

Table 9. Statistical analysis of R2 in various sensors.

	M-S	SAR	M-S + SAR	P-C	H-S
Mean	0.62	0.66	0.70	**0.71**	0.65
STD	0.23	0.22	0.18	**0.15**	0.24
Min	−0.07	0.00	0.10	0.35	0.00
1st quartile	0.49	0.53	0.60	0.62	0.55
Median	0.66	0.72	0.68	**0.74**	0.69
3rd quartile	0.79	0.82	0.85	0.82	0.83
Max	**0.998**	0.990	0.990	0.950	0.980
Count	**2384**	456	126	116	214

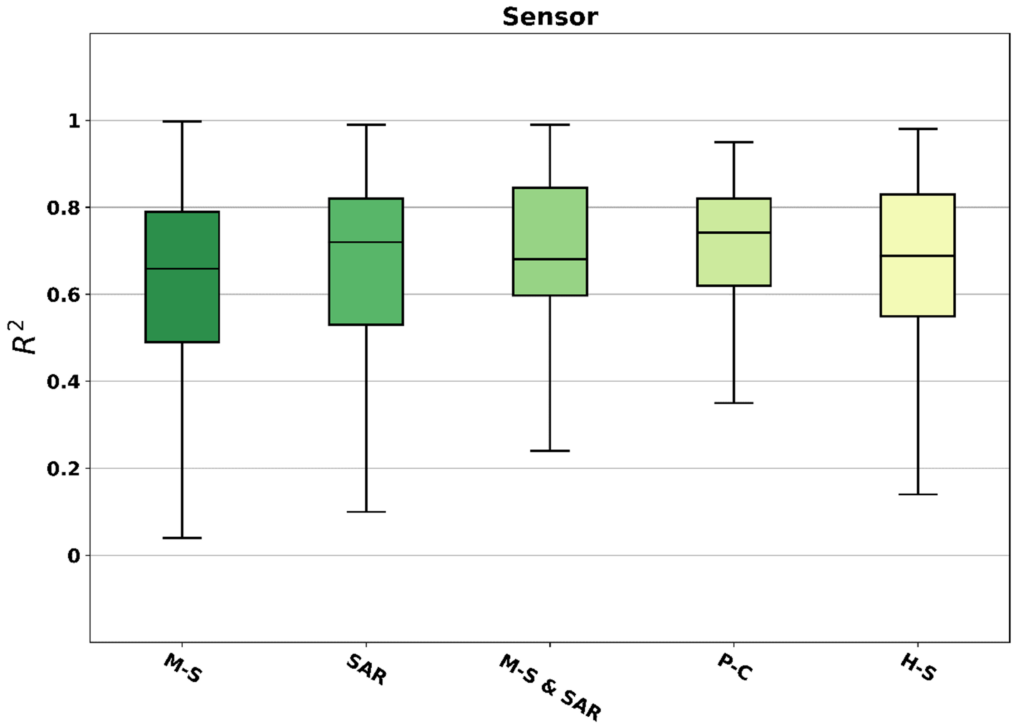

Figure 20. The coefficient of determination (R^2) of various sensors (M-S: multispectral; P-C: point-cloud; H-S: hyperspectral).

Figure 21 shows the potential of the various remote sensing sensors for crop parameter estimation. Research exploiting the multispectral RapidEye and WorldView satellites had the highest median accuracy of all optical sensors (Table 10). This may be a function of the red-edge band available from these sensors. RapidEye and WorldView also have a higher spatial resolution than other satellite systems, contributing to higher accuracy for studies using these satellites. MODIS yielded relatively low accuracy compared to other optical sensors. This result could be due to this sensor's low spatial resolution and the absence of red-edge bands on MODIS.

Table 10. Statistical analysis of R^2 in various specific sensors.

	Sentinel-2	**Landsat**	**Sentinel-1**	**RADARSAT**	**UAV**	**RapidEye**	**MODIS**	**HJ**
Mean	0.65	0.62	0.58	0.66	0.62	0.81	0.55	0.60
STD	0.20	0.23	0.25	0.20	0.23	0.15	0.24	0.20
Min	0.01	−0.07	0.00	0.01	0.00	0.36	−0.07	0.01
1st quartile	0.55	0.49	0.42	0.53	0.49	0.73	0.39	0.49
Median	0.69	0.64	0.60	0.69	0.68	**0.86**	0.57	0.62
3rd quartile	0.80	0.79	0.77	0.81	0.79	0.91	0.71	0.74
Max	0.970	0.992	0.976	0.990	0.990	0.970	0.993	0.960
Count	503	445	122	252	**649**	54	240	132
	Worldview	**TerraSAR-X**	**G-S**	**TLS**	**LiDAR**	**SPOT**	**Hyperion**	**QuickBird**
Mean	0.71	**0.82**	0.61	0.70	0.75	0.66	0.63	0.63
STD	0.18	**0.11**	0.25	**0.11**	0.14	0.24	0.16	0.17
Min	0.31	0.66	0.00	0.47	0.35	0.10	0.02	0.19
1st quartile	0.58	0.74	0.49	0.64	0.73	0.51	0.55	0.56
Median	0.75	0.80	0.65	0.71	0.80	0.68	0.62	0.68
3rd quartile	0.86	0.92	0.80	0.74	0.83	0.87	0.69	0.73
Max	**0.998**	0.959	0.990	0.880	0.950	0.990	0.980	0.930
Count	143	12	623	12	73	165	77	72

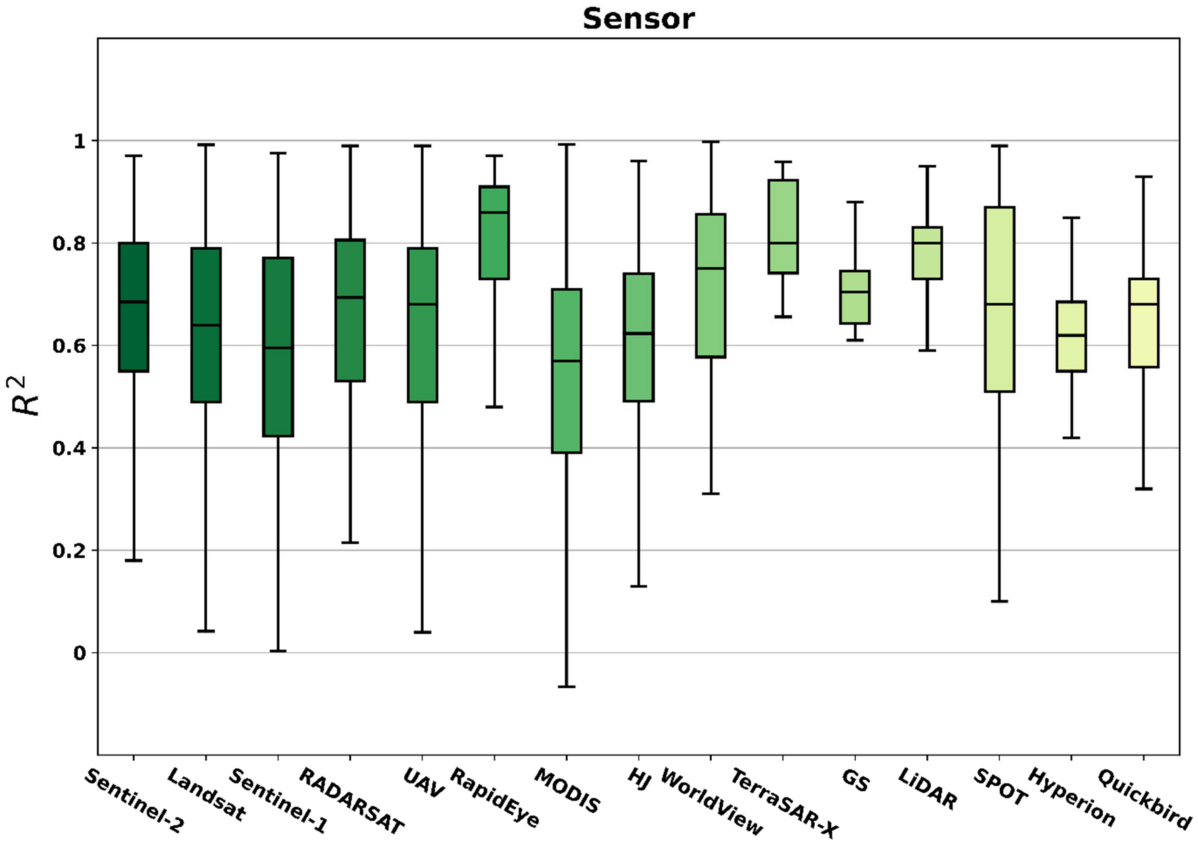

Figure 21. The coefficient of determination (R^2) of specific sensors.

TerraSAR-X showed significant potential in estimating crop biophysical parameters, perhaps a function of the higher spatial resolution associated with X-band sensors and the interaction of these shorter microwaves with the upper parts of the crop canopies. TerraSAR-X can acquire dual-polarized data with one co- and one cross-polarized channel (HH and HV; VV and VH). A number of studies reported that TerraSAR-X co-polarized backscatter was strongly correlated with crop parameters [20,121,122]. Although some penetration in canopies is required, it can be beneficial to use SAR wavelengths that interact within the canopy but do not penetrate farther and scatter from the soil. The number of studies that used TerraSAR-X is significantly lower than RADARSAT and Sentinel-1 data. As shown in Table 10, research that exploited RADARSAT yielded higher accuracies (mean and median) when compared to studies that used data from Sentinel-1. Several studies have shown the potential of fully polarimetric SAR data in estimating crop parameters [41,123,124] and the lack of a polarimetric capability on Sentinel-1 may explain the difference in results using these two C-band satellites.

4. Discussion

This metadata analysis assessed research papers investigating various remote sensing technologies and methodologies to estimate different biophysical parameters for various crop types. The primary goal of these researchers was to discover and report on optimum data and the most accurate algorithms for crop parameter determination.

4.1. Earth Observation Platform

Earth observation systems provide essential information spanning a multitude of disciplines. In agriculture, remote sensing research is consequential in applications to optimize production and minimize environmental footprints, such as precision agriculture and larger-scale initiatives to mitigate food insecurity. The technology has changed substantially in the years under investigation in this metadata analysis, and the number of satellites has

increased considerably. Moreover, open data policies have driven innovation and provided more opportunities and data for the scientific community. Other technological advancements have accelerated research into collecting and analyzing data from sensors on drones and UAVs. Sensor capabilities have also advanced, including improvements in spatial resolutions but also the ability of sensors to acquire more complex data. This leap in sensor innovation is particularly evident with SARs, where single-polarization sensors have been superseded by SARs that collect complex polarimetric data. The legacy of remote sensing for crop monitoring is multispectral moderate-resolution satellites/instruments, such as Landsat, NOAA AVHRR, and MODIS. Optical imagery is also more intuitive for users than other sensors. Access to optical sensors dates back to the 1970s. Analysis of optical data is more straightforward than SAR imagery since these data require less complicated processing and more analytical software packages are available [125]. This access has resulted in greater use of optical imagery relative to SAR and LiDAR. However, with increasing accessibility to SAR imagery, this technology is making inroads in agricultural monitoring. As this analysis of the literature has discovered, substantial research has been conducted using space-borne platforms [18,61,89,121,126–128], airborne platforms [129–134], and ground-based [135–138] platforms to estimate crop parameters and yields. However, ground-based and airborne platforms are not conducive to monitoring crop parameters at large spatial scales [19].

Yu et al. [139] investigated the potential of three spaceborne satellites, including Landsat 7/8 and Sentinel-2, to estimate corn LAI using PROSAIL and a look-up table. They utilized three VIs for Landsat and Sentinel-2 data, including NDVI, EVI2, and green chlorophyll index (CIgreen), and one VI for Sentinel-2 data (red-edge chlorophyll index). Moreover, they used four spectral bands for extracting the VIs mentioned above. Their results showed that the green band of Sentinel-2 performed better among all the spectral bands they utilized in their study. They also stated that, compared to the three red-edge spectral bands, the green band performed better. These researchers pointed out that CIgreen yielded better accuracy than other VIs extracted from Sentinel-2 data. Results showed that the combination of CIgreen extracted from Landsat 7/8 data and the three red-edge bands of Sentinel-2 were optimal for inversion methods. They also stated that the red-edge bands of Sentinel-2 were more accurate (RMSE = 0.64) than the Landsat 7/8 VI (RMSE = 0.72).

Estévez et al. [140] studied the potential of spaceborne Sentinel-2 level-1C and level-2A data to estimate the LAI of several crops. They studied several models, including PROSAIL, a look-up table, GPR, and variational heteroscedastic GPR. They stated that by using level-1C and level-2A and variational heteroscedastic GPR, a high R^2 could be obtained (R^2 = 0.80), but the RMSE of level-1C data is slightly lower than that of level-2A (i.e., 0.57 vs. 0.60).

Other technological advancements have accelerated research into collecting and analyzing data from sensors on drones and UAVs. Sensor capabilities have also advanced, including improvements in spatial resolutions but also the ability of sensors to acquire more complex data. Darvishzadeh et al. [141] utilized the PROSAIL RTM model, a look-up table for inversion, and PLSR to estimate grassland LAI using hyperspectral airborne sensors. They stated whether using all spectral bands or a subset of spectral bands by PLSR yielded the same R^2 (R^2 = 0.87); however, the RMSE of a subset of spectral bands was lower (RMSE = 0.64 compared to 0.68). These researchers stated that the optimum spectral bands for grassland LAI retrieval include bands in the NIR and SWIR regions. In this same study, a feature selection was applied to the hyperspectral data. Finally, a total of 107 bands were selected and used for the modeling.

Nie et al. [73] assessed the potential of airborne LiDAR data to estimate corn LAI, utilizing the Beer-Lambert law and LR in their study. Various sample radii were considered to determine which radius delivered higher accuracy. These researchers declared that using a radius of 3.5 m for samples using the Beer-Lambert law had higher accuracy (R^2 = 0.85). Zhang et al. [32] utilized a UAV RGB sensor to estimate grassland biomass and height. The

results revealed that using LR, grassland height could be estimated with R^2 of 0.90, while dry biomass could be retrieved using a logarithmic regression model with R^2 of 0.89.

Ground-based sensors, such as scatterometers and spectrometers, have shown promise in estimating crop parameters. Singh [142] investigated the potential of a ground-based scatterometer operating at X-band, with VV and HH polarizations, to estimate LAI, dry biomass, and height of soybeans. This research utilized the WCM to compute the backscattering coefficient and MLR and PLSR at various incident angles. Their results showed that, given the parametric regression results, dry biomass could be retrieved with higher accuracy (R^2) than LAI and crop height. Moreover, the VV polarization showed a better ability to estimate crop parameters than the HH polarization. For dry soybean biomass and crop height estimation, a 40° incident angle and VV and HH polarizations yielded the best accuracy (R^2 of 0.98 for the VV polarization and 0.96 for the HH polarization). For LAI, using the HH polarization, as reported for dry biomass and plant height, an incident angle of 40° delivered the best results; however, using VV polarization, a slightly shallower angle of 50° delivered better accuracy. Shen et al. [143] assessed the potential of several VIs to estimate the dry biomass of five grasslands using LR and MLR models. They extracted VIs from a hyperspectral ground-based spectrometer. Their results revealed that NDVI, SAVI, and EVI showed significant potential in retrieving dry biomass.

Xing et al. [144] gathered data from a hyperspectral ground sensor and data from the Sentinel-2 satellite to estimate wheat LAI using parametric linear and nonlinear regression models. They utilized 14 VIs and proposed a new VI (the transformed triangular vegetation index (TTVI)). The results from the ground sensor data showed that TTVI, MTVI2, and EVI were ranked one to three in performance, with R^2 of 0.62, 0.60, and 0.60, respectively. In addition, their results revealed that using Sentinel-2 VIs, TTVI, EVI, and TVI were ranked one to three in accuracy among all VIs with R^2 of 0.59, 0.55, and 0.52, respectively. Overall, the results obtained by the ground-based sensing TTVI, for LAI less than 4, achieved an R^2 of 0.78.

In another study, Afrasiabian et al. [145] investigated the effect of spatial, temporal, and spectral resolution on wheat and barley LAI retrieval. To this end, they used various spaceborne sensors (i.e., Sentinel-2, Landsat 8, and MODIS) and a hyperspectral ground-based sensor. Their results revealed that spatial and temporal resolution did not have any remarkable effect on crop LAI estimation accuracy; however, they reported a significant correlation between several VIs and wheat and barley LAI. The best performance related to Landsat 8 derived VIs was the LSWI and NDWI with R^2 of 0.69 and 0.65. Similarly, for Sentinel-2 data, LSWI and NDWI yielded a higher accuracy (R^2 = 0.60 and 0.58, respectively). These researchers hypothesized that the improved performance of Landsat 8 VIs, compared to Sentinel-2 VIs, may be explained by the narrower NIR bandwidth of Landsat 8 spectral channels. They pointed out that the high temporal resolution of MODIS data did not significantly improve the LAI estimation. The highest accuracy yielded by the VIs reported in this study was related to the VI calculated from the normalized difference of the 1115 nm and 1135 nm spectra (R^2 = 0.85) collected by the hyperspectral ground sensor.

4.2. Remote Sensing Systems

One approach to categorizing sensors is to divide these technologies into passive and active instruments. Passive sensors measure the energy emitted from or reflected by the Earth at wavelengths selected across the electromagnetic spectrum. The received signal by the sensor is a function of many Earth and atmospheric parameters. Examples of space-based passive remote sensors commonly used in agriculture include Landsat, Sentinel-2, MODIS, and Worldview. In contrast, active sensors generate their waveforms and propagate this energy toward the target of interest. Active sensors then measure the energy's characteristics (intensity, phase) scattered and returned to the sensor. These sensors also range or locate the target's position using the time between transmitting and receiving propagated signals. LiDAR and SAR are two active remote sensing technologies.

4.2.1. Optical Earth Observations

Optical sensors have been widely used in crop mapping and monitoring. These sensors measure reflected energy from the vegetation. This energy varies according to plant and canopy properties and depends on leaf orientation, shadowing illumination angle, and background properties such as soil characteristics. These sensors gather data in the electromagnetic spectrum's visible, near-infrared, shortwave, and thermal infrared regions. In addition, spectral vegetation indices (VIs) are used to estimate many crop biophysical parameters. Figure 12 revealed that Sentinel-2, MODIS, and Landsat sensors/satellites are widely utilized in crop parameter estimation. Critically, Sentinel-2 (A and B) data are free and accessible, and the combination of these two satellites yields good temporal (5-day revisit at the equator with two satellites), spectral, and spatial (10–20 m in the visible and near-infrared bands) resolutions. The 10 m spatial resolution bands include B2 (490 nm), B3 (560 nm), B4 (665 nm), and B8 (842 nm), while 20 m spatial resolution bands are B5 (705 nm), B6 (740 nm), B7 (783 nm), B8a (865 nm), B11 (1610 nm), and B12 (2190 nm). Sentinel-2 also provides additional bands in the red-edge spectral region, effective in crop mapping and parameter estimation. MODIS is a passive sensor on board the Aqua (launched in 1999) and Terra (launched in 2002) satellites that obtains data in the visible and infrared spectral domains, including thermal infrared. MODIS has 36 bands; bands 1 and 2 have a 250 m resolution, bands 3 to 7 have a 500 m resolution, and bands 8 to 36 have a 1 km spatial resolution. Landsat is a joint mission program between NASA and the United States Geological Survey, gathering data from 1972 until today. The current active and orbiting satellites are Landsat 8 and Landsat 9. The first satellite of the program was launched on July 1972. The continuity of the Landsat program has ensured access to data to support the tracking of land-use and land cover change. The Landsat 8 and 9 operational land imager (OLI) and thermal infrared sensor (TIRS) have 11 spectral bands, consisting of visible, NIR, SWIR, and TIR. The spatial resolution for multispectral bands is 30 m, except for the panchromatic band, which is 15 m. The spatial resolution for the TIR bands is 100 m.

Jin et al. [146] utilized 14 VIs (e.g., NDVI, TCARI, and NDII) extracted from simulated Sentinel-2 optical data and LAI to estimate the biomass of corn. Their results showed that the three-band water index (TBWI) led to higher accuracy. Liao et al. [147] analyzed MODIS and Landsat 8 satellite data to extract phenology, dry biomass, and yield of corn and soybeans and reported an RMSE for corn and soybean yield of 146.33 g/m^2 and 82.86 g/m^2, respectively. Punalekar et al. [148] used Sentinel-2 satellite images and proximal hyperspectral data to estimate pasture LAI and biomass.

Within the peer-reviewed literature, high spatial resolution optical satellite data provided by sensors such as RapidEye and WorldView are exploited less in crop monitoring studies when compared to lower spatial resolution data (e.g., Sentinel-2 and Landsat). This is likely due to the higher cost associated with these commercial sensors. Nevertheless, studies that exploited these high spatial resolution data reported high accuracy. RapidEye consists of five identical satellites gathering data in five bands of blue, green, red, red-edge, and NIR. The ground sampling distance (GSD) at the nadir is 6.5 m. WorldView constellation satellites are a mission owned by DigitalGlobe. The first satellite, WorldView-1, was launched on September 2007 and gathered panchromatic data at a 0.5 m resolution. WorldView-2 added eight spectral bands to its panchromatic capability. This second-generation satellite collects imagery in the red, green, blue, red-edge, and NIR spectral regions, with a GSD at the nadir of about 1.8 m.

Reisi Gahrouei et al. [92] utilized multi-temporal RapidEye data to estimate the LAI and biomass of canola, soybeans, and corn. They extracted 11 VIs (e.g., GNDVI, SR, and EVI) to assess the potential of optical data in predicting crop biophysical parameters. Their model delivered an RMSE of 0.59 m^2/m^2 for canola LAI, 0.27 m^2/m^2 for corn LAI, and 0.21 m^2/m^2 for soybean LAI. In the study by Bahrami et al. [40], using the same satellite and ground dataset as Reisi Gahrouei et al., the random forest feature importance showed that the red-edge VIs had higher significance than the conventional VIs, such as NDVI. Maimaitijiang et al. [149] analyzed several spectral bands and VIs extracted from

WorldView-2/3 and UAV RGB images to estimate soybean dry biomass and LAI. They also used the digital elevation model (DEM) and digital surface model (DSM) extracted from the UAV points cloud to estimate crop height. Their results showed that UAV crop height measurements were strongly correlated with crop height ground measurements (R^2 = 0.90). In addition to crop height measured by the UAV sensor, they calculated crop canopy cover using RGB UAV images. Lu and He [150] used Sentinel-1, WorldView-2, and DEM data to estimate vegetation LAI. Their results showed that optical WorldView-2 data delivered the best accuracy with an R^2 of 0.630 and RMSE of 0.701. Wei et al. [151] used four high-resolution satellite datasets, including Pleiades-1A, WorldView-2 and -3, and Spot6, to estimate winter oilseed rape LAI through an integrated model (combination of radiative transfer model and RF and K-NN as inversion model). These researchers used RF to select the best features and calculated accuracy date by date (separately), achieving a high accuracy (R^2 of 0.998) using the five top features. Kross et al. [54] investigated RapidEye data to estimate crop LAI and biomass, focusing on red-edge VIs and parametric regression models. Their results showed that the simple ratio red-edge delivered an R^2 of 0.97 for corn. However, the red-edge VIs did not significantly improve biomass and LAI estimation compared to conventional VIs. Campos-Taberner et al. [152] achieved an R^2 of 0.97 for a study area in Spain using Sentinel-2 spectral bands. In this study, inversion of the radiative transfer model using GPR was applied to estimate rice LAI. Yue et al. [37] utilized spectral bands and VIs extracted from a hyperspectral sensor and RGB camera mounted on a UAV to estimate winter wheat dry biomass and LAI. Combining crop height and VIs did not improve estimation accuracy compared to using spectral bands alone. However, these researchers stated that multiplying crop height and VIs could improve the estimation accuracy. In a study by Sibanda et al. [153], red-edge and infrared bands were the most effective in estimating grassland dry biomass using simulated Sentinel-2 data. Moreover, they stated that using hyperspectral infrared imaging (HyspIRI), the red-edge and middle infrared bands were the most efficient bands. They also declared that using VIs extracted from Sentinel-2 and HyspIRI significantly improved the estimation accuracy.

4.2.2. SAR Earth Observations

SAR sensors have shown potential in retrieving crop biophysical parameters. Unlike optical sensors, SAR sensors can gather data in cloudy weather conditions as these longer microwaves are, by and large, unaffected by atmospheric conditions. Microwave scattering is sensitive to the larger-scale physical characteristics of vegetation but also depends on sensor configurations (microwave wavelength, polarization of transmitted and received wave, and incident propagation angle). Although various studies have examined single- or dual-polarization SAR data, their analytical power is significantly less than when fully polarimetric data are used [154,155]. Fully polarimetric SARs transmit and receive two orthogonal polarizations that provide valuable observations about the target. With intensity and phase to exploit, these data can be used to synthesize a range of polarimetric features and to determine scattering mechanisms. Polarimetric decompositions have been used to determine the target's physical characteristics [156,157]. Standard decompositions exploited in the literature include Cloude–Pottier [158], Freeman–Durden [159], and Yamaguchi [160]. In two studies by [7,41], these decomposition methods were used to estimate crop biophysical parameters.

SAR data from sensors operating at X-band, C-band, and L-band have been used in crop monitoring and mapping research. However, as evident in Figure 11, C-band data dominate research in this field, followed by X-band and L-band. Access to C-band satellite data dates back to the early 1990s, and in 2014 the Sentinel-1A satellite began acquiring standard coverages and releasing these C-band data as open access. The Sentinel-1 A and B constellation provided multitemporal coverage (6-day revisit with two satellites). The future generation of these satellites (Sentinel C and D) will provide longer-term data continuity. The Canadian C-band RADARSAT-2 satellite has fueled agricultural research, considering that since 2007 this satellite has provided the capacity to acquire fully po-

larimetric space-based data [161]. Given the diversity of data synthesized from a fully polarimetric mode, these data have attracted considerable attention from the scientific community. However, the current engineering challenge with a fully polarimetric mode is the limited swath width at which these data can be acquired.

Generally, satellite and UAV images, specifically Sentinel-1 satellite data, showed great potential in retrieving rice crop parameters, such as dry biomass, LAI, and crop height, using parametric and non-parametric algorithms [128,162–164]. Mansaray et al. [165] utilized combinations of Sentinel-1 C- VV and C-VH data to estimate the dry biomass of rice, ultimately achieving an R^2 of 0.73 and RMSE of 462.4 g/m^2. Using these polarizations from Sentinel-1, Mandal et al. [93] predicted wet biomass and plant area index (PAI) for wheat, canola, and soybeans. Using the WCM, the correlation between observed and estimated C-VV backscatter was high for wheat and canola. For soybeans, the correlation was higher using the VH polarization. Estimates of wheat PAI were poorer during the early tillering stages, likely because of the contribution of soil in radar backscatter. An underestimation occurred at a PAI greater than 5 m^2m^{-2} because of the saturation of the C-band signal at high biomass.

Hosseini and McNairn [88] tested both space-based C-band (RADARSAT-2) and airborne L-band (UAVSAR) SAR to estimate the biomass of spring wheat. Their results showed that with C-VV and C-VH data, wheat biomass could be estimated with an RMSE of 78.834 g/m^2. In addition, their results showed that RADARSAT-2 HH-HV and VV-HV are the best polarizations to retrieve wheat total biomass and head biomass, respectively (R = 0.83 for total biomass and R = 0.70 for the biomass of heads of wheat). The highest error using RADARSAT-2 data was reported when retrieving biomass in the fruit/ripening stage. Errors were higher when retrieving biomass using UAVSAR L-band data. Expanding the research to corn and soybeans, Hosseini et al. [87] used RADARSAT-2 C-band and UAVSAR L-band data to estimate LAI for these two crops. Their results showed that RADARSAT-2 HH-HV and VV-HV provided reasonable estimates of corn LAI (R = 0.83 and 0.81, respectively). At C-band, RADARSAT-2 outperformed UAVSAR-L-band data for estimating corn LAI. High correlations between observed and estimated LAI for soybeans were also reported from RADARSAT-2 data, with poor results found with the UAVSAR-L-band data.

Although C-band SAR studies have dominated, data from X-band sensors have also been studied. Although shorter X-band microwaves have lower penetration into vegetation canopies [156], these sensors provide higher-resolution data. Ahmadian et al. [121] used TerraSAR-X dual-polarization data to estimate the wet and dry biomass of wheat, barley, and canola. Results for wheat showed that X-HH had better accuracy than X-VV. Inoue et al. [66] utilized five SAR wavelengths (C, L, Ka, Ku, X) to estimate rice biomass and LAI. Their results revealed that C-band HH and HV intensities are well-correlated with rice LAI, while L-band HH and the cross-polarization are well-correlated with wet biomass. Ott et al. [166] illustrated that L-band was sensitive to biomass and VWC, while Reisi-Gahrouei et al. [7] analyzed airborne L-band polarimetric data to estimate the biomass of canola, corn, and soybeans. Canisius and Fernandes [38] assessed the potential of the Advanced Land Observing Satellite (ALOS) phased array synthetic aperture radar (PALSAR) L-band data and ENVISAT C-band ASAR data to estimate the LAI of corn, soybean, and pasture. ASAR did not have a polarimetric mode and therefore they could not compare the performance of L-band and C-band polarimetry. However, using HH and HV polarizations acquired at C- and L-band frequencies, Canisius and Fernandes [38] showed that both C-HH and C-HV delivered weak results for corn and soybean LAI. They stated that the C-band signal tended to saturate when the LAI reached a value between 2 and 3. In contrast to C-band, L-band produced promising results for corn and soybean LAI estimation (R^2 = 0.76 and 80 for HV and HH polarizations, respectively). They stated that their results showed no evidence of saturation of the L-band signal for the crops studied. In addition to the studies mentioned above, combining two or more bands may improve accuracy. According to Figure 11, the combination of L- and C-band was studied most often.

The angle at which the radar beam hits the Earth (incident angle) affects the characteristics of SAR scattering. The physics of wave propagation dictates that the intensity of scattering decreases as the incident angle increases; therefore, the same object has a different backscatter intensity in images obtained by various incident angles [167]. This angle also impacts how the wave interacts within, for example, a crop canopy. Steep (small) incident angles generally allow for greater penetration into the crop canopy and may lead to greater scattering contributions from the soil depending on the radar wavelength. Chakraborty et al. [168] illustrated that a shallower incident angle (>40°) led to improved mapping of rice crops using RADARSAT-1 C-band data. In studying winter wheat and barley, Ahmadian et al. [121] discovered that X-VV and X-HH backscatter (31° incident angle) increased from stem elongation to the start of the flowering period. Jiao et al. [169] reported that C-HV backscatter at both steep and shallow angles was well-correlated with corn and soybean LAI. Inoue et al. [66] used four incident angles (25°, 35°, 45°, and 55°) to estimate the LAI and biomass of rice. They discovered that L-band HH backscatter could accurately estimate biomass at all incident angles with R^2 between 0.95 to 0.99 (with the highest accuracy at 45°). Baghdadi et al. [20] studied data from TerraSAR-X, ENVISAT ASAR, and ALOS PALSAR acquired at various incident angles (from 18° to 53°). The larger incident angles and longer wavelengths delivered the best estimates of sugarcane height. In addition to the impact on backscatter intensity, the angle of wave propagation also impacts scattering characteristics.

4.2.3. Combination of Optical and SAR Images

The combination of SAR and multispectral images has shown potential in retrieving crop parameters. Yadav et al. [170] assessed the potential of Sentinel-1 and Sentinel-2 data in estimating wheat LAI. They compared the results of the original WCM and a modified version. Their results showed that using Sentinel-1 VV intensiy in the modified WCM was more sensitive to crop growth features and was strongly correlated with LAI (R^2 = 0.974). Results were better than those obtained with C-VV intensity using the original WCM or C-VH using either the modified WCM or original WCM. The LAI of wheat could be retrieved with the modified WCM and C-VV intensity, with high accuracy (R^2 = 0.901).

Jin et al. [171] utilized Huanjing (HJ) optical data and RADARSAT-2 SAR data to estimate wheat dry biomass and LAI. First, they assessed results using only optical or only SAR data and then evaluated performance when SAR and optical data were combined. They examined various VIs and SAR polarimetric decompositions using several parametric methods and PLSR. Among VIs extracted from the optical images, MTVI and EVI had better accuracy in estimating LAI and biomass, respectively. With respect to SAR features, RVI and double-bounce eigenvalue relative differences had higher accuracy in estimating LAI and biomass, respectively. Jin et al. [171] then multiplied six of the VIs with the two best radar features to produce a new series of combined features, then calcuated the accuracy of the parametric regression. Their results showed that this method could improve LAI and biomass retrievals (R^2 = 0.68 for LAI and 0.80 for biomass). When LR and PLSR were used to combine VIs and radar features, PLSR delivered the best estimates of LAI and biomass with R^2 of 0.83 and 0.90, respectively.

Baghdadi et al. [27] studied the potential of RADARSAT-2 and Landsat 7/8 data to estimate soil moisture and several crop parameters, including LAI and biomass. They utilized NN and considered six configurations for estimating the crop parameters under various conditions, such as the sole use of SAR or a combination of SAR and optical features. Moreover, they calculated several polarimetric decompositions, including Shannon entropy (SE) and the Pauli component. The C-band HH polarization was the most suitable for estimating grassland biophysical parameters. In addition, they stated that dual polarization or full polarimetric decomposition parameters did not improve vegetation parameter estimation nor soil moisture retrieval for grasslands.

Luo et al. [61] analyzed the potential of Sentinel-1/2 and Landsat 8 data for crop monitoring. They utilized spectral and texture features from optical and SAR data as inputs

to SVR and MLR models to estimate corn biomass and LAI. Their results showed that the texture features of both SAR and optical data could improve the accuracy of biomass and LAI estimation.

Koppe et al. [172] assessed the potential of hyperspectral (EO-1 Hyperion) and microwave (Envisat ASAR) satellite data to estimate wheat dry biomass. Their results showed that the exclusive use of hyperspectral data yielded better accuracy (R^2 = 0.83) than results from Envisat ASAR data (R^2 = 0.75). They also stated that the combination of EO-1 Hyperion and Envisat ASAR data resulted in the highest accuracy when compared to results when only microwave or hyperspectral data were used (R^2 = 0.9).

4.2.4. Laser-Based Sensors for Crop Parameters Estimation

In addition to optical and SAR sensors, laser-based sensors, such as airborne LiDAR and terrestrial laser scanner (TLS), can also be used to estimate crop height and biomass. Active laser technologies gather data in three dimensions. The 3D points collected by laser-based sensors provide longitude, latitude, and ellipsoidal height data. The ellipsoidal heights can then be converted to the elevation. Li et al. [141] used TLS to estimate rice aboveground biomass and the biomass of individual canopy components. They also modeled rice development throughout the growing season. Zhu et al. [131] analyzed multisource data from two multispectral cameras and a LiDAR sensor mounted on three UAVs to estimate aboveground corn biomass. High-precision crop height measurements can lead to more accurate corn biomass. They showed that using this precise data, R^2 of wet biomass increased by 0.01, 0.07, 0.19, and 0 (t/ha), and RMSE decreased by 0.02, 0.89, 1.65, and 0 (t/ha) for MLR, RF, ANN, and SVR, respectively. Zhu et al. [173] also exploited multispectral images and LiDAR data to estimate aboveground corn biomass and demonstrated that integrating these two data sources improved retrieval accuracy.

4.3. Analytical Methods

Over the last three decades, many methods have been developed to retrieve crop parameters and estimate yield from remote sensing data. As stated in the previous section, these methods can be divided into four main categories: (1) parametric regression methods, (2) non-parametric regression methods, (3) physically based models, and (4) empirical and semi-empirical models. Our results showed that using high-resolution optical data, almost all models, such as parametric and non-parametric regression models and physical, empirical, and semi-empirical models, yielded high accuracy for crop parameter estimation [37,132,141,164].

4.3.1. Parametric Regression Models

Parametric regression methods build a direct relationship between one dependent variable and one or more independent variables. Rueda-Ayala et al. [174] combined aerial and ground remote sensing data to estimate pasture biomass, plant volume, and plant height using simple linear regression (LR). Elsayed and Darwish [175] used LR to assess the potential of hyperspectral remote sensing data to predict corn VWC, dry and wet biomass, yield, canopy water mass (CWM), and grain yield (GY). Ahmadian et al. [121] used LR, Pow-R, and Exp-R to estimate LAI, wet and dry biomass, and VWC of wheat, barley, and canola. Acorsi et al. [130] used UAV data to estimate black oat height, dry biomass, and wet biomass using parametric regression models. These researchers divided data collection into three missions; the first mission was conducted at the booting stage, the second at the flowering stage, and the third at the grain-filling stage. Their results showed that the crop height of black oat could be retrieved with high accuracy during the first and second missions with R^2 of 0.86 and 0.92, respectively. The accuracy of retrievals during the third mission was poor. Wet and dry biomass, as with crop height, could be well estimated during booting and flowering stages (for dry biomass, R^2 = 0.81 and 0.92, and wet biomass, R^2 = 0.87 and 0.94, respectively); however, the results at the grain-filling stage were again, poor.

Using multiple parametric regression models, Eitel et al. [22] utilized TLSs and RapidEye images to predict dry wheat biomass, LAI, and crop height. Their results showed that crop heights extracted from the TLS were strongly correlated with in situ measurements with an R^2 of 0.87. Han et al. [17] investigated the potential of several parametric regression models, including power, exponential, linear, logarithmic, and quadratic regression models, to estimate the dry biomass of winter oilseed rape using several VIs extracted from four high-resolution satellite images (WorldView-2/3, SPOT-6, and Pleiades-1A). They used several VIs, including EVI, EVI2, RVI, NDVI, RDVI, OSAVI, SAVI, and MTVI2. Their results showed that power regression had a higher R^2 for all VIs (ranging from 0.71 to 0.77). The exponential regression model was the second best, with accuracies ranging from 0.66 to 0.76. Their results revealed that NDVI delivered higher accuracy using power regression compared to other VIs and parametric regression models. They stated that all VIs had a strong near-linear dependency to dry biomass at the seeding and stem elongation stages. Moreover, they observed that the samples were distributed away from the fitting line at the podding stage. Additionally, they reported that at the period of high biomass, NDVI tended to saturate to a greater extent than other VIs.

4.3.2. Non-Parametric Regression Models

Kernel-based machine learning algorithms have recently received significant attention because of their high generalization performance and ability to learn the nonlinear relationship between features and target parameters [114]. As shown in Table 5, although PLRS has a higher count number, it produces relatively higher accuracy than RF compared to the other non-parametric regression models. Sibanda et al. [153] used PLSR to estimate dry grassland biomass. They utilized leave-one-out cross-validation in their research to train the PLSR model. Their results revealed that using PLSR, dry grassland biomass could be efficiently estimated using simulated bands and VIs. Their results also showed that using spectral bands and VIs extracted from simulated Sentinel-2 data, grassland dry biomass could be estimated with high accuracy (R^2 ranging from 0.52 to 90 using raw spectral bands and from 0.51 to 0.97 using VIs). They also declared that using spectral bands and VIs simulated from the Hyperspectral Infrared Imager (HyspIRI), grassland dry biomass could be estimated with R^2 ranging from 0.65 to 90 for spectral bands and ranging from 0.70 to 0.97 for VIs.

Yue et al. [37] utilized two non-parametric regression models, i.e., RF and PLSR, and several parametric models to estimate wheat dry biomass and LAI. Their results revealed that parametric regression models did not provide good results for the three crop development stages. However, their results showed that using RF and PLSR regression, dry biomass and LAI could be accurately retrieved. Utilizing VIs extracted from a digital camera delivered better results than VIs extracted from a hyperspectral sensor mounted on a UAV. The results by RF models were better than PLSR. The R^2 for dry biomass and LAI using RF was 0.94 and 0.93 for digital camera VIs and 0.93 and 0.93 for hyperspectral VIs, respectively, while the R^2 for dry biomass and LAI using PLSR was 0.61 and 0.50 for the digital camera and 0.34 and 0.45 for hyperspectral, respectively. They also achieved a high accuracy by using all VIs and crop height. In this scenario, the R^2 was 0.96 and 0.77 for the digital camera and 0.94 and 0.64 for hyperspectral VIs for dry biomass using RF and PLSR, respectively.

Mansaray et al. [25] utilized data from three satellites, including Sentinel-2, Landsat 8, and the Chinese Huanjing (HJ-1 A and B), to estimate rice dry biomass using RF, SVR, k-NN, and gradient boosting decision tree (GB). They stated that EVI was highly correlated with crop biophysical parameters while being less susceptible to saturation at high biomass. GB delivered the best estimation of dry rice biomass before the heading period (R^2 = 0.82). Furthermore, K-NN led to the best results after the rice heading stage (R^2 = 0.43). Duan et al. [162] also assessed the potential of SVR to estimate rice LAI using a UAV dataset. In this study, the researchers calculated the simple correlation between several spectral bands, VIs, and VI-based Fourier spectra with rice LAI. Their results showed that compared to

the spectral bands, NDVI and EVI extracted from the UAV data were the most strongly correlated features with rice LAI. VI-based Fourier features, when input to the SVR model, delivered better accuracy than VIs.

Li et al. [164] utilized several parametric and non-parametric regression methods (LR, MLR, principal component regression (PCR), PLSR, RF, and SVR) to estimate rice LAI using combined optical indices and texture features. Kiala et al. [176] investigated the potential of PLSR and SVR to estimate grassland LAI using a ground hyperspectral field spectrometer. They stated that at the beginning and end of summer, PLSR outperformed SVR. They also observed that at the peak of the growing season (mid-summer), when saturation occurred, SVR performed better than PLSR. Moreover, they reported that for the whole dataset, SVR was slightly better than PLSR (R^2 = 0.74 for SVR and 0.73 for PLSR). PLSR and SVR yielded R^2 of 0.87 and 0.86 for the beginning of summer, 0.89 and 0.90 for the middle of summer, and 0.85 and 0.83 for end of summer, respectively.

Khan et al. [177] applied ANN to Landsat 8 optical data to estimate Mentha crop biomass yield over India. They extracted several VIs, including NDVI, GNDVI, and SAVI, and achieved an R^2 of 0.76. Zhu et al. [131] assessed four non-parametric machine learning algorithms, including RF, MLR, ANN, and SVR, to estimate corn biomass and height. Their results showed that the estimation accuracy of MLR was close to the results obtained by RF and SVR, indicating that non-parametric regression methods do not efficiently improve rice wet and dry biomass estimation. In addition, they expressed that ANN performed poorly in estimating corn biomass when compared to SVR and RF methods. High-spatial-resolution crop-height data was deemed a key parameter in estimating crop biomass. Khan et al. [177] utilized several non-parametric machine learning algorithms, including OLSR, RF, SVR, and extreme learning regression (ELR). Their results showed that combining data from satellite and UAV platforms delivered higher accuracy estimates of dry biomass and LAI, when evaluated against data collect using only UAV or only satellite images. Also, ELR and RF outperformed other machine learning algorithms in retrieving dry biomass (R^2 = 0.92 for ELR and 0.92 for RF). The LAI of soybeans could be accurately estimating by combining satellite and UAV data, with ELR delivering slightly better results relative to other models (R^2 = 0.93). This research showed that soybean parameters could be accurately estimated using high-spatial-resolution images and machine learning algorithms.

Recently, GPR has received considerable attention for retrieving crop and vegetation biophysical parameters [178]. GPR comprises a Bayesian framework to solve regression and probabilistic classification problems. As observed in Table 5 and Figure 17, GPR has the highest mean and median R^2 among non-parametric methods. This finding could be explained by the fact that GPR does not have numerous parameters, making this method a suitable choice to resolve overfitting and underfitting problems [179]. Yin et al. [180] utilized GPR coupled with gap-filling methods to produce aboveground grassland biomass. Several studies showed that GPR outperformed other ML algorithms [181,182]. Mao et al. [183] assessed the potential of five ML methods and Sentinel-2 spectral bands to estimate cotton LAI, including ANN, SVR, RF, GPR, and GB. Grid search cross-validation was implemented to find the best parameters for tuning the machine learning models. To avoid biased results caused by the random selection of training and testing samples, they conducted 20 repetitions of the machine learning algorithms using different training and testing sample sets. GB had the highest accuracy among various machine learning models (R^2 = 0.854 on average). Although GB outperformed other non-parametric machine learning algorithms, it was a less robust algorithm because of its wide distribution range of R^2 and RMSE. After GB, the best results were from ANN, SVR, RF, and GPR. Mao et al. [183] also found that SVR delivered good results (R^2 = 0.83 on average) and was the most robust model as evident in its narrower distribution of R^2 and RMSE. ANN delivered the best results when feature selection was conducted for the Sentinel-2 spectral bands (R^2 = 0.88 on average). After SVR, GPR was next most robust model for estimating the LAI of cotton, when considering the standard error of the models.

4.3.3. Physical-Based Models

Physical-based models have significant potential in crop characterization and are easily transferable to various crop types [184,185]. Generally, complex RTM models are more realistic but with many parameters, retrievals are challenging because of the complexity of the inversion task. The number of independent observations is typically less than the number of unknown parameters; for this reason, physically based models can be ill-posed. Several methods have been suggested to overcome this challenge, including look-up table and hybrid approaches to model inversion.

Physical-based models have been widely used to estimate LAI, dry and wet biomass, and other crop parameters [151,186]. Klingler et al. [187] utilized several methods based on RTM models. Their results showed that these methods had a lower error than direct green LAI (GLAI) measurements. Chen et al. [188] also utilized PROSAIL, as an RTM-based method, to generate simulated hyperspectral GF-5 reflectance data under various soil and vegetation conditions. They used Sentinel-2 multispectral and GF-5 hyperspectral data in their research. They applied three feature selection methods, including RF, mean impact value, and K-means clustering, and three regression methods, including RF, NN, and K-NN, to develop various scenarios. RF was the most efficient method. Chen et al. [188] also used nine spectral bands and five VIs, e.g., NDVI and four red-edge VIs, as input variables. Based on the feature selection results, blue, red, and red-edge bands were the best features. They stated that when using the spectral bands and 5 VIs without performing feature selection, RF obtained the highest accuracy and lowest error (i.e., R^2 = 0.83 and RMSE of 0.84). Although feature selection did not improve the model performance, they stated that by using RF feature selection, the most useful data was preserved.

In another study, Sun et al. [126] simulated the canopy spectral reflectance using the PROSAIL RTM model [122,123]. Their study used five VIs extracted from Sentinel-2 data, including NDVI, red-edge and green chlorophyll index, broad dynamic range vegetation index, and modified simple ratio. They concluded that the red-edge 2 and red-edge 3 bands were the most optimal. However, some saturation was observed at high LAI. Yuping et al. [189] regionalized and adjusted the WOFOST model in north China and combined it with LAI and the PROSAIL RTM model to simulate SAVI.

4.3.4. Empirical and Semi-Empirical Models

In addition to the above methods, several empirical and semi-empirical methods have been studied to retrieve crop descriptors [93]. The WCM is a well-known semi-empirical model widely used in agriculture. Hosseini et al. [89] assessed corn dry and wet biomass estimation using calibrated WCM and SAR data from RADARSAT-2. Moreover, they extracted four VIs from RapidEye optical data, including NDVI, red-edge simple ratio, SR, and the red-edge triangular vegetation index (RETVI). This approached achieved an R of 0.73 and 0.74 between estimated and observed backscatter for the dry biomass, respectively. However, the correlation for wet biomass was lower (0.73 and 0.61 for HH and HV polarizations, respectively). Their results also revealed that almost all VIs delivered an acceptable correlation with dry and wet biomass.

Ahmadian et al. [121] studied the impact of crop biomass on radar backscatter intensity using the WCM. Their results showed a strong correlation between X-band VV backscatter, and barley and canola dry biomass (R^2 = 0.87 for barley and 0.96 for canola). However, the HH polarization was more accurate in estimating dry wheat biomass. They also observed a high correlation between HH polarization and barley and canola wet biomass. Utilizing MLR for dry biomass, they achieved an accuracy (R^2) of 0.75 for wheat, 0.87 for barley, and 0.66 for canola. In addition, they reported accuracy (R^2) of 0.80 for wheat, 0.93 for barley, and 0.74 for canola dry biomass. Using MLR, the results revealed that the accuracy for dry biomass is higher than wet biomass. They also utilized RF and found better results than when applying MLR, in all cases. The correlations (R^2) were reported as 0.8 and 0.92 for wheat dry and wet biomass, 0.96 and 0.96 for barley dry and wet biomass, and 0.74 and 0.68 for canola dry and wet biomass.

Han et al. [190] applied the WCM and MLR to SAR and optical data from Sentinel-1 and Sentinel-2 satellites to estimate the water content of winter wheat. Their results showed that estimation of the water content from Sentinel-2 optical data delivered higher accuracy than when Sentinel-1 SAR data were used. Hosseini and McNairn [88] coupled the WCM and the Ulaby soil moisture model to estimate spring wheat biomass and surface soil moisture from RADARSAT-2 C-band and UAVSAR L-band data. Their results revealed that, for wheat biomass during development stage, a correlation coefficient of 0.70 was obtained for a validation dataset using RADARSAT data. However, the results for UAVSAR L-band were not as promising; the highest correlation coefficient was 0.47 for wheat biomass estimation.

4.4. Crop Characterization

Estimating crop biophysical parameters using remote sensing data depends on the model, the spatial and spectral resolution of the sensor, and landscape heterogeneity [191]. LAI, dry biomass, and wet biomass have been studied more extensively than other biophysical parameters. Biomass and LAI are primary crop growth parameters [146] and indicate general crop health and biochemical status [55,145,171,183,192–195]. Accurate estimation of aboveground biomass can be linked with the yield of some crops [196]. Mansaray et al. (2020a) stated that dry biomass is one of the most critical crop growth parameters for rice. Paris [197] illustrated that K-band HH and VV polarized backscatter could be used to retrieve the LAI of corn. Pandey et al. [198] found that scattering measured with a ground-based X-band radar correlated well with ladyfinger's biomass and LAI but was poorly correlated with plant height.

Ganeva and Roumenina [199] used SPOT VEGETATION and simulated PROBA-V data to estimate several crop descriptors, including fAPAR, wet biomass, and LAI. Their results showed that Exp-R models coupled with simulated PROBA-V data delivered R^2 of 0.90 and 0.93 for wet biomass and 0.91 and 0.93 for LAI. Wong and Fung [194] extracted several VIs from EO1-Hyperion data and texture features from ENVISAT ASAR imagery to estimate mangrove LAI. Radar texture had a low correlation with mangrove LAI. Their research investigated the potential of two parametric regression models, including LR and MLR. LR, triangular vegetation index (TVI), and NDVI delivered the highest and lowest R^2, respectively (R^2 = 0.69 for the TVI and 0.02 for the NDVI). Jigh accuracy could be reached using MLR and a combination of the modified chlorophyll absorption ratio index and angular second moment texture feature (R^2 = 0.79).

Xing et al. [200] coupled ENVISAT ASAR with Landsat 5 optical satellite imagery to estimate aboveground biomass over mixed vegetation. They utilized the modified WCM and a look-up table in their research. Dry biomass could be retrieved with an R^2 of 0.8 and RMSE of 0.28 kg/m^2. Campos-Taberner et al. [201] studied optical data from Landsat 7 and Landsat 8 and discovered that the LAI of rice could be estimated with an R^2 of 0.89. Reisi Gahrouei et al. [92] reported a high correlation between RapidEye VIs and corn, soybean, and canola biomass and LAI. These researchers examined SVR and ANN for modeling crop biomass and LAI. They extracted 11 VIs from RapidEye imagery, including NDVI, EVI, SAVI, red-edge NDVI, and red-edge SR. For dry biomass, the SVR model delivered higher accuracy for canola (R^2 = 0.93). Using both SVR and ANN models produced good accuracy for soybeans (R^2 = 0.89 and 0.83 for SVR and ANN, respectively). The results for all crops using ANN were poor compared to the SVR model. Estimating LAI using both SVR and ANN produced promising results for all crops. For canola, R^2 was reported as 0.94 and 0.84 for SVR and ANN models, respectively. For corn, R^2 was 0.93 and 0.88 for SVR and ANN, respectively; the R^2 for soybean was 0.98 and 0.9 using SVR and ANN, respectively. Reisi-Gahrouei et al. [7] evaluated ANN and MLR to estimate the dry biomass of three crops from SAR observations. Polarimetric SAR L-band data delivered high correlations when estimating the dry biomass of corn, canola, and soybeans. They stated that using MLR and a combination of HH and HV polarization intensities, an acceptable correlation could be reached for canola (R = 0.60). HH backscatter and entropy (H parameter from

Cloude-Pottier decomposition) polarimetric feature produced a higher accuracy and a lowest error for corn (R = 0.91 and RMSE = 211.01 g/m^2). For soybean, HH and entropy parameter produced the best correlation (R = 0.79). In ANN, VV backscatter and double scattering derived from Freeman–Durden decomposition delivered better result for canola (R = 0.72). In ANN, HH backscatter and entropy features produced the best accuracy (R = 0.92). Finally, the best correlation they reported for soybean using ANN was R = 0.82.

Yue et al. [37] highlighted a high correlation between VIs extracted from UAV-based cameras and LAI and biomass. In studying corn, Li et al. [50] reported that with LiDAR and GF-1 remote sensing data, LAI, height, and biomass could be estimated with an RMSE of 0.37 m^2/m^2, 0.17 m, and 0.49 kg/m^2, respectively. This was accomplished with a logarithmic regression and a multiplicative model. Paloscia et al. [202] reported a strong correlation between X-band data collected by Cosmo-SkyMed and crop VWC. Using LR, X-HH backscatter was sensitive to the VWC of sunflowers (R^2 of 0.76) and wheat (R^2 of 0.68). Lobell et al. [203] estimated the fraction of absorbed photosynthetically active radiation (fAPAR) from Landsat-5 and Landsat-8, then used the fAPAR in a light-use efficiency (LUE) model to predict the yield of wheat.

4.5. Challenges and Opportunities

Despite the notable advances in sensor technologies, challenges remain in applying remote sensing to map and monitor agricultural landscapes. Success is contingent upon technological advances in computing, algorithm development, and data policies.

1. As discovered in this literature review, integrating data from multiple data sources is advantageous. This is not limited to, for example, the advantages of SAR acquisitions during periods of cloud cover. In addition, it recognizes that multi-sensor approaches exploit differences in how canopies impact different spectral and microwave wavelengths. The integration of data across Sentinel platforms (Sentinel-1A/B and Sentinel-2A/B) has provided outstanding outcomes, and more research using multi-sensors is required. Landsat-9 (launched in 2021) and the NASA–Indian Space Research Organization (ISRO) SAR (NISAR) (soon to be launched) will be of interest for crop mapping and estimation of LAI, biomass and crop phenology. NISAR will have two L- and S-band sensors. This SAR satellite will acquire images consistently over the globe with an exact 12-day repeat. Following the lead of the Landsat and Sentinel programs, NISAR data will be free and open. Operating as a virtual constellation, the revisit time for Landsat-8 and Landsat-9 is eight days, narrowing the temporal gap and providing essential opportunities to map crop growth. More research on data fusion and assimilation algorithms is needed to develop solutions to fill temporal and spatial resolution gaps.
2. Calibration, either absolute (to a standard) or relative (platform to platform and consistency over time), is always challenging. Although calibration is always necessary, the demands are exceptionally high when remote sensing data model biophysical and biochemical crop parameters. Furthermore, inter-sensor calibration is particularly important considering recent trends in constellations of satellites.
3. Many studies have developed relationships between reflectance and/or backscatter crop by crop. Implementing these crop-specific models would be complex for large-scale monitoring (nationally, for example), and a universal model may be required. The robustness of models developed for limited geographies and temporal periods must be evaluated if the goal is to adopt these methods for monitoring operations. The pooling of data and resources over multiple sites and research teams could provide a partial solution.
4. In the optical domain, many satellite sensors are limited to imaging in the near-infrared and visible spectral regions. They thus do not capture significant absorption and reflectance features in the more extended shortwave-infrared region [204]. Moreover, one of the main problems of remote sensing sensors operating in visible, near-infrared, and shortwave infrared is their sensitivity to atmospheric and weather conditions,

particularly to cloud cover. This challenge leads to inconsistency in data collections and data loss in vital months of the growing season.

5. The trend toward more free and open data policies is still mostly limited to publicly owned and operated satellites. It has led to substantial increases in the volume of data in remote sensing archives. The Sentinel and Landsat archives are two good examples. As well, accessibility to these large datasets through open-source data computing platforms, such as Google Earth Engine and Amazon Cloud Computing, is also improving [205]. This extensive archive of available data, coupled with access to computing platforms and open-source image processing tools, will continue to advance the use of remote sensing for monitoring agricultural landscapes.
6. Researchers can develop more complex machine learning modeling approaches as computing capacity increases. This review demonstrated that advanced machine learning and deep learning improve model outcomes. Nevertheless, continued advancement to create robust models over space and time will rely on big data's ongoing availability and sharing.
7. Several companies have announced plans to launch diverse satellite constellations into Earth's orbit, in the coming years. One target application of these constellations is precision agriculture. Many of these constellations will provide data at high spatial resolutions. As discovered in our meta-review research, sensors which provide higher-resolution data tend to deliver more accuracy estimates of crop biophysical parameters, when compared to medium- and low-resolution sensors.

5. Conclusions

This research provides a meta-analysis of 277 papers published in the last three decades which focused on retrieving crop biophysical parameters from remote sensing data. This study gathered publications in crop parameter estimation and provided a statistical analysis of trends in this field of research. The outcomes of this meta-analysis can be summarized as follows:

- China (75), Canada (37), and the USA (34) were the countries where most studies were conducted. The ground data provided by SMAPVEX12 and SMAPVEX16 experiments over Canada fueled many studies because of the open-access policy of the SMAPVEX team.
- The largest number of publications occurred in 2019. The COVID-19 pandemic may have diminished publications in 2020 because of a limited ability to travel to study sites. Most papers were published in the Remote Sensing (44) and Remote Sensing of Environment (RSE) (29) journals.
- The number of studies that utilized remote sensing data has steadily increased from 2009 up to now. The availability of free remote sensing data, such as Landsat, and the launching of satellites such as RapidEye, WorldView1/2, and RADARSAT-2, likely contributed to this increase.
- Wheat and corn were the most studied crops, reflecting the importance of these two crops to global acreages and food supply. In addition, biophysical parameters for rice have been retrieved with higher mean and median accuracies when compared to other crops.
- Significant variances were observed in the retrieval of crop parameters associated with almost all crops. These variances may be related to the variety of remote sensing sensors and methodologies exploited by researchers.
- Among the three crop biophysical parameters studied the most (i.e., LAI, dry and wet biomass), LAI was estimated with higher accuracy. The results showed that coupling spaceborne remote sensing data with airborne data led to improved accuracy. Moreover, the results revealed that combining multispectral and SAR sensors provided higher accuracy for crop biophysical parameter estimation when compared to retrievals based solely on SAR or optical sensors.

- Historical access to data from a wide range of optical sensors has led to significant use of VIs extracted from visible, NIR, and SWIR in agriculture monitoring.
- The NDVI has had a long history in agricultural monitoring and mapping, which is reflected in this meta-analysis. It is the most studied vegetation index for retrieving crop parameters, such as the leaf area index (LAI), dry biomass, and wet biomass.
- The most widely used platforms in agricultural studies were spaceborne, airborne, and ground-based platforms, respectively. Data from Sentinel-2 (51) has been most frequently exploited for this application. Despite the dominance of satellite observations, data acquired by UAVs (57) and ground-based platforms (45) were also frequently exploited. Finally, more research was conducted using optical sensors than SAR and LiDAR sensors.
- Because of the more limited availability of multi-frequency SAR data, a significant gap in multi-frequency analysis is observed. Most studies utilized single frequency data because of challenges in the availability of data at more than one SAR frequency. Several studies concluded that greater access to data gathered using multiple SAR frequencies would significantly benefit agricultural research and applications development.
- Based on our results, using a combination of satellite and airborne platforms delivered better accuracy.
- Generally, our assessments showed that high-resolution optical data delivered higher accuracy. TerraSAR-X, RapidEye, and WorldView provided better accuracy than other remote sensing satellite sensors.
- The results showed that linear regression was the most frequently used method to estimate crop biophysical parameters. Among parametric methods, exponential and polynomial regression methods showed great potential in crop parameter estimation. The results also revealed that from 2010, non-parametric methods were increasingly used to predict crop parameters and provided comparatively better accuracies. A comparison between non-parametric and parametric methods showed that the average accuracy of non-parametric algorithms is generally higher than parametric regression methods. The highest accuracy among non-parametric methods was reported using random forest (RF).

Author Contributions: Methodology: H.B., M.M., S.H. and H.M.; Software: H.B.; Validation: H.B., H.M., M.M. and S.H.; Formal analysis: H.B., H.M., M.M. and S.H.; Investigation: H.B., H.M., S.H. and M.M.; Writing—original draft preparation: H.B., H.M., S.H. and M.M.; Writing—review and editing: H.B., H.M., S.H. and M.M.; Visualization: H.B., M.M. and S.H.; Supervision: M.M. and S.H. All authors have read and agreed to the published version of the manuscript.

Funding: This research received no external funding.

Conflicts of Interest: The authors declare no conflict of interest.

References

1. Liu, C.-A.; Chen, Z.-X.; Yun, S.; Chen, J.-S.; Hasi, T.; Pan, H.-Z. Research advances of SAR remote sensing for agriculture applications: A review. *J. Integr. Agric.* **2019**, *18*, 506–525. [CrossRef]
2. Tao, H.; Feng, H.; Xu, L.; Miao, M.; Long, H.; Yue, J.; Li, Z.; Yang, G.; Yang, X.; Fan, L. Estimation of Crop Growth Parameters Using UAV-Based Hyperspectral Remote Sensing Data. *Sensors* **2020**, *20*, 1296. [CrossRef] [PubMed]
3. Akhavan, Z.; Hasanlou, M.; Hosseini, M.; McNairn, H. Decomposition-based soil moisture estimation using UAVSAR fully polarimetric images. *Agronomy* **2021**, *11*, 145. [CrossRef]
4. Jiao, X.; McNairn, H.; Shang, J.; Pattey, E.; Liu, J.; Champagne, C. The sensitivity of RADARSAT-2 polarimetric SAR data to corn and soybean leaf area index. *Can. J. Remote Sens.* **2011**, *37*, 69–81. [CrossRef]
5. Jin, X.; Kumar, L.; Li, Z.; Xu, X.; Yang, G.; Wang, J. Estimation of winter wheat biomass and yield by combining the aquacrop model and field hyperspectral data. *Remote Sens.* **2016**, *8*, 972. [CrossRef]
6. Battude, M.; Al Bitar, A.; Morin, D.; Cros, J.; Huc, M.; Sicre, C.M.; Le Dantec, V.; Demarez, V. Estimating maize biomass and yield over large areas using high spatial and temporal resolution Sentinel-2 like remote sensing data. *Remote Sens. Environ.* **2016**, *184*, 668–681. [CrossRef]

7. Reisi-Gahrouei, O.; Homayouni, S.; McNairn, H.; Hosseini, M.; Safari, A. Crop biomass estimation using multi regression analysis and neural networks from multitemporal L-band polarimetric synthetic aperture radar data. *Int. J. Remote Sens.* **2019**, *40*, 6822–6840. [CrossRef]
8. Mandal, D.; Rao, Y. SASYA: An integrated framework for crop biophysical parameter retrieval and within-season crop yield prediction with SAR remote sensing data. *Remote Sens. Appl. Soc. Environ.* **2020**, *20*, 100366. [CrossRef]
9. Dhillon, M.S.; Dahms, T.; Kuebert-Flock, C.; Borg, E.; Conrad, C.; Ullmann, T. Modelling Crop Biomass from Synthetic Remote Sensing Time Series: Example for the DEMMIN Test Site, Germany. *Remote Sens.* **2020**, *12*, 1819. [CrossRef]
10. Panday, U.S.; Pratihast, A.K.; Aryal, J.; Kayastha, R.B. A review on drone-based data solutions for cereal crops. *Drones* **2020**, *4*, 41. [CrossRef]
11. Zhang, Y.; Chipanshi, A.; Daneshfar, B.; Koiter, L.; Champagne, C.; Davidson, A.; Reichert, G.; Bédard, F. Effect of using crop specific masks on earth observation based crop yield forecasting across Canada. *Remote Sens. Appl. Soc. Environ.* **2019**, *13*, 121–137. [CrossRef]
12. Liu, J.; Huffman, T.; Qian, B.; Shang, J.; Li, Q.; Dong, T.; Davidson, A.; Jing, Q. Crop yield estimation in the Canadian Prairies using Terra/MODIS-derived crop metrics. *IEEE J. Sel. Top. Appl. Earth Obs. Remote Sens.* **2020**, *13*, 2685–2697. [CrossRef]
13. Wiseman, G.; McNairn, H.; Homayouni, S.; Shang, J. RADARSAT-2 polarimetric SAR response to crop biomass for agricultural production monitoring. *IEEE J. Sel. Top. Appl. Earth Obs. Remote Sens.* **2014**, *7*, 4461–4471. [CrossRef]
14. Hoogenboom, G. Contribution of agrometeorology to the simulation of crop production and its applications. *Agric. For. Meteorol.* **2000**, *103*, 137–157. [CrossRef]
15. Li, F.; Zeng, Y.; Luo, J.; Ma, R.; Wu, B. Modeling grassland aboveground biomass using a pure vegetation index. *Ecol. Indic.* **2016**, *62*, 279–288. [CrossRef]
16. Zheng, Y.; Zhang, M.; Zhang, X.; Zeng, H.; Wu, B. Mapping winter wheat biomass and yield using time series data blended from PROBA-V 100-and 300-m S1 products. *Remote Sens.* **2016**, *8*, 824. [CrossRef]
17. Han, J.; Wei, C.; Chen, Y.; Liu, W.; Song, P.; Zhang, D.; Wang, A.; Song, X.; Wang, X.; Huang, J. Mapping above-ground biomass of winter oilseed rape using high spatial resolution satellite data at parcel scale under waterlogging conditions. *Remote Sens.* **2017**, *9*, 238. [CrossRef]
18. Bao, N.; Li, W.; Gu, X.; Liu, Y. Biomass Estimation for Semiarid Vegetation and Mine Rehabilitation Using Worldview-3 and Sentinel-1 SAR Imagery. *Remote Sens.* **2019**, *11*, 2855. [CrossRef]
19. Alebele, Y.; Zhang, X.; Wang, W.; Yang, G.; Yao, X.; Zheng, H.; Zhu, Y.; Cao, W.; Cheng, T. Estimation of canopy biomass components in paddy rice from combined optical and sar data using multi-target gaussian regressor stacking. *Remote Sens.* **2020**, *12*, 2564. [CrossRef]
20. Baghdadi, N.; Boyer, N.; Todoroff, P.; El Hajj, M.; Bégué, A. Potential of SAR sensors TerraSAR-X, ASAR/ENVISAT and PALSAR/ALOS for monitoring sugarcane crops on Reunion Island. *Remote Sens. Environ.* **2009**, *113*, 1724–1738. [CrossRef]
21. Jiao, X.; Kovacs, J.M.; Shang, J.; McNairn, H.; Walters, D.; Ma, B.; Geng, X. Object-oriented crop mapping and monitoring using multi-temporal polarimetric RADARSAT-2 data. *ISPRS J. Photogramm. Remote Sens.* **2014**, *96*, 38–46. [CrossRef]
22. Eitel, J.U.; Magney, T.S.; Vierling, L.A.; Greaves, H.E.; Zheng, G. An automated method to quantify crop height and calibrate satellite-derived biomass using hypertemporal lidar. *Remote Sens. Environ.* **2016**, *187*, 414–422. [CrossRef]
23. Viljanen, N.; Honkavaara, E.; Näsi, R.; Hakala, T.; Niemeläinen, O.; Kaivosoja, J. A novel machine learning method for estimating biomass of grass swards using a photogrammetric canopy height model, images and vegetation indices captured by a drone. *Agriculture* **2018**, *8*, 70. [CrossRef]
24. Guerini Filho, M.; Kuplich, T.M.; Quadros, F.L.D. Estimating natural grassland biomass by vegetation indices using Sentinel 2 remote sensing data. *Int. J. Remote Sens.* **2020**, *41*, 2861–2876. [CrossRef]
25. Mansaray, L.R.; Kanu, A.S.; Yang, L.; Huang, J.; Wang, F. Evaluation of machine learning models for rice dry biomass estimation and mapping using quad-source optical imagery. *GIScience Remote Sens.* **2020**, *57*, 785–796. [CrossRef]
26. Shang, J.; Liu, J.; Huffman, T.C.; Qian, B.; Pattey, E.; Wang, J.; Zhao, T.; Geng, X.; Kroetsch, D.; Dong, T. Estimating plant area index for monitoring crop growth dynamics using Landsat-8 and RapidEye images. *J. Appl. Remote Sens.* **2014**, *8*, 085196. [CrossRef]
27. Baghdadi, N.N.; El Hajj, M.; Zribi, M.; Fayad, I. Coupling SAR C-band and optical data for soil moisture and leaf area index retrieval over irrigated grasslands. *IEEE J. Sel. Top. Appl. Earth Obs. Remote Sens.* **2015**, *9*, 1229–1243. [CrossRef]
28. Dong, T.; Meng, J.; Shang, J.; Liu, J.; Wu, B.; Huffman, T. Modified vegetation indices for estimating crop fraction of absorbed photosynthetically active radiation. *Int. J. Remote Sens.* **2015**, *36*, 3097–3113. [CrossRef]
29. Betbeder, J.; Fieuzal, R.; Baup, F. Assimilation of LAI and dry biomass data from optical and SAR images into an agro-meteorological model to estimate soybean yield. *IEEE J. Sel. Top. Appl. Earth Obs. Remote Sens.* **2016**, *9*, 2540–2553. [CrossRef]
30. Dong, T.; Liu, J.; Qian, B.; Zhao, T.; Jing, Q.; Geng, X.; Wang, J.; Huffman, T.; Shang, J. Estimating winter wheat biomass by assimilating leaf area index derived from fusion of Landsat-8 and MODIS data. *Int. J. Appl. Earth Obs. Geoinf.* **2016**, *49*, 63–74. [CrossRef]
31. Jannoura, R.; Brinkmann, K.; Uteau, D.; Bruns, C.; Joergensen, R.G. Monitoring of crop biomass using true colour aerial photographs taken from a remote controlled hexacopter. *Biosyst. Eng.* **2015**, *129*, 341–351. [CrossRef]
32. Zhang, H.; Sun, Y.; Chang, L.; Qin, Y.; Chen, J.; Qin, Y.; Du, J.; Yi, S.; Wang, Y. Estimation of grassland canopy height and aboveground biomass at the quadrat scale using unmanned aerial vehicle. *Remote Sens.* **2018**, *10*, 851. [CrossRef]

33. Eskandari, R.; Mahdianpari, M.; Mohammadimanesh, F.; Salehi, B.; Brisco, B.; Homayouni, S. Meta-analysis of unmanned aerial vehicle (UAV) imagery for agro-environmental monitoring using machine learning and statistical models. *Remote Sens.* **2020**, *12*, 3511. [CrossRef]
34. Ali, I.; Cawkwell, F.; Dwyer, E.; Green, S. Modeling managed grassland biomass estimation by using multitemporal remote sensing data—A machine learning approach. *IEEE J. Sel. Top. Appl. Earth Obs. Remote Sens.* **2016**, *10*, 3254–3264. [CrossRef]
35. Hunt, E.R.; Daughtry, C.S.; Mirsky, S.B.; Hively, W.D. Remote sensing with simulated unmanned aircraft imagery for precision agriculture applications. *IEEE J. Sel. Top. Appl. Earth Obs. Remote Sens.* **2014**, *7*, 4566–4571. [CrossRef]
36. Li, W.; Niu, Z.; Chen, H.; Li, D. Characterizing canopy structural complexity for the estimation of maize LAI based on ALS data and UAV stereo images. *Int. J. Remote Sens.* **2017**, *38*, 2106–2116. [CrossRef]
37. Yue, J.; Feng, H.; Jin, X.; Yuan, H.; Li, Z.; Zhou, C.; Yang, G.; Tian, Q. A comparison of crop parameters estimation using images from UAV-mounted snapshot hyperspectral sensor and high-definition digital camera. *Remote Sens.* **2018**, *10*, 1138. [CrossRef]
38. Canisius, F.; Fernandes, R. ALOS PALSAR L-band polarimetric SAR data and in situ measurements for leaf area index assessment. *Remote Sens. Lett.* **2012**, *3*, 221–229. [CrossRef]
39. McNairn, H.; Shang, J. A review of multitemporal synthetic aperture radar (SAR) for crop monitoring. In *Multitemporal Remote Sensing*; Springer: Berlin/Heidelberg, Germany, 2016; pp. 317–340.
40. Holtgrave, A.-K.; Röder, N.; Ackermann, A.; Erasmi, S.; Kleinschmit, B. Comparing Sentinel-1 and-2 data and indices for agricultural land use monitoring. *Remote Sens.* **2020**, *12*, 2919. [CrossRef]
41. Bahrami, H.; Homayouni, S.; Safari, A.; Mirzaei, S.; Mahdianpari, M.; Reisi-Gahrouei, O. Deep Learning-Based Estimation of Crop Biophysical Parameters Using Multi-Source and Multi-Temporal Remote Sensing Observations. *Agronomy* **2021**, *11*, 1363. [CrossRef]
42. Fontanelli, G.; Crema, A.; Azar, R.; Stroppiana, D.; Villa, P.; Boschetti, M. Agricultural crop mapping using optical and SAR multi-temporal seasonal data: A case study in Lombardy region, Italy. In Proceedings of the 2014 IEEE Geoscience and Remote Sensing Symposium, Quebec City, QC, Canada, 13–18 July 2014; pp. 1489–1492.
43. Schuster, C.; Schmidt, T.; Conrad, C.; Kleinschmit, B.; Förster, M. Grassland habitat mapping by intra-annual time series analysis–Comparison of RapidEye and TerraSAR-X satellite data. *Int. J. Appl. Earth Obs. Geoinf.* **2015**, *34*, 25–34. [CrossRef]
44. McNairn, H.; Champagne, C.; Shang, J.; Holmstrom, D.; Reichert, G. Integration of optical and Synthetic Aperture Radar (SAR) imagery for delivering operational annual crop inventories. *ISPRS J. Photogramm. Remote Sens.* **2009**, *64*, 434–449. [CrossRef]
45. Bahrami, H.; Homayouni, S.; McNairn, H.; Hosseini, M.; Mahdianpari, M. Regional Crop Characterization Using Multi-Temporal Optical and Synthetic Aperture Radar Earth Observations Data. *Can. J. Remote Sens.* **2022**, *48*, 258–277. [CrossRef]
46. Dong, T.; Meng, J.; Shang, J.; Liu, J.; Wu, B. Evaluation of chlorophyll-related vegetation indices using simulated Sentinel-2 data for estimation of crop fraction of absorbed photosynthetically active radiation. *IEEE J. Sel. Top. Appl. Earth Obs. Remote Sens.* **2015**, *8*, 4049–4059. [CrossRef]
47. Du, X.; Li, Q.; Dong, T.; Jia, K. Winter wheat biomass estimation using high temporal and spatial resolution satellite data combined with a light use efficiency model. *Geocarto Int.* **2015**, *30*, 258–269. [CrossRef]
48. Dusseux, P.; Hubert-Moy, L.; Corpetti, T.; Vertès, F. Evaluation of SPOT imagery for the estimation of grassland biomass. *Int. J. Appl. Earth Obs. Geoinf.* **2015**, *38*, 72–77. [CrossRef]
49. Leroux, L.; Baron, C.; Zoungrana, B.; Traoré, S.B.; Seen, D.L.; Bégué, A. Crop monitoring using vegetation and thermal indices for yield estimates: Case study of a rainfed cereal in semi-arid West Africa. *IEEE J. Sel. Top. Appl. Earth Obs. Remote Sens.* **2015**, *9*, 347–362. [CrossRef]
50. Li, W.; Niu, Z.; Wang, C.; Huang, W.; Chen, H.; Gao, S.; Li, D.; Muhammad, S. Combined use of airborne LiDAR and satellite GF-1 data to estimate leaf area index, height, and aboveground biomass of maize during peak growing season. *IEEE J. Sel. Top. Appl. Earth Obs. Remote Sens.* **2015**, *8*, 4489–4501. [CrossRef]
51. Marshall, M.; Thenkabail, P. Advantage of hyperspectral EO-1 Hyperion over multispectral IKONOS, GeoEye-1, WorldView-2, Landsat ETM+, and MODIS vegetation indices in crop biomass estimation. *ISPRS J. Photogramm. Remote Sens.* **2015**, *108*, 205–218. [CrossRef]
52. Kamal, M.; Phinn, S.; Johansen, K. Assessment of multi-resolution image data for mangrove leaf area index mapping. *Remote Sens. Environ.* **2016**, *176*, 242–254. [CrossRef]
53. Tanaka, S.; Kawamura, K.; Maki, M.; Muramoto, Y.; Yoshida, K.; Akiyama, T. Spectral index for quantifying leaf area index of winter wheat by field hyperspectral measurements: A case study in gifu prefecture, central Japan. *Remote Sens.* **2015**, *7*, 5329–5346. [CrossRef]
54. Kross, A.; McNairn, H.; Lapen, D.; Sunohara, M.; Champagne, C. Assessment of RapidEye vegetation indices for estimation of leaf area index and biomass in corn and soybean crops. *Int. J. Appl. Earth Obs. Geoinf.* **2015**, *34*, 235–248. [CrossRef]
55. Zhou, X.; Zhu, X.; Dong, Z.; Guo, W. Estimation of biomass in wheat using random forest regression algorithm and remote sensing data. *Crop J.* **2016**, *4*, 212–219.
56. Haldar, D.; Tripathy, R.; Dave, V.; Dave, R.; Bhattacharya, B.; Misra, A. Monitoring cotton crop condition through synergy of optical and radar remote sensing. *Geocarto Int.* **2020**, *37*, 377–395. [CrossRef]
57. Ranjbar, S.; Zarei, A.; Hasanlou, M.; Akhoondzadeh, M.; Amini, J.; Amani, M. Machine learning inversion approach for soil parameters estimation over vegetated agricultural areas using a combination of water cloud model and calibrated integral equation model. *J. Appl. Remote Sens.* **2021**, *15*, 018503. [CrossRef]

58. Wang, B.; Ono, A.; Muramatsu, K.; Fujiwara, N. Automated detection and removal of clouds and their shadows from Landsat TM images. *IEICE Trans. Inf. Syst.* **1999**, *82*, 453–460.
59. Haboudane, D.; Miller, J.R.; Pattey, E.; Zarco-Tejada, P.J.; Strachan, I.B. Hyperspectral vegetation indices and novel algorithms for predicting green LAI of crop canopies: Modeling and validation in the context of precision agriculture. *Remote Sens. Environ.* **2004**, *90*, 337–352. [CrossRef]
60. Fu, Y.; Yang, G.; Wang, J.; Song, X.; Feng, H. Winter wheat biomass estimation based on spectral indices, band depth analysis and partial least squares regression using hyperspectral measurements. *Comput. Electron. Agric.* **2014**, *100*, 51–59. [CrossRef]
61. Luo, P.; Liao, J.; Shen, G. Combining Spectral and Texture Features for Estimating Leaf Area Index and Biomass of Maize Using Sentinel-1/2, and Landsat-8 Data. *IEEE Access* **2020**, *8*, 53614–53626. [CrossRef]
62. Moreira, A.; Prats-Iraola, P.; Younis, M.; Krieger, G.; Hajnsek, I.; Papathanassiou, K.P. A tutorial on synthetic aperture radar. *IEEE Geosci. Remote Sens. Mag.* **2013**, *1*, 6–43. [CrossRef]
63. Carver, K.R.; Elachi, C.; Ulaby, F.T. Microwave remote sensing from space. *Proc. IEEE* **1985**, *73*, 970–996. [CrossRef]
64. Li, Z.; Guo, X. Can Polarimetric Radarsat-2 Images Provide a Solution to Quantify Non-Photosynthetic Vegetation Biomass in Semiarid Mixed Grassland? *Can. J. Remote Sens.* **2017**, *43*, 593–607. [CrossRef]
65. Wu, S.-t. Potential application of multipolarization SAR for pine-plantation biomass estimation. *IEEE Trans. Geosci. Remote Sens.* **1987**, *3*, 403–409. [CrossRef]
66. Inoue, Y.; Kurosu, T.; Maeno, H.; Uratsuka, S.; Kozu, T.; Dabrowska-Zielinska, K.; Qi, J. Season-long daily measurements of multifrequency (Ka, Ku, X, C, and L) and full-polarization backscatter signatures over paddy rice field and their relationship with biological variables. *Remote Sens. Environ.* **2002**, *81*, 194–204. [CrossRef]
67. Karjalainen, M.; Kaartinen, H.; Hyyppä, J. Agricultural monitoring using Envisat alternating polarization SAR images. *Photogramm. Eng. Remote Sens.* **2008**, *74*, 117–126. [CrossRef]
68. Jimenez-Sierra, D.A.; Benítez-Restrepo, H.D.; Vargas-Cardona, H.D.; Chanussot, J. Graph-Based Data Fusion Applied to: Change Detection and Biomass Estimation in Rice Crops. *Remote Sens.* **2020**, *12*, 2683. [CrossRef]
69. Cable, J.W.; Kovacs, J.M.; Jiao, X.; Shang, J. Agricultural monitoring in northeastern Ontario, Canada, using multi-temporal polarimetric RADARSAT-2 data. *Remote Sens.* **2014**, *6*, 2343–2371. [CrossRef]
70. Gao, S.; Niu, Z.; Huang, N.; Hou, X. Estimating the Leaf Area Index, height and biomass of maize using HJ-1 and RADARSAT-2. *Int. J. Appl. Earth Obs. Geoinf.* **2013**, *24*, 1–8. [CrossRef]
71. Chen, F.; Weber, K.T.; Gokhale, B. Herbaceous biomass estimation from SPOT 5 imagery in semiarid rangelands of Idaho. *GIScience Remote Sens.* **2011**, *48*, 195–209. [CrossRef]
72. Davenport, I.; Bradbury, R.; Anderson, G.; Hayman, G.; Krebs, J.; Mason, D.; Wilson, J.; Veck, N. Improving bird population models using airborne remote sensing. *Int. J. Remote Sens.* **2000**, *21*, 2705–2717. [CrossRef]
73. Nie, S.; Wang, C.; Dong, P.; Xi, X.; Luo, S.; Zhou, H. Estimating leaf area index of maize using airborne discrete-return LiDAR data. *IEEE J. Sel. Top. Appl. Earth Obs. Remote Sens.* **2016**, *9*, 3259–3266. [CrossRef]
74. Lefsky, M.A.; Cohen, W.B.; Parker, G.G.; Harding, D.J. Lidar remote sensing for ecosystem studies: Lidar, an emerging remote sensing technology that directly measures the three-dimensional distribution of plant canopies, can accurately estimate vegetation structural attributes and should be of particular interest to forest, landscape, and global ecologists. *BioScience* **2002**, *52*, 19–30.
75. Agrawal, S.; Khairnar, G. A comparative assessment of remote sensing imaging techniques: Optical, sar and lidar. *Int. Arch. Photogramm. Remote Sens. Spat. Inf. Sci.* **2019**, *XLII-5/W3*, 1–6. [CrossRef]
76. Anderson, K.E.; Glenn, N.F.; Spaete, L.P.; Shinneman, D.J.; Pilliod, D.S.; Arkle, R.S.; McIlroy, S.K.; Derryberry, D.R. Estimating vegetation biomass and cover across large plots in shrub and grass dominated drylands using terrestrial lidar and machine learning. *Ecol. Indic.* **2018**, *84*, 793–802. [CrossRef]
77. Lumme, J.; Karjalainen, M.; Kaartinen, H.; Kukko, A.; Hyyppä, J.; Hyyppä, H.; Jaakkola, A.; Kleemola, J. Terrestrial laser scanning of agricultural crops. *Int. Arch. Photogramm. Remote Sens. Spat. Inf. Sci* **2008**, *37*, 563–566.
78. Hoffmeister, D.; Waldhoff, G.; Korres, W.; Curdt, C.; Bareth, G. Crop height variability detection in a single field by multi-temporal terrestrial laser scanning. *Precis. Agric.* **2016**, *17*, 296–312. [CrossRef]
79. García-Berná, J.A.; Ouhbi, S.; Benmouna, B.; Garcia-Mateos, G.; Fernández-Alemán, J.L.; Molina-Martínez, J.M. Systematic mapping study on remote sensing in agriculture. *Appl. Sci.* **2020**, *10*, 3456. [CrossRef]
80. Ali, I.; Greifeneder, F.; Stamenkovic, J.; Neumann, M.; Notarnicola, C. Review of machine learning approaches for biomass and soil moisture retrievals from remote sensing data. *Remote Sens.* **2015**, *7*, 16398–16421. [CrossRef]
81. Chao, Z.; Liu, N.; Zhang, P.; Ying, T.; Song, K. Estimation methods developing with remote sensing information for energy crop biomass: A comparative review. *Biomass Bioenergy* **2019**, *122*, 414–425. [CrossRef]
82. Hatfield, J.L.; Prueger, J.H.; Sauer, T.J.; Dold, C.; O'Brien, P.; Wacha, K. Applications of vegetative indices from remote sensing to agriculture: Past and future. *Inventions* **2019**, *4*, 71. [CrossRef]
83. Ke, L.; Zhou, Q.-B.; Wu, W.-B.; Tian, X.; Tang, H.-J. Estimating the crop leaf area index using hyperspectral remote sensing. *J. Integr. Agric.* **2016**, *15*, 475–491.
84. Steele-Dunne, S.C.; McNairn, H.; Monsivais-Huertero, A.; Judge, J.; Liu, P.-W.; Papathanassiou, K. Radar remote sensing of agricultural canopies: A review. *IEEE J. Sel. Top. Appl. Earth Obs. Remote Sens.* **2017**, *10*, 2249–2273. [CrossRef]

85. Verrelst, J.; Camps-Valls, G.; Muñoz-Marí, J.; Rivera, J.P.; Veroustraete, F.; Clevers, J.G.; Moreno, J. Optical remote sensing and the retrieval of terrestrial vegetation bio-geophysical properties—A review. *ISPRS J. Photogramm. Remote Sens.* **2015**, *108*, 273–290. [CrossRef]
86. Weiss, M.; Jacob, F.; Duveiller, G. Remote sensing for agricultural applications: A meta-review. *Remote Sens. Environ.* **2020**, *236*, 111402. [CrossRef]
87. Hosseini, M.; McNairn, H.; Merzouki, A.; Pacheco, A. Estimation of Leaf Area Index (LAI) in corn and soybeans using multi-polarization C-and L-band radar data. *Remote Sens. Environ.* **2015**, *170*, 77–89. [CrossRef]
88. Hosseini, M.; McNairn, H. Using multi-polarization C-and L-band synthetic aperture radar to estimate biomass and soil moisture of wheat fields. *Int. J. Appl. Earth Obs. Geoinf.* **2017**, *58*, 50–64. [CrossRef]
89. Hosseini, M.; McNairn, H.; Mitchell, S.; Robertson, L.D.; Davidson, A.; Homayouni, S. Synthetic aperture radar and optical satellite data for estimating the biomass of corn. *Int. J. Appl. Earth Obs. Geoinf.* **2019**, *83*, 101933. [CrossRef]
90. Homayouni, S.; McNairn, H.; Hosseini, M.; Jiao, X.; Powers, J. Quad and compact multitemporal C-band PolSAR observations for crop characterization and monitoring. *Int. J. Appl. Earth Obs. Geoinf.* **2019**, *74*, 78–87. [CrossRef]
91. Mandal, D.; Kumar, V.; McNairn, H.; Bhattacharya, A.; Rao, Y. Joint estimation of Plant Area Index (PAI) and wet biomass in wheat and soybean from C-band polarimetric SAR data. *Int. J. Appl. Earth Obs. Geoinf.* **2019**, *79*, 24–34. [CrossRef]
92. Reisi Gahrouei, O.; McNairn, H.; Hosseini, M.; Homayouni, S. Estimation of Crop Biomass and Leaf Area Index from Multitemporal and Multispectral Imagery Using Machine Learning Approaches. *Can. J. Remote Sens.* **2020**, *46*, 84–99. [CrossRef]
93. Mandal, D.; Kumar, V.; Lopez-Sanchez, J.M.; Bhattacharya, A.; McNairn, H.; Rao, Y. Crop biophysical parameter retrieval from Sentinel-1 SAR data with a multi-target inversion of Water Cloud Model. *Int. J. Remote Sens.* **2020**, *41*, 5503–5524. [CrossRef]
94. Shewry, P.R.; Hey, S.J. The contribution of wheat to human diet and health. *Food Energy Secur.* **2015**, *4*, 178–202. [CrossRef]
95. Hazell, P.B. *The Asian Green Revolution*; International Food Policy Research Institute: Washington, DC, USA, 2009; Volume 911.
96. Grote, U.; Fasse, A.; Nguyen, T.T.; Erenstein, O. Food security and the dynamics of wheat and maize value chains in Africa and Asia. *Front. Sustain. Food Syst.* **2021**, *4*, 317. [CrossRef]
97. Huang, S.; Tang, L.; Hupy, J.P.; Wang, Y.; Shao, G. A commentary review on the use of normalized difference vegetation index (NDVI) in the era of popular remote sensing. *J. For. Res.* **2021**, *32*, 1–6. [CrossRef]
98. Rouse, J.W.; Haas, R.H.; Schell, J.A.; Deering, D.W. Monitoring vegetation systems in the Great Plains with ERTS. *NASA Spec. Publ.* **1974**, *351*, 309.
99. Townshend, J.R.; Justice, C. Analysis of the dynamics of African vegetation using the normalized difference vegetation index. *Int. J. Remote Sens.* **1986**, *7*, 1435–1445. [CrossRef]
100. Quarmby, N.; Milnes, M.; Hindle, T.; Silleos, N. The use of multi-temporal NDVI measurements from AVHRR data for crop yield estimation and prediction. *Int. J. Remote Sens.* **1993**, *14*, 199–210. [CrossRef]
101. Huete, A.; Didan, K.; Miura, T.; Rodriguez, E.P.; Gao, X.; Ferreira, L.G. Overview of the radiometric and biophysical performance of the MODIS vegetation indices. *Remote Sens. Environ.* **2002**, *83*, 195–213. [CrossRef]
102. Huete, A.R. A soil-adjusted vegetation index (SAVI). *Remote Sens. Environ.* **1988**, *25*, 295–309. [CrossRef]
103. Jordan, C.F. Derivation of leaf-area index from quality of light on the forest floor. *Ecology* **1969**, *50*, 663–666. [CrossRef]
104. Rondeaux, G.; Steven, M.; Baret, F. Optimization of soil-adjusted vegetation indices. *Remote Sens. Environ.* **1996**, *55*, 95–107. [CrossRef]
105. Gitelson, A.A.; Kaufman, Y.J.; Merzlyak, M.N. Use of a green channel in remote sensing of global vegetation from EOS-MODIS. *Remote Sens. Environ.* **1996**, *58*, 289–298. [CrossRef]
106. Gitelson, A.A. Wide dynamic range vegetation index for remote quantification of biophysical characteristics of vegetation. *J. Plant Physiol.* **2004**, *161*, 165–173. [CrossRef] [PubMed]
107. Qi, J.; Chehbouni, A.; Huete, A.R.; Kerr, Y.H.; Sorooshian, S. A modified soil adjusted vegetation index. *Remote Sens. Environ.* **1994**, *48*, 119–126. [CrossRef]
108. Jiang, Z.; Huete, A.R.; Didan, K.; Miura, T. Development of a two-band enhanced vegetation index without a blue band. *Remote Sens. Environ.* **2008**, *112*, 3833–3845. [CrossRef]
109. Shang, J.; McNairn, H.; Champagne, C.; Jiao, X. Application of multi-frequency synthetic aperture radar (SAR) in crop classification. In *Advances in Geoscience and Remote Sensing*; IntechOpen: London, UK, 2009.
110. McNairn, H.; Kross, A.; Lapen, D.; Caves, R.; Shang, J. Early season monitoring of corn and soybeans with TerraSAR-X and RADARSAT-2. *Int. J. Appl. Earth Obs. Geoinf.* **2014**, *28*, 252–259. [CrossRef]
111. Mohan, S.; Das, A.; Haldar, D.; Maity, S. Monitoring and retrieval of vegetation parameter using multi-frequency polarimetric SAR data. In Proceedings of the 2011 3rd International Asia-Pacific Conference on Synthetic Aperture Radar (APSAR), Seoul, Korea, 26–30 September 2011; pp. 1–4.
112. Brisco, B.; Brown, R.; Gairns, J.; Snider, B. Temporal ground-based scatterometer observations of crops in western Canada. *Can. J. Remote Sens.* **1992**, *18*, 14–21. [CrossRef]
113. Sishodia, R.P.; Ray, R.L.; Singh, S.K. Applications of remote sensing in precision agriculture: A review. *Remote Sens.* **2020**, *12*, 3136. [CrossRef]
114. Fu, Y.; Yang, G.; Song, X.; Li, Z.; Xu, X.; Feng, H.; Zhao, C. Improved estimation of winter wheat aboveground biomass using multiscale textures extracted from UAV-based digital images and hyperspectral feature analysis. *Remote Sens.* **2021**, *13*, 581. [CrossRef]

115. Jin, X.-L.; Diao, W.-Y.; Xiao, C.-H.; Wang, F.-Y.; Chen, B.; Wang, K.-R.; Li, S.-K. Estimation of wheat agronomic parameters using new spectral indices. *PLoS ONE* **2013**, *8*, e72736. [CrossRef]
116. Kujawa, S.; Niedbała, G. Artificial Neural Networks in Agriculture. *Agriculture* **2021**, *11*, 497. [CrossRef]
117. Abubakar, B.S. Weed detection using machine learning: A systematic literature review. *Syst. Lit. Rev. Meta-Anal. J.* **2021**, *2*, 61–73. [CrossRef]
118. Khairunniza-Bejo, S.; Mustaffha, S.; Ismail, W.I.W. Application of artificial neural network in predicting crop yield: A review. *J. Food Sci. Eng.* **2014**, *4*, 1.
119. Camps-Valls, G.; Bruzzone, L.; Rojo-Álvarez, J.L.; Melgani, F. Robust support vector regression for biophysical variable estimation from remotely sensed images. *IEEE Geosci. Remote Sens. Lett.* **2006**, *3*, 339–343. [CrossRef]
120. Yue, J.; Feng, H.; Yang, G.; Li, Z. A comparison of regression techniques for estimation of above-ground winter wheat biomass using near-surface spectroscopy. *Remote Sens.* **2018**, *10*, 66. [CrossRef]
121. Ahmadian, N.; Ullmann, T.; Verrelst, J.; Borg, E.; Zölitz, R.; Conrad, C. Biomass assessment of agricultural crops using multi-temporal dual-polarimetric TerraSAR-X data. *PFG–J. Photogramm. Remote Sens. Geoinf. Sci.* **2019**, *87*, 159–175. [CrossRef]
122. Fieuzal, R.; Baup, F.; Marais-Sicre, C. Sensitivity of TerraSAR-X, RADARSAT-2 and ALOS satellite radar data to crop variables. In Proceedings of the 2012 IEEE International Geoscience and Remote Sensing Symposium, Munich, Germany, 22–27 July 2012; pp. 3740–3743.
123. Liu, C.; Shang, J.; Vachon, P.W.; McNairn, H. Multiyear crop monitoring using polarimetric RADARSAT-2 data. *IEEE Trans. Geosci. Remote Sens.* **2012**, *51*, 2227–2240. [CrossRef]
124. Mattia, F.; Le Toan, T.; Picard, G.; Posa, F.I.; D'Alessio, A.; Notarnicola, C.; Gatti, A.M.; Rinaldi, M.; Satalino, G.; Pasquariello, G. Multitemporal C-band radar measurements on wheat fields. *IEEE Trans. Geosci. Remote Sens.* **2003**, *41*, 1551–1560. [CrossRef]
125. Mahdianpari, M.; Granger, J.E.; Mohammadimanesh, F.; Salehi, B.; Brisco, B.; Homayouni, S.; Gill, E.; Huberty, B.; Lang, M. Meta-analysis of wetland classification using remote sensing: A systematic review of a 40-year trend in North America. *Remote Sens.* **2020**, *12*, 1882. [CrossRef]
126. Sun, Y.; Qin, Q.; Ren, H.; Zhang, T.; Chen, S. Red-Edge Band Vegetation Indices for Leaf Area Index Estimation From Sentinel-2/MSI Imagery. *IEEE Trans. Geosci. Remote Sens.* **2019**, *58*, 826–840. [CrossRef]
127. Deb, D.; Deb, S.; Chakraborty, D.; Singh, J.; Singh, A.K.; Dutta, P.; Choudhury, A. Aboveground biomass estimation of an agro-pastoral ecology in semi-arid Bundelkhand region of India from Landsat data: A comparison of support vector machine and traditional regression models. *Geocarto Int.* **2020**, *37*, 1043–1058. [CrossRef]
128. Sharifi, A.; Hosseingholizadeh, M. Application of Sentinel-1 Data to Estimate Height and Biomass of Rice Crop in Astaneh-ye Ashrafiyeh, Iran. *J. Indian Soc. Remote Sens.* **2020**, *48*, 11–19. [CrossRef]
129. Grüner, E.; Astor, T.; Wachendorf, M. Biomass prediction of heterogeneous temperate grasslands using an SfM approach based on UAV imaging. *Agronomy* **2019**, *9*, 54. [CrossRef]
130. Acorsi, M.G.; das Dores Abati Miranda, F.; Martello, M.; Smaniotto, D.A.; Sartor, L.R. Estimating biomass of black oat using UAV-based RGB imaging. *Agronomy* **2019**, *9*, 344. [CrossRef]
131. Zhu, W.; Sun, Z.; Peng, J.; Huang, Y.; Li, J.; Zhang, J.; Yang, B.; Liao, X. Estimating Maize Above-Ground Biomass Using 3D Point Clouds of Multi-Source Unmanned Aerial Vehicle Data at Multi-Spatial Scales. *Remote Sens.* **2019**, *11*, 2678. [CrossRef]
132. Liu, Y.; Liu, S.; Li, J.; Guo, X.; Wang, S.; Lu, J. Estimating biomass of winter oilseed rape using vegetation indices and texture metrics derived from UAV multispectral images. *Comput. Electron. Agric.* **2019**, *166*, 105026. [CrossRef]
133. Song, Y.; Wang, J.; Shang, J. Estimating effective leaf area index of winter wheat using simulated observation on unmanned aerial vehicle-based point cloud data. *IEEE J. Sel. Top. Appl. Earth Obs. Remote Sens.* **2020**, *13*, 2874–2887. [CrossRef]
134. Panday, U.S.; Shrestha, N.; Maharjan, S.; Pratihast, A.K.; Shrestha, K.L.; Aryal, J. Correlating the Plant Height of Wheat with Above-Ground Biomass and Crop Yield Using Drone Imagery and Crop Surface Model, A Case Study from Nepal. *Drones* **2020**, *4*, 28. [CrossRef]
135. Dayananda, S.; Astor, T.; Wijesingha, J.; Chickadibburahalli Thimappa, S.; Dimba Chowdappa, H.; Nidamanuri, R.R.; Nautiyal, S.; Wachendorf, M. Multi-Temporal Monsoon Crop Biomass Estimation Using Hyperspectral Imaging. *Remote Sens.* **2019**, *11*, 1771. [CrossRef]
136. Carneiro, F.M.; Furlani, C.E.A.; Zerbato, C.; de Menezes, P.C.; da Silva Gírio, L.A.; de Oliveira, M.F. Comparison between vegetation indices for detecting spatial and temporal variabilities in soybean crop using canopy sensors. *Precis. Agric.* **2019**, *21*, 979–1007. [CrossRef]
137. Tong, X.; Duan, L.; Liu, T.; Singh, V.P. Combined use of in situ hyperspectral vegetation indices for estimating pasture biomass at peak productive period for harvest decision. *Precis. Agric.* **2019**, *20*, 477–495. [CrossRef]
138. Li, P.; Zhang, X.; Wang, W.; Zheng, H.; Yao, X.; Tian, Y.; Zhu, Y.; Cao, W.; Chen, Q.; Cheng, T. Estimating aboveground and organ biomass of plant canopies across the entire season of rice growth with terrestrial laser scanning. *Int. J. Appl. Earth Obs. Geoinf.* **2020**, *91*, 102132. [CrossRef]
139. Yu, L.; Shang, J.; Cheng, Z.; Gao, Z.; Wang, Z.; Tian, L.; Wang, D.; Che, T.; Jin, R.; Liu, J. Assessment of Cornfield LAI Retrieved from Multi-Source Satellite Data Using Continuous Field LAI Measurements Based on a Wireless Sensor Network. *Remote Sens.* **2020**, *12*, 3304. [CrossRef]

140. Estévez, J.; Vicent, J.; Rivera-Caicedo, J.P.; Morcillo-Pallarés, P.; Vuolo, F.; Sabater, N.; Camps-Valls, G.; Moreno, J.; Verrelst, J. Gaussian processes retrieval of LAI from Sentinel-2 top-of-atmosphere radiance data. *ISPRS J. Photogramm. Remote Sens.* **2020**, *167*, 289–304. [CrossRef]
141. Darvishzadeh, R.; Atzberger, C.; Skidmore, A.; Schlerf, M. Mapping grassland leaf area index with airborne hyperspectral imagery: A comparison study of statistical approaches and inversion of radiative transfer models. *ISPRS J. Photogramm. Remote Sens.* **2011**, *66*, 894–906. [CrossRef]
142. Singh, D. Scatterometer performance with polarization discrimination ratio approach to retrieve crop soybean parameter at x-band. *Int. J. Remote Sens.* **2006**, *27*, 4101–4115. [CrossRef]
143. Shen, M.; Tang, Y.; Klein, J.; Zhang, P.; Gu, S.; Shimono, A.; Chen, J. Estimation of aboveground biomass using in situ hyperspectral measurements in five major grassland ecosystems on the Tibetan Plateau. *J. Plant Ecol.* **2008**, *1*, 247–257. [CrossRef]
144. Xing, N.; Huang, W.; Xie, Q.; Shi, Y.; Ye, H.; Dong, Y.; Wu, M.; Sun, G.; Jiao, Q. A Transformed Triangular Vegetation Index for Estimating Winter Wheat Leaf Area Index. *Remote Sens.* **2020**, *12*, 16. [CrossRef]
145. Afrasiabian, Y.; Noory, H.; Mokhtari, A.; Nikoo, M.R.; Pourshakouri, F.; Haghighatmehr, P. Effects of spatial, temporal, and spectral resolutions on the estimation of wheat and barley leaf area index using multi-and hyper-spectral data (case study: Karaj, Iran). *Precis. Agric.* **2020**, *22*, 660–688. [CrossRef]
146. Jin, X.; Li, Z.; Feng, H.; Ren, Z.; Li, S. Deep neural network algorithm for estimating maize biomass based on simulated Sentinel 2A vegetation indices and leaf area index. *Crop J.* **2020**, *8*, 87–97. [CrossRef]
147. Liao, C.; Wang, J.; Dong, T.; Shang, J.; Liu, J.; Song, Y. Using spatio-temporal fusion of Landsat-8 and MODIS data to derive phenology, biomass and yield estimates for corn and soybean. *Sci. Total Environ.* **2019**, *650*, 1707–1721. [CrossRef] [PubMed]
148. Punalekar, S.M.; Verhoef, A.; Quaife, T.L.; Humphries, D.; Bermingham, L.; Reynolds, C.K. Application of Sentinel-2A data for pasture biomass monitoring using a physically based radiative transfer model. *Remote Sens. Environ.* **2018**, *218*, 207–220. [CrossRef]
149. Maimaitijiang, M.; Sagan, V.; Sidike, P.; Daloye, A.M.; Erkbol, H.; Fritschi, F.B. Crop Monitoring Using Satellite/UAV Data Fusion and Machine Learning. *Remote Sens.* **2020**, *12*, 1357. [CrossRef]
150. Lu, B.; He, Y. Leaf Area Index Estimation in a Heterogeneous Grassland Using Optical, SAR, and DEM Data. *Can. J. Remote Sens.* **2019**, *45*, 618–633. [CrossRef]
151. Wei, C.; Huang, J.; Mansaray, L.R.; Li, Z.; Liu, W.; Han, J. Estimation and mapping of winter oilseed rape LAI from high spatial resolution satellite data based on a hybrid method. *Remote Sens.* **2017**, *9*, 488. [CrossRef]
152. Campos-Taberner, M.; García-Haro, F.J.; Camps-Valls, G.; Grau-Muedra, G.; Nutini, F.; Busetto, L.; Katsantonis, D.; Stavrakoudis, D.; Minakou, C.; Gatti, L. Exploitation of SAR and optical Sentinel data to detect rice crop and estimate seasonal dynamics of leaf area index. *Remote Sens.* **2017**, *9*, 248. [CrossRef]
153. Sibanda, M.; Mutanga, O.; Rouget, M. Comparing the spectral settings of the new generation broad and narrow band sensors in estimating biomass of native grasses grown under different management practices. *GIScience Remote Sens.* **2016**, *53*, 614–633. [CrossRef]
154. Marti-Cardona, B.; Lopez-Martinez, C.; Dolz-Ripolles, J.; Bladè-Castellet, E. ASAR polarimetric, multi-incidence angle and multitemporal characterization of Doñana wetlands for flood extent monitoring. *Remote Sens. Environ.* **2010**, *114*, 2802–2815. [CrossRef]
155. Mahdianpari, M.; Salehi, B.; Mohammadimanesh, F.; Brisco, B. An assessment of simulated compact polarimetric SAR data for wetland classification using random forest algorithm. *Can. J. Remote Sens.* **2017**, *43*, 468–484. [CrossRef]
156. Adeli, S.; Salehi, B.; Mahdianpari, M.; Quackenbush, L.J.; Brisco, B.; Tamiminia, H.; Shaw, S. Wetland monitoring using SAR data: A meta-analysis and comprehensive review. *Remote Sens.* **2020**, *12*, 2190. [CrossRef]
157. Yang, R.; Dai, B.; Tan, L.; Liu, X.; Yang, Z.; Li, H. Target Polarimetric Decompositions of PolSAR Image. In *Polarimetric Microwave Imaging*; Springer: Berlin/Heidelberg, Germany, 2021; pp. 385–425.
158. Cloude, S.R.; Pottier, E. A review of target decomposition theorems in radar polarimetry. *IEEE Trans. Geosci. Remote Sens.* **1996**, *34*, 498–518. [CrossRef]
159. Freeman, A.; Durden, S.L. A three-component scattering model for polarimetric SAR data. *IEEE Trans. Geosci. Remote Sens.* **1998**, *36*, 963–973. [CrossRef]
160. Yamaguchi, Y.; Moriyama, T.; Ishido, M.; Yamada, H. Four-component scattering model for polarimetric SAR image decomposition. *IEEE Trans. Geosci. Remote Sens.* **2005**, *43*, 1699–1706. [CrossRef]
161. McNairn, H.; Brisco, B. The application of C-band polarimetric SAR for agriculture: A review. *Can. J. Remote Sens.* **2004**, *30*, 525–542. [CrossRef]
162. Duan, B.; Liu, Y.; Gong, Y.; Peng, Y.; Wu, X.; Zhu, R.; Fang, S. Remote estimation of rice LAI based on Fourier spectrum texture from UAV image. *Plant Methods* **2019**, *15*, 124. [CrossRef]
163. Wali, E.; Tasumi, M.; Moriyama, M. Combination of Linear Regression Lines to Understand the Response of Sentinel-1 Dual Polarization SAR Data with Crop Phenology—Case Study in Miyazaki, Japan. *Remote Sens.* **2020**, *12*, 189. [CrossRef]
164. Li, S.; Yuan, F.; Ata-UI-Karim, S.T.; Zheng, H.; Cheng, T.; Liu, X.; Tian, Y.; Zhu, Y.; Cao, W.; Cao, Q. Combining color indices and textures of UAV-based digital imagery for rice LAI estimation. *Remote Sens.* **2019**, *11*, 1763. [CrossRef]
165. Mansaray, L.R.; Zhang, K.; Kanu, A.S. Dry biomass estimation of paddy rice with Sentinel-1A satellite data using machine learning regression algorithms. *Comput. Electron. Agric.* **2020**, *176*, 105674. [CrossRef]

166. Ott, J.; Kasischke, E.; French, N.; Gross, M.; Klemas, V. Preliminary evaluation of a multi-channel SAR data set for a mid-Atlantic coastal marsh. In Proceedings of the 10th Annual International Symposium on Geoscience and Remote Sensing, College Park, MD, USA, 20–24 May 1990; pp. 453–456.
167. Kaplan, G.; Fine, L.; Lukyanov, V.; Manivasagam, V.; Tanny, J.; Rozenstein, O. Normalizing the Local Incidence Angle in Sentinel-1 Imagery to Improve Leaf Area Index, Vegetation Height, and Crop Coefficient Estimations. *Land* **2021**, *10*, 680. [CrossRef]
168. Chakraborty, M.; Manjunath, K.; Panigrahy, S.; Kundu, N.; Parihar, J. Rice crop parameter retrieval using multi-temporal, multi-incidence angle Radarsat SAR data. *ISPRS J. Photogramm. Remote Sens.* **2005**, *59*, 310–322. [CrossRef]
169. Jiao, X.; McNairn, H.; Shang, J.; Pattey, E.; Liu, J.; Champagne, C. The sensitivity of RADARSAT-2 quad-polarization SAR data to crop LAI. In Proceedings of the Remote Sensing and Modeling of Ecosystems for Sustainability VI, San Diego, CA, USA, 20 August 2009; p. 74540O.
170. Yadav, V.P.; Prasad, R.; Bala, R. Leaf area index estimation of wheat crop using modified water cloud model from the time-series SAR and optical satellite data. *Geocarto Int.* **2019**, *36*, 791–802. [CrossRef]
171. Jin, X.; Yang, G.; Xu, X.; Yang, H.; Feng, H.; Li, Z.; Shen, J.; Lan, Y.; Zhao, C. Combined multi-temporal optical and radar parameters for estimating LAI and biomass in winter wheat using HJ and RADARSAR-2 data. *Remote Sens.* **2015**, *7*, 13251–13272. [CrossRef]
172. Koppe, W.; Gnyp, M.L.; Hennig, S.D.; Li, F.; Miao, Y.; Chen, X.; Jia, L.; Bareth, G. Multi-temporal hyperspectral and radar remote sensing for estimating winter wheat biomass in the North China Plain. *Photogramm. -Fernerkund. -Geoinf.* **2012**, *2012*, 281–298. [CrossRef]
173. Zhu, Y.; Zhao, C.; Yang, H.; Yang, G.; Han, L.; Li, Z.; Feng, H.; Xu, B.; Wu, J.; Lei, L. Estimation of maize above-ground biomass based on stem-leaf separation strategy integrated with LiDAR and optical remote sensing data. *PeerJ* **2019**, *7*, e7593. [CrossRef]
174. Rueda-Ayala, V.P.; Peña, J.M.; Höglind, M.; Bengochea-Guevara, J.M.; Andújar, D. Comparing UAV-based technologies and RGB-D reconstruction methods for plant height and biomass monitoring on grass ley. *Sensors* **2019**, *19*, 535. [CrossRef]
175. Elsayed, S.; Darwish, W. Hyperspectral remote sensing to assess the water status, biomass, and yield of maize cultivars under salinity and water stress. *Bragantia* **2017**, *76*, 62–72. [CrossRef]
176. Kiala, Z.; Odindi, J.; Mutanga, O.; Peerbhay, K. Comparison of partial least squares and support vector regressions for predicting leaf area index on a tropical grassland using hyperspectral data. *J. Appl. Remote Sens.* **2016**, *10*, 036015. [CrossRef]
177. Khan, M.S.; Semwal, M.; Sharma, A.; Verma, R.K. An artificial neural network model for estimating Mentha crop biomass yield using Landsat 8 OLI. *Precis. Agric.* **2020**, *21*, 18–33. [CrossRef]
178. Danner, M.; Berger, K.; Wocher, M.; Mauser, W.; Hank, T.J.I.J.o.P.; Sensing, R. Efficient RTM-based training of machine learning regression algorithms to quantify biophysical & biochemical traits of agricultural crops. *ISPRS J. Photogramm. Remote Sens.* **2021**, *173*, 278–296.
179. Svendsen, D.H.; Martino, L.; Campos-Taberner, M.; García-Haro, F.J.; Camps-Valls, G. Joint Gaussian processes for biophysical parameter retrieval. *IEEE Trans. Geosci. Remote Sens.* **2017**, *56*, 1718–1727. [CrossRef]
180. Yin, G.; Li, A.; Wu, C.; Wang, J.; Xie, Q.; Zhang, Z.; Nan, X.; Jin, H.; Bian, J.; Lei, G. Seamless upscaling of the field-measured grassland aboveground biomass based on gaussian process regression and gap-filled landsat 8 OLI reflectance. *ISPRS Int. J. Geo-Inf.* **2018**, *7*, 242. [CrossRef]
181. Campos-Taberner, M.; García-Haro, F.J.; Camps-Valls, G.; Grau-Muedra, G.; Nutini, F.; Crema, A.; Boschetti, M. Multitemporal and multiresolution leaf area index retrieval for operational local rice crop monitoring. *Remote Sens. Environ.* **2016**, *187*, 102–118. [CrossRef]
182. Camps-Valls, G.; Verrelst, J.; Munoz-Mari, J.; Laparra, V.; Mateo-Jimenez, F.; Gomez-Dans, J. A survey on Gaussian processes for earth-observation data analysis: A comprehensive investigation. *IEEE Geosci. Remote Sens. Mag.* **2016**, *4*, 58–78. [CrossRef]
183. Mao, H.; Meng, J.; Ji, F.; Zhang, Q.; Fang, H. Comparison of machine learning regression algorithms for cotton leaf area index retrieval using Sentinel-2 spectral bands. *Appl. Sci.* **2019**, *9*, 1459. [CrossRef]
184. Kganyago, M.; Mhangara, P.; Adjorlolo, C. Estimating crop biophysical parameters using machine learning algorithms and Sentinel-2 imagery. *Remote Sens.* **2021**, *13*, 4314. [CrossRef]
185. Xu, X.; Lu, J.; Zhang, N.; Yang, T.; He, J.; Yao, X.; Cheng, T.; Zhu, Y.; Cao, W.; Tian, Y. Inversion of rice canopy chlorophyll content and leaf area index based on coupling of radiative transfer and Bayesian network models. *ISPRS J. Photogramm. Remote Sens.* **2019**, *150*, 185–196. [CrossRef]
186. Quan, X.; He, B.; Yebra, M.; Yin, C.; Liao, Z.; Zhang, X.; Li, X. A radiative transfer model-based method for the estimation of grassland aboveground biomass. *Int. J. Appl. Earth Obs. Geoinf.* **2017**, *54*, 159–168. [CrossRef]
187. Klingler, A.; Schaumberger, A.; Vuolo, F.; Kalmár, L.B.; Pötsch, E.M. Comparison of Direct and Indirect Determination of Leaf Area Index in Permanent Grassland. *PFG–J. Photogramm. Remote Sens. Geoinf. Sci.* **2020**, *88*, 369–378. [CrossRef]
188. Chen, Z.; Jia, K.; Xiao, C.; Wei, D.; Zhao, X.; Lan, J.; Wei, X.; Yao, Y.; Wang, B.; Sun, Y. Leaf Area Index Estimation Algorithm for GF-5 Hyperspectral Data Based on Different Feature Selection and Machine Learning Methods. *Remote Sens.* **2020**, *12*, 2110. [CrossRef]
189. Yuping, M.; Shili, W.; Li, Z.; Yingyu, H.; Liwei, Z.; Yanbo, H.; Futang, W. Monitoring winter wheat growth in North China by combining a crop model and remote sensing data. *Int. J. Appl. Earth Obs. Geoinf.* **2008**, *10*, 426–437. [CrossRef]
190. Han, D.; Liu, S.; Du, Y.; Xie, X.; Fan, L.; Lei, L.; Li, Z.; Yang, H.; Yang, G. Crop Water Content of Winter Wheat Revealed with Sentinel-1 and Sentinel-2 Imagery. *Sensors* **2019**, *19*, 4013. [CrossRef] [PubMed]

191. Dhakar, R.; Sehgal, V.K.; Chakraborty, D.; Sahoo, R.N.; Mukherjee, J. Field scale wheat LAI retrieval from multispectral Sentinel 2A-MSI and LandSat 8-OLI imagery: Effect of atmospheric correction, image resolutions and inversion techniques. *Geocarto Int.* **2019**, *36*, 2044–2064. [CrossRef]
192. Bendig, J.; Bolten, A.; Bennertz, S.; Broscheit, J.; Eichfuss, S.; Bareth, G. Estimating biomass of barley using crop surface models (CSMs) derived from UAV-based RGB imaging. *Remote Sens.* **2014**, *6*, 10395–10412. [CrossRef]
193. Li, X.; Zhang, Y.; Luo, J.; Jin, X.; Xu, Y.; Yang, W. Quantification winter wheat LAI with HJ-1CCD image features over multiple growing seasons. *Int. J. Appl. Earth Obs. Geoinf.* **2016**, *44*, 104–112. [CrossRef]
194. Li, Z.; Wang, J.; Tang, H.; Huang, C.; Yang, F.; Chen, B.; Wang, X.; Xin, X.; Ge, Y. Predicting grassland leaf area index in the meadow steppes of northern china: A comparative study of regression approaches and hybrid geostatistical methods. *Remote Sens.* **2016**, *8*, 632. [CrossRef]
195. Asad, M.H.; Bais, A. Crop and Weed Leaf Area Index Mapping Using Multi-Source Remote and Proximal Sensing. *IEEE Access* **2020**, *8*, 138179–138190. [CrossRef]
196. Geng, L.; Che, T.; Ma, M.; Tan, J.; Wang, H. Corn Biomass Estimation by Integrating Remote Sensing and Long-Term Observation Data Based on Machine Learning Techniques. *Remote Sens.* **2021**, *13*, 2352. [CrossRef]
197. Paris, J. The effect of leaf size on the microwave backscattering by corn. *Remote Sens. Environ.* **1986**, *19*, 81–95. [CrossRef]
198. Pandey, A.; Thapa, K.B.; Prasad, R.; Singh, K. General regression neural network and radial basis neural network for the estimation of crop variables of lady finger. *J. Indian Soc. Remote Sens.* **2012**, *40*, 709–715. [CrossRef]
199. Ganeva, D.; Roumenina, E. Remote estimation of crop canopy parameters by statistical regression algorithms for winter rapeseed using Sentinel-2 multispectral images. *Aerosp. Res. Bulg* **2018**, *30*, 75–95. [CrossRef]
200. Xing, M.; Quan, X.; Li, X.; He, B. An extended approach for biomass estimation in a mixed vegetation area using ASAR and TM data. *Photogramm. Eng. Remote Sens.* **2014**, *80*, 429–438. [CrossRef]
201. Campos-Taberner, M.; García-Haro, F.J.; Busetto, L.; Ranghetti, L.; Martínez, B.; Gilabert, M.A.; Camps-Valls, G.; Camacho, F.; Boschetti, M. A critical comparison of remote sensing leaf area index estimates over rice-cultivated areas: From Sentinel-2 and Landsat-7/8 to MODIS, GEOV1 and EUMETSAT Polar system. *Remote Sens.* **2018**, *10*, 763. [CrossRef]
202. Paloscia, S.; Santi, E.; Fontanelli, G.; Montomoli, F.; Brogioni, M.; Macelloni, G.; Pampaloni, P.; Pettinato, S. The sensitivity of cosmo-skymed backscatter to agricultural crop type and vegetation parameters. *IEEE J. Sel. Top. Appl. Earth Obs. Remote Sens.* **2014**, *7*, 2856–2868. [CrossRef]
203. Lobell, D.B.; Asner, G.P.; Ortiz-Monasterio, J.I.; Benning, T.L. Remote sensing of regional crop production in the Yaqui Valley, Mexico: Estimates and uncertainties. *Agric. Ecosyst. Environ.* **2003**, *94*, 205–220. [CrossRef]
204. Khanal, S.; KC, K.; Fulton, J.P.; Shearer, S.; Ozkan, E. Remote sensing in agriculture—Accomplishments, limitations, and opportunities. *Remote Sens.* **2020**, *12*, 3783. [CrossRef]
205. Gorelick, N.; Hancher, M.; Dixon, M.; Ilyushchenko, S.; Thau, D.; Moore, R. Google Earth Engine: Planetary-scale geospatial analysis for everyone. *Remote Sens. Environ.* **2017**, *202*, 18–27. [CrossRef]